國 立 交 通 大 學

材 料 科 學 與 工 程 學 系

博 士 論 文

奈米顆粒及化學改質對藥物載體材料之物理性質與

生物醫學特性影響研究

Influence of nanoparticles and chemical modification on physical properties and biomedical characteristics of drug carrier materials

研 究 生：劉澤英

指導教授：陳三元 博士

中華民國 九十五年六月

奈米顆粒及化學改質對藥物載體材料之物理性質與生物醫學特性影響研究

Influence of nanoparticles and chemical modification on physical properties and biomedical characteristics of drug carrier materials

研 究 生：劉澤英　　Student：Tse-Ying Liu

指導教授：陳三元 博士　　Advisor：Dr. San-Yuan Chen

國 立 交 通 大 學

材料科學與工程系

博 士 論 文

A Dissertation

Submitted to Department of Materials Science and Engineering

And Institute of Materials Science and Engineering

College of Engineering

National Chiao Tung University

in Partial Fulfillment of the Requirements

for the Degree of

Doctor of Philosophy

in Materials Science and Engineering

June 2006

Hsinchu, Taiwan, Republic of China

中華民國九十五年六月

奈米顆粒及化學改質對藥物載體材料之物理性質與生物醫學特性影響研究

研究生：劉澤英　　指導教授：陳三元 博士

國立交通大學材料科學與工程學系 博士班

摘　　要

本研究主要是研究缺鈣氫氧基磷灰石(Ca-deficient hydroxyapatite, CDHA) 奈米顆粒對於 PMMA 與幾丁聚醣高分子物理性質及藥物釋放行為的影響。首先，PMMA-CDHA 的流變行為與 CDHA 形貌與濃度的關聯性如下：增加 CDHA 濃度會使 shear-thinning 行為變得顯著，代表奈米顆粒間以凡得瓦力與機械接觸構成交互作用使流變行為偏離牛頓流體，同時，複合材料中奈米顆粒的堆積效率與流變降服強度均與奈米顆粒長寬比有高度相關。至於以 CDHA 奈米顆粒做為牛血清蛋白載體時，其攜藥奈米載體的合成方式(原位製程與非原位製程)對牛血清蛋白攜帶量及後續蛋白質釋放行為的影響如下：對這兩種製程而言，奈米載體之牛血清蛋白攜帶量均隨合成環境 pH 值增加而減少，在 pH 值超過 8 時，相對原位製程而言，透過非原位製程所合成的奈米載體具有較大的蛋白質攜帶量，然而，其也明顯地對應一個突放(bursting release)的藥物釋放行為，這個突放行為主要歸因於牛血清蛋白分子的脫附(desorption)；相反地，透過原位製程所合成的奈米載體則表現出較和緩的釋放行為，原因為透過原位製程使得牛血清蛋白分子與奈米載體產生較強的交互作用，這樣的解釋可以透過高解析度穿透式電子顯微鏡(HR-TEM)來證明；另一方面，在低 pH 值環境下以原位製程所合成的奈米載體，則表現出兩階段釋放行為，第一階段突放是來自於牛血清蛋白分子的脫附，第二階段的釋放是來自於奈米顆粒 c 軸(長軸)溶解時所釋放出的蛋白質分子。另外，CDHA 奈米顆粒對於攜藥幾丁聚醣

複合薄膜藥物釋放行為的影響如下： CDHA 奈米顆粒的添加量與複合材料合成方式均會對擴散機制造成影響，以原位合成所製備的複合薄膜，其擴散機制由擴散控制機制朝向膨潤控制機制變化。

為了進一步調控奈米粒子與幾丁聚醣高分子間之作用力，並擴展幾丁聚醣的生醫適應性使其可包覆雙性藥物分子及 DNA 等會在酸性環境中變性的生物分子，本研究成功地合成一種無細胞毒性的雙性幾丁聚醣(NOCHC)，其上之己醯基對於細胞存活率並無顯著負面影響，本材料因有高度的親水性及部份疏水基所造成的靜電遮蔽效用，使得纖維母細胞非常不易貼附，然而，己醯基的進一步增加似乎有助於纖維母細胞的貼附；另外，己醯基的導入對於吸水率產生了非常顯著的影響，其在低溼度時會使水接合位置增加，在飽和狀態時則會增加分子間的空間使得大量的自由水可以存在，這個現象，也造成了 NOCHC 的酸鹼敏感性大於 NOCC(*N,O*-carboxymethyl chitosan)；而且，疏水性的己醯基會影響水分子的移動使材料的保水能力提升；另外，相較於 NOCC 與未改質的幾丁聚醣，NOCHC 可以包覆較多的雙性藥物 Ibuprofen，然而， NOCHC 因膨潤度大所以導致過於快速的藥物釋放，為了改善此特性，本研究使用疏水性的 *O*-hexanoyl chitosan (OHC)微球來分散於 NOCHC 基底中，可以達到程序式釋放的目的；另一方面，CDHA 奈米顆粒的混摻亦可調控此二者的藥物釋放行為，CDHA 奈米顆粒對於此二幾丁聚醣衍生物藥物釋放行為的影響如下：CDHA 對於 NOCHC 有類似交聯的效應，可減緩釋放速度並使擴散機制改變，然而，CDHA 則會破壞 OHC 的疏水結構使水份容易進入材料內部，加速降解導致釋放速度增加。

Influence of nanoparticles and chemical modification on physical properties and biomedical characteristics of drug carrier materials

Student: Tse-Ying Liu Advisor: Dr. San-Yuan Chen

Department of Materials Science and Engineering
National Chiao Tung University

ABSTRACT

Ca-deficient hydroxyapatite (CDHA) nanoparticles were incorporated with poly(methyl methacrylate) (PMMA), bovine serum albumin (BSA) and chitosan-based materials to explore the influence of filler-filler interaction, nanocarrier-protein interaction and filler-polymer interaction on the physical properties and drug release behaviors of the bioactive nanocomposites. Rheological behaviors of the PMMA-CDHA melting suspensions were systematically investigated in terms of solid loading and aspect ratio of the CDHA nanoparticles. It was found that an increase in solid contents causes pronounced shear-thinning behavior. This result suggests that a strong interaction, including van der Waals attraction and mechanical interlocking, between the CDHA nanoparticles makes the nanocomposite mixture more non-Newtonian. In addition, the packing efficiency and yield strength in the suspension were strongly influenced by the aspect ratio of nanoparticles. For the BSA-incorporated CDHA nanocarrier, the amount of BSA uptake by CDHA decreases with increasing pH. Besides, the release profile showed a bursting behavior for the nano-carrier prepared via the ex-situ process, which is probably due to the desorption of BSA molecules. In contrast, for the sample synthesized via the in-situ process at a higher pH level, a slower release profile without bursting behavior due to the dissolution of the BSA-incorporated CDHA crystal as seen from high solution TEM that indicates different extent of interaction between BSA and CDHA.

In addition, the effect of CDHA nanofiller on drug release kinetics of chitosan-CDHA

nanocomposite monolithic membrane was investigated. It demonstrates that the drug diffusion mechanism is altered by the CDHA-chitosan interaction which is strongly influenced by both the synthesis process and the concentration of the CDHA nanofiller in the membrane. In order to encapsulate the partially hydrophobic agents to prevent the agent from denature in acid environment, a novel carboxymethyl-hexanoyl (NOCHC) hydrogel with amphiphatic nature and pH-sensitivity was synthesized. The cell viability results indicate that carboxymethyl-hexanoyl chitosan did not show any sign of cytotoxicity in vitro. The degree of hexanoyl substitution did not affect the number of vital cells. In addition, the amount of fibroblast with spread out morphology increased with degree of the hexanoyl substitution. On the other hand, the hexanoyl substitution affected significantly the water-absorption ability by altering the number of water-binding sites and the state of water under low humidity and the fully-swollen state, respectively. Moreover, the presence of hydrophobic hexanoyl substitution retarded significantly water mobility during deswelling, causing better water-retention ability. Besides, compared with that of pristine chitosan and *N,O*-carboxymethyl chitosan (NOCC), the encapsulation efficiency of ibuprofen (IBU, partially hydrophobic agent) was significantly enhanced with the incorporation of the hexanoyl group. However, the bursting release of IBU was less prominent for the NOCHC samples with high degree of carboxymethyl substitution. Moreover, the pH-sensitivity was more pronounced for NOCHC than NOCC. In order to regulate the bursting release behavior of the NOCHC hydrogel in a highly swollen state, the release kinetics of microsphere-embedded hydrogel prepared by NOCHC and *O*-hexanoyl chitosan (OHC) was further investigated by incorporating various amounts of CDHA nanoparticles. It was found that the release duration of IBU from NOCHC was prolonged with the amounts of CDHA. On the contrary, the release duration of IBU from OHC (hydrophobic phase) was shortened through increasing the CDHA amount, which is due to the hydrophilic nature of the CDHA nanoparticles, destroying the intermolecular hydrophobic interaction and accelerating OHC degradation.

誌　　謝

“昨夜西風凋碧樹，獨上高樓，望盡天涯路”道盡博士班研究生在多少長夜裡面對研究挫折的徬徨與心境上的孤寂，如果沒有師長的指導與家人的支持，很難順利走完蕭瑟的研究旅程!

首先要感謝指導教授陳三元博士與劉典謨博士在研究策略規劃上的導引及科學邏輯的訓練，使我能夠順利從金屬材料背景順利切入高分子生醫材料的領域，繼續砌築知識之磚；另外，衷心感謝國防醫學大學王順德教授、吳慶祥教授以及仁愛醫院夏清智主任提供生物醫學實驗設施及寶貴的知識與建議，使得研究成果未來得以真正與生物醫學領域相銜接；在高分子專業領域部份，感謝韋光華教授與林宏洲教授在授課過程中的指引；對於中興大學徐善慧教授在細胞毒性實驗上的協助，在此也謹致感謝之意! 另外，在電子顯微鏡學部份，非常感謝劉思謙博士的協助與指導!同時也謝謝同步輻射中心李信義博士在 X-Ray 繞射儀使用上的協助!

感謝若豪及怡伶兩位學妹在協同研究上的貢獻，使得整體研究能夠順利進行；也謝謝實驗室夥伴：晉慶、志成、繼聖、定宇、彥妤、昆和、翔詮、佳惠、冠廷、泓洲、尚秀、虹蓓、書萍、白嘉、泰彥、彥谷、昀碩、茹蘭與琬琳的相伴，共享研究瓶頸之苦與工四館烤肉之趣；同時也感謝國防醫學院學弟妹: 耀文、尚群、典妮與俊彥在生物實驗上的協助；另外，所上其他同學及過去華通電腦老長官與伙伴在這四年中所給予的鼓勵與協助在此一併致謝!

我要特別感謝妻子文如在過去四年獨立負擔家計與辛勤養育女兒翔瑜，她們二位讓我有無比的勇氣面對所有的挫折與挑戰；另外，衷心地感激岳父岳母給予的支持與勉勵，讓我無後顧之憂地從產業界轉戰學術界;最後，我要將最誠摯的謝意獻給我的父母，感謝他們多年來的茹苦養育與默默的付出，謹以此論文獻給我摯愛的家人，感謝他們為我所做的一切!!

CONTENTS:

LIST OF TABLES

LIST OF FIGURES

CHAPTER 1

Introduction

1.1. Introduction to bioactive composite for drug carrier

Synthetic bioactive and biodegradable composite materials are becoming increasingly important as scaffolds for tissue engineering. Next-generation biomaterials should combine bioactive and biodegradable properties to activate in vivo mechanisms of tissue regeneration, stimulating the body to heal itself and leading to replacement of the scaffold by the regenerating tissue. The key successful point of the implantable devices for tissue regeneration is not only the suitable matrix with sufficient bioactivity and mechanical strength for progenitor cells, but also the sustained release of antibiotics and growth factors to eliminate infection and insure cell differentiation, respectively. Hence, drug-loaded implants with controlled release function were developed to optimize the therapeutic concentration of drug to the specific site of action, which eliminates the need for multiple intravenous injections and maintains the biological activity of the agents with short half-life such as platelet-derived growth factor and fibroblast growth factor.

Synthetic biocompatiable and biodegradable polymers are easily fabricated into complex structure via injection molding or solution casting method, yet insufficient bioactivity and mechanical strength are hard to meet the demands of surgery and in vivo physiologic environment. On the other hand, certain bioactive ceramics such as hydroxyapatite (HA) react with physiologic fluids to form tenacious bonds with hard tissue. However, these bioactive materials are relatively stiff, brittle, and difficult to be fabricated into complex shapes. Therefore, the tailored properties of bioactive composites such as rheological behavior, molecular relaxation kinetics, biologic response, mechanical strength and drug release profile as well as predictable degradation behavior can be manipulated through incorporating

bioactive inorganic phases into biomedical polymers. Moreover, the characteristics of polymers can be further manipulated through chemical modification by which both biological responses to implants and material responses to the physiological environment can be regulated.

1.2. Motivation of this dissertation

Poly(methymethacrylate) (PMMA), a self-curing cement, is the current standard for cement held prostheses, providing immediate structural support. However, the clinical use of this type of bone cement is typically accompanied by several complications. These complications are a result of the cement's limited mechanical properties and poor adhesion with bone which may lead to implant failure and periprosthetic osteolysis. On the other hand, chitosan (CS) is abundant in nature and currently receiving a great deal of attention for medical and pharmaceutical applications due to its biodegradable nature and biocompatibility, allowing its use in various medical applications such as bone substitute and drug-loaded scaffolds for bone tissue engineering. Nevertheless, chitosan lacks sufficient mechanical strength, which restricts its uses for load-bearing applications, especially in orthopedics. On this base, many researchers proposed that the incorporation of hydroxyapatite particles (HAp) into PMMA and chitosan can enhance osteoconductivity and mechanical strength to meet the requirement of orthopedic application. However, natural bone mineral is essentially a calcium-deficient apatitic structure (Ca-deficient hydroxyapatite, CDHA) with a Ca/P ratio of about 1.5. Therefore, CDHA is considered to be a candidate material with respect to both mechanical reinforcement and biological activity for orthopedic application. In this study, CDHA nanoparticles were incorporated into PMMA and chitosan to understand the role of CDHA nanoparticles in the rheological behaviors of the PMMA-CDHA nanocomposite and the drug release behaviors of the chitosan-CDHA nanocomposite, which are very important for the fabrication of bone-fixation devices and drug-loaded scaffolds, respectively.

Secondly, chitosan is one of the most abundant natural materials and has been used for wound dressing, cartilage tissue engineering and drug-loaded implants due to its glycosaminoglycan-like structure and low price. However, insufficient swelling ability in neutral physiological condition, poor solubility in organic solvents, and lack of amphiphatic nature have limited its uses. In addition, chitosan is a cationic polysaccharide with an isoelectric point (IEP) of 6.2. It is soluble in diluted acids and the resulting gelled-solution aggregates under neutral physiological conditions, which is unfavorable for incorporating CDHA nanoparticles and encapsulating the bioactive agents such as DNA and protein whose conformation will be altered in acidic environments. Therefore, it is necessary to develop a water-soluble chitosan-based hydrogel with amphiphatic nature to encapsulate the bioactive agents with a wide range of hydrophilic/hydrophobic nature and the agent will denature in neutral environment. In this study, a novel carboxymethyl-hexanoyl chitosan hydrogel was developed to meet above-mentioned requirement. The basic properties of hydrogel were systemically investigated in terms of the degrees of carboxymethyl and hexanoyl substitutions.

1.3. Outline of this dissertation

1. Influence of the aspect ratio of bioactive nanofillers on rheological behavior of PMMA-based orthopedic materials.

In this investigation, calcium-deficient hydroxyapatite nanocrystals with needlelike geometry were synthesized and incorporated with poly(methyl methacrylate), PMMA, to form CDHA-PMMA nanocomposites. Rheological behaviors of the PMMA-CDHA melting suspensions were systematically investigated in terms of the solid content and the aspect ratio of the CDHA nanoparticles.

2. BSA-loaded calcium-deficient hydroxyapatite nano-carriers for controlled drug

delivery.

Calcium-deficient hydroxyapatite nano-crystals incorporated with bovine serum albumin (BSA) to form BSA-loaded nano-carriers were synthesized via both in-situ and ex-situ processes. The amount of BSA uptake by the CDHA nano-crystals and the subsequent release behaviors of the BSA-loaded nano-carriers were investigated.

3. Drug release behaviour of CDHA/Chitosan nanocomposites-Effect of CDHA nanoparticles.

With the aim of the manipulation of release kinetics via bioactive nanofillers for orthopedic drug-loaded implants, the effect of CDHA nanofiller on drug release kinetics was studied by adopting vitamin B_{12} as a model drug for chitosan/Ca-deficient hydroxyapatite (CS/CDHA) nanocomposite membranes prepared in terms of different synthetic processes, i.e. in-situ and ex-situ routes, and various amounts of CDHA.

4. Synthesis and characterization of amphiphilic carboxymethyl-hexanoyl chitosan hydrogel.

Carboxymethyl-hexanoyl chitosan (NOCHC) amphiphatic hydrogel with excellent water-absorption and water-retention abilities in neutral condition was successfully synthesized for the first time and then employed as a carrier for delivering amphiphatic agents. NOCHC is a water-soluble chitosan derivative bearing the carboxymethyl (hydrophilic) group and the hexanoyl (hydrophobic) group. Water-absorption ability (W_c), water-retention ability, and drug encapsulation efficiency of the NOCHC hydrogel were investigated in terms of the degrees of carboxymethyl and hexanoyl substitution.

5. Synthesis and characterization of amphiphilic carboxymethyl-hexanoyl chitosan hydrogel: pH sensitivity and drug release behavior.

Carboxymethyl-hexanoyl chitosan (NOCHC) amphiphatic hydrogel with excellent swelling ability in neutral condition was successfully synthesized using *N,O*-carboxymethyl chitosan (NOCC) as the starting precursor. Swelling ratio under various pH values (pH-sensitivity) and release behaviors of the NOCHC hydrogel were investigated in terms of the degrees of carboxymethyl and hexanoyl substitution.

6. Sequential release behaviors of carboxymethyl-hexanoyl chitosan/*O*-hexanoyl chitosan hydrogel: Role of hydroxyapatite nanoparticles.

In order to explore the effect of nanofiller on the regulation of the drug release behavior from microsphere-embedded hydrogel prepared by carboxymethyl-hexanoyl chitosan (NOCHC) and *O*-hexanoyl chitosan (OHC), the release kinetics was investigated in terms of various amounts of calcium-deficient hydroxyapatite nanoparticles incorporated.

CHAPTER 2

Literature Review

2.1. Inorganic nanomaterials for orthopedic application

2.1.1. Introduction to nanomaterials

Nanoscience/nanotechnology is the science of fabricating, characterizing, and utilizing structures at the atomic, molecular and supramolecular levels in order to understand, create and use material structures, devices and systems with fundamentally new properties and functions resulting from their small structure. Nanomaterials are functional materials comprised of objects with at least one dimension on a scale of 1-100 nm (although the upper limit of 100 nm may be relaxed to greater sizes in some cases, depending on the material and the specific property being investigated) [1]. These objects may be either nanoparticles (small ensembles of molecules) or even individual molecules. One of the most exciting aspects of nanoobjects is that the remarkable effects on novel properties (catalytic, magnetic, ferroelectric, mechanical, optical and electronic) may arise from the critical size reduction. It occurs as we reduce the dimensions from a practically infinite (and periodic) solid crystal to a system composed of a relatively small number of atoms. For example, silver nanoparticles show biological (antimicrobial) activity whereas silver metal does not [2]. Similarly the conductivity of metal particles undergoes a marked change as their size decreases and the optical and electronic properties of inorganic semiconductor nanoparticles are known to depend upon the particle size [3]. The definition of some terms used in the field of nanostructureed materials are presented in Table 2-1 [4].

2.1.2. Bioceramics and calcium phosphate ceramics

Many kinds of surgical intervention with the involvement of an internal device or

prosthesis require that the objects to be implanted be made of ceramic materials. Bioceramics are generally very well tolerated and integrated by living tissues and have no significant toxicity. In general, there are three types of tissue response to a biomaterial as shown in Table 2-2 [5]. The present uses of bioceramics are shown in Table 2-3 [6].

Inert bioceramics are those which do not exert any influence on tissues and are not influenced by them. Their function is generally to sustain high mechanical loads. Differently from inert bioceramics, those which are defined as bioactive ceramics are able to exert some biological influence on tissues and are influenced by them. They are chemically composed with atomic species managed by the biological cycles, and generally they are calcium phosphates. Calcium phosphates ceramics (CPCs) were taken into consideration in early bioceramic studies for surgical application on bone [7-10]. Several calcium phosphate cements (CPC) have been developed and have potential use in orthopedic field as shown in Table 2-4 [11]. The most utilized are hydroxyapatite (HA) and tricalcium phosphate (TCP). The stable phases of calcium phosphate ceramics depend considerably upon temperature and the presence of water, either during processing or in the use environment. At body temperature, only two calcium phosphates are stable when in contact with aqueous media such as body fluids. At pH < 4.2, the stable phase is $CaHPO_4 \cdot 2H_2O$ (dicalcium phosphate dehydrate or hrushite, C_2P), while at pH > 4.2 the stable phase is $Ca_{10}(PO_4)_6(OH)_2$ (HA). At higher temperatures, other phases such as $Ca_3(PO_4)_2$ (β-tricalcium phosphate, C_3P, or β-TCP) and $Ca_4P_2O_9$ (tetracalcium phosphate, C_4P) are present.

2.1.3. Hydroxyapatite and Ca-deficient hydroxyapatite

The main constituents of bone are collagen (20 wt. %), calcium phosphate (69 wt. %), and water (9 wt. %). Additionally, other organic materials, such as proteins, polysaccharides, and lipids are also present in small quantities. Collagen, which can be considered as the matrix, is in the form of small microfibers. The diameter of the collagen microfibers varies

from 100 to 2000 nm. Calcium phosphate in the form of crystallized hydroxyapatite and/or amorphous calcium phosphate (ACP) provides stiffness to the bone [12]. The hydroxyapatite crystals, present in the form of plates or needles, are about 40-60 nm long, 20 nm wide, and 1.5-5 nm thick. They are deposited parallel to the collagen fibers, such that the larger dimension of crystals is along the long axis of the fiber [12].

Hydroxyapatite (HA, chemical formula $Ca_{10}(PO_4)_6(OH)_2$) is the main mineral constituent of teeth and bones. Hydroxyapatite is one of apatites with the lattice parameters: $a_1=a_2=$ 0.9432 nm and $c=$ 0.6881 nm [13]. Apatite is a general name for compounds having symmetry $P6_3/m$ and chemical formulas $A_{10}(BO_4)_2X_2$. A is cations of 1 to 3 valences, B anions have 3 to 7 valences and X denotes anions of 0 to 3 valences, where A: Ca, Pb, Cd, Sr, Ni, Eu, Al, Y, La, Ce, Na, K, B: P, As, V, Cr, Si, C, Al, S, Re and X: OH, F, Cl, Br, I, O, N, CO_3, H_2O, vacancy [13-16]. A structural model along the [0001] zone axis projected along the *c*-axis is shown in Figure 2-1 [16], from where the Ca atoms occupy two series of non-equivalent sites. Hydroxyl groups (OH^-) are situated on the 6-fold c-axis. These ions are slightly below and above the mirror planes at $Z=1/4$ and 3/4. Posner *et al*. first refined the structure of HA and reported the coordination of different Ca atoms in HA [14]. The Ca(1) atoms are coordinated by nine oxygen atoms situated in six different phosphate tetrahedral. The Ca(2) atoms, situated around the hexagonal screw axes, each has an irregular sevenfold coordination with six oxygen of five phosphate groups in addition to the hydroxyl ion. Elliott *et al*. reported that the space group of HA has three kinds of vertical or columnar symmetry [15]. There are columns of Ca^{2+} ions spaced by one half of the c-axis parameter along three-fold axes which account for two fifths of the Ca^{2+} ions in the structure. These ions are given as Ca(1). The Ca^{2+} ions are linked together by PO_4 tetrahedra in which three oxygen atoms come from one column and the fourth comes from an adjacent column. The result is a three-dimension network of PO_4 tetrahedra with enmeshed Ca^{2+} ions, and channels that contain the residual calcium, Ca(2), and ions such as OH^- which make up the HA structure. The substitution of

phosphate ions $(PO_4)^{3-}$ by hydrogenophosphate ones $(HPO_4)^{2-}$ allows a continuous variation of the Ca/P atomic ratio between 9/6 and 10/6 [17]. This leads to calcium deficient hydroxyapatites (CDHA, $Ca_{10-x}(PO_4)_{6-x}(HPO_4)_x(OH)_{2-x}$, with $0 \leqq x \leqq 1$). CDHA powders can be precipitated from conventional wet chemical methods and decomposed into a mixture of HAp and TCP by thermal treatment above 700°C.

From the point of view of biocompatibility, hydroxyapatite seems to be the most appropriate ceramic material for artificial teeth or bones due to excellent biocompatibility and bioactivity. HA ceramics does not exhibit any cytotoxicity. It shows excellent biocompatibility with hard tissues and also with skin and muscle tissues. Moreover, HA can directly bond to the bone. Unfortunately, mechanical properties of pure HA ceramics are poor. For example, fracture toughness (K_{Ic}) does not exceed the value of about 1.0 MPa $\cdot$ $m^{1/2}$ (human bone: 2–12 MPa$\cdot m^{1/2}$). Additionally, the Weibull modulus (n) is low in wet environments (n=5–12) which indicates low reliability of HA implants. Presently, the HA ceramics cannot be used as heavy-loaded implants, such as artificial teeth or bones. Its medical applications are limited to small unloaded implants, powders, coatings, and low-loaded porous implants [18]. In order to improve the reliability of HA ceramics, various reinforcements (ceramic, metallic, or polymer) have been used. Moreover, HA-coated metals have been introduced as artificial bones or teeth.

2.2. Polymer-based orthopedic materials

2.2.1. Acrylic bone cement

Acrylic based bone cement was developed in the early 1960s by Charnley and Smith [19]. Acrylic bone cements are based on polymethyl methacrylate (PMMA) which is accepted as a biocompatible polymer when cured. The bone cement is usually prepared by mixing the two components of the dose: a transparent liquid and a white powder. The main ingredients are shown in Table 2-5 [20]. The *N*,*N*-dimethyl-*para*-toluidine (DMPT) acts as accelerant of

the polymerization reaction, which activates the initiator mixed with the powder. The hydroquinone (OHC_6H_4OH, HQ) is an inhibitor, which prevents the premature polymerization of the monomer. The benzoil peroxide ($COC_6H_5OOCC_6H_5O$, BP) acts as the initiator, producing free radicals when it reacts with the amine (DMPT). $BaSO_4$ or ZrO_2 are added in order to obtain a radio-opaque cement. The diameter of most of the PMMA particles in the cement ranges between 30 and 150 μm and their shape depends on the manufacturing process used.

2.2.2. PMMA-HAp nanocomposites

PMMA is a bio-inert material thus causing weak linkage between bone and cement. It is also a brittle material with relative low fracture energy which causes the failure of implant [21]. In order to solve these problems, many PMMA-CPCs composites have been used in surgery to fix joint replacements into the bone. Hydroxyapatite particle filled PMMA composites are the most common used materials in clinical applications. Dalby et al. proposed that HAp/PMMA was a better substrate for human osteoblast (HOB) cells, resulting in increased proliferation and alkaline phosphatase (ALP) activity [22]. Scanning electron microscopy (SEM) and transmission electron microscopy (TEM) showed that HOB cells cultured on the HAp-filled PMMA preferentially anchored to HA particles exposed at the cement surface, with a close intimacy observed between HAp and HOB cells. Aizawa et al. fabricated the HAp-PMMA hybrid material having mechanical properties similar to those of the cortical bone, using porous HA ceramics with well-controlled pore sizes and bulk polymerization of MMA monomer without solvents [23]. Lee et al. studied a hydroxyapatite filled 4-META/MMA-TBB adhesive bone cement [24]. In this study, histologic examinations showed that the exposed HA particles at the surface of the cured cement were generally associated with intimate attachment to bone without fibrous tissue, as well as interdigitation of cement to bone. Moursi reported similar results [25]. Extracellular matrix production was

examined by immunohistochemistry which indicated that osteoblasts cultured on PMMA/HAp showed a more distinct networked pattern of organized fibronectin. Histochemical staining of mineralization was examined by confocal microscopy which demonstrated a higher degree of mineralization in nodules formed on PMMA/HAp as compared to PMMA. Together, these results indicate that the addition of HAp in a PMMA matrix improves osteoblast response as compared to PMMA alone. Liu showed that the surface hydroxyl groups of hydroxyapatite have the ability to react with organic isocyanate groups. It provide a good reason to use HAp as a reinforce agent in PMMA bonecement [26].

2.2.3. Chitosan and its derivatives

Polysaccharides are aboundant in nature. Their molecular structures and hence their properties vary over a broad range. Of the many kinds of polysaccharides, cellulose and chitin are the most important biomass resources; cellulose is synthesized mainly in plants, whereas chitin is synthesized mainly in lower animals. Chitin is structurally similar to cellulose, but it is an amino polysaccharide having acetamide groups at the C-2 positions in place of hydroxyl groups (Figure 2-2) [27]. Chitin is a co-polymer of *N*-acetyl-glucosamine and *N*-glucosamine units randomly or block distributed throughout the biopolymer chain depending on the processing method used to derive the biopolymer. When the number of *N*-acetyl-glucosamine units is higher than 50%, the biopolymer is termed chitin. Conversely, when the number of *N*-glucosamine units is higher, the term chitosan (CS) is used [27-29].

The presence of amino groups in chitosan is highly advantageous for providing distinctive biological functions and for conducting modification reactions. Recent progress regarding some typical chemical modifications including acylation, phthaloylation, tosylation, alkylation, Schiff base formation, reductive alkylation, *O*-carboxymethylation, *N*-carboxyalkylation, silylation, and graft copolymerization have been reported.

2.2.3.1. Hydrophobic Modification

In order to resolve the issue that poor solubility in organic solvents, chemical modification of chitosan, in particular, *N*-alkylation [30, 31], *N*-acylation [32, 33], *O*-acylation [34], and *N*-carboxyalkylation [35], has been studied. For example, Fujii et al. have reported on the acyl modification of chitosan reacted with long-chain acyl chloride for improving the organic solubility [36, 37]. Nishimura et al. [38] have also reported on phthaloylation of chitosan with phthalic anhydride.

2.2.3.2. Hydrophilic modification

On the other hand, a special emphasis has been placed on the chemical modifications to prepare several chitosan derivatives with higher solubility in water, such as *O, N*-carboxymethyl-chitosan [39], *N*-carboxymethyl-chitosan [40], *O*-carboxymethyl-chitosan [41], *N*-sulfate-chitosan [42], *O*-sulfate chitosan [43], *O*-butyryl-chitosan [44], *N*-methylene phosphonic chitosan [45], hydroxypropyl chitosan [46], *N*-trimethyl chitosan [47], *N*-succinyl-chitosan [48], *N*-carboxyethyl chitosan [49], *N*-benzyl phosphoryl chitosan [50], and *O*-succinyl chitosan [51].

2.2.3.3. Amphiphatic modification

Special attention was paid to chemical modification preparing several chitosan derivatives with amphiphatic nature. Lee et al. reported a non-covalently cross-linked palmitoyl glycol chitosan hydrogel evaluated as an erodible controlled release system for the delivery of hydrophilic macromolecules [52]. Ramos et al. introduced an alkyl chain onto a water soluble modified chitosan (*N*-methylene phosphonic chitosan) offer the presence of hydrophobic and hydrophilic branched for controlling solubility properties [53]. A series of novel chitosan derivative carrying long chain alkyl groups as hydrophobic moieties and sulfated groups as hydrophilic moieties (*N*-alkyl-*O*-sulfate chitosan) were synthesized as a

carrier to encapsulate taxol [54]. In addition, an amphiphilic chitosan derivative, *O,O'*-dipalmitoyl chitosan (DPCT), was synthesized and its miscibility with cholesterol of DPCT were studied by Tong et al.[55].

2.2.4. Chitosan-HAp nanocomposites

There were many researchers has reported HAp-Chitosan nanocomposite. Li et al. prepared the HAp-filled Chitosan composite by in-situ precipitation [56]. It was observed that the mechanical properties of the composite in the dry condition improved as the percentage of CS content increased. Mechanical properties of such CS/HAp composite rod are much better than that prepared via traditional method. They also showed that the water absorption of CS/HAp composite decreased when adding of HA powders into CS matrix, which contributes to postponing the attenuation of mechanical properties of CS/HAp composite under moisture condition. This result provides very useful information for HAp-CS drug delivery system. Chen et al. also proposed that the nano-structure of hydroxyapatite/chitosan composite will have the best biomedical properties in the biomaterials applications [57]. Zhao et al. prepared a biodegradable scaffold by phase separation method for bone tissue engineering which used hydroxyapatite/chitosan-gelatin network (HAp/CS-Gel) composite [58]. Histological and immunohistochemical staining and scanning electron microscopy observation indicated that the osteoblasts attached to and proliferated on the scaffolds. Extracellular matrices including collagen I and proteoglycan-like substrate were synthesized, while osteoid and bone-like tissue formed during the culture period. This report provided a powerful methodology to characterize the scaffolds by the presence of ECM. Sivakumar et al. proposed that the a-axis lattice constant of coralline hydroxyapatite-chitosan composite may decrease with the increase in the amount of chitosan [59]. This result indicated the interaction of the polymer backbone with HAp. The mechanical properties of chitosan-HAp nanocomposite was studied [60]. It showed that the typical aggregation length corresponded approximately to a chitosan

molecule length and the c-axes of the constituent HAp crystallites were well aligned in parallel with the chitosan molecules. The growth of the HAp crystallites is considered to occur at the nucleation sites that were most probably the complexes of amino groups on chitosan bounded with calcium ions. The compact composites obtained have been found mechanically flexible, and this flexibility has been further improved by heating at 120 degrees C in an autoclave with saturated steam pressure.

2.3. Drug release kinetics

2.3.1. Undegradable matrices

2.3.1.1. Monolithic systems (Matrix systems)

In these systems, the drug is distributed, ideally uniformly, throughout a solid polymer. Diffusion in polymers is complex and the diffusion rates should lie between those in liquids and in solids, which depends strongly on the concentration and degree of swelling of polymers. The first mathematical treatment of diffusion was established by Fick [61] who developed a law for diffusion in one dimension:

$$J = -Aj = -AD(\partial c / \partial z) \qquad 2\text{-}(1)$$

where J is the mass flow, j the flux per unit area, A the area across which diffusion occurs, D the diffusion coefficient, c the concentration, z the distance and $(\partial c / \partial z)$ the gradient of the concentration along the z axis. This equation is also known as Fick's first law. In the case of diffusion without convection and a unitary area, Eqn. 2-(1) can be written as

$$J = -D(\partial c / \partial z) \qquad 2\text{-}(2)$$

In the study of solvent diffusion in polymers, different behaviors have been observed. It is known that the diffusion of the solvent is linked to the physical properties of the polymer network and the interactions between the polymer and the solvent itself. Wang et al. proposed a classification according to the solvent diffusion rate and the polymer relaxation rate: Fickian (Case I) and non-Fickian (Case II and anomalous) diffusions [62]. The amount of solvent

absorbed per unit area of polymer at time t, M_t, is represented by

$$M_t=kt^n \quad \text{(Power low)} \qquad 2\text{-}(3)$$

where k is a constant and n a parameter related to the diffusion mechanism, the value of which lies between 1/2 and 1 for the sample with slab geometry [63].

A. Fickian diffusion

The influence of matrix relaxation and the diffusion process on drug release can be estimated by the Deborah number De:

$$De=\lambda/\theta \qquad 2\text{-}(4)$$

where De is the ratio of a characteristic relaxation time (λ) to a characteristic diffusion time (θ). Eqn. 2-(4) indicates that De << 1 is obtained when the relaxation is much faster than the diffusion, and in this case drug release is controlled by diffusion in the fluid filling the swollen matrix. This condition usually occurs with swellable systems well above the glass transition temperature (Tg) that swell rapidly and reach equilibrium before drug release takes place. De>> 1 indicates that the matrix is characterized by a very long relaxation and drug release is controlled by diffusion in an unchanged matrix. The drug diffuses in fact from an unswollen region, such as from a matrix in the glassy state (well below the Tg). In the cases of De<< 1 and De>> 1, the drug is released by diffusion through a system with constant boundary conditions. The relaxation process does not interact with drug release, so the same speculations reported above for Fickian diffusion release from undegradable and unswellable devices can be applied. This process is also defined as Case I transport. The diffusion distance is proportional to the square-root of time (Higuichi model) [64]

$$M_t=kt^{1/2} \qquad 2\text{-}(5)$$

B. Non-Fickian diffusion

A second case of drug release from swellable and undegradable matrices is observed when the glassy fraction of a swelling system relaxes with observable rate, but much more slowly than the diffusion of the drug in the rubbery fraction of the matrix. In this process,

defined as Case II transport, the release kinetic is controlled by the relaxation of the glassy fraction of the matrix. For a thin film, the diffusion distance is directly proportional to time

$$M_t=kt \qquad 2\text{-}(6)$$

When the characteristic relaxation time and diffusion time are comparable (De~1), the relaxation interacts with the diffusion process and drug release takes place under nonconstant boundary conditions. This anomalous non-Fickian transport is observed when the drug is released during a change of the matrix from a glassy to a rubber state. Anomalous diffusion lies in between and is characterized by the following equation:

$$M_t=kt^n \text{ and } 0.5<n<1. \qquad 2\text{-}(7)$$

Thus, Eqn. 2-(7) has two distinct physical realistic meanings in the two special cases of n=0.5 (indicating diffusion-controlled drug release) and n=1.0 (indicating swelling-controlled drug release). Values of n between 0.5 and 1.0 can be regarded as an indicator for the superposition of both phenomena (anomalous transport). The two extreme values for the exponent n, 0.5 and 1.0, are only valid for slab geometry. For spheres and cylinders different values have been derived [65, 66], as listed in Table 2-6.

2.3.1.2. Reservoir systems

In this type of system, a core of drug is sourrounded by a polymer and diffusion of the drug through the polymer is the rate-limiting step. In other words, reservoir systems are usually designed so that the drug is contained in an oversaturation concentration in the core of the system and release is controlled by diffusion through a surrounding undegradable membrane. Release is defined by the first Fick's law, which describes the flux of a substance through the membrane at a steady state:

$$J_d= -Ddc/dx \qquad 2\text{-}(8)$$

The first Fick's equation can be elaborated for matrices with different geometrical shape. For a cylindrical device of height h, inner radius r_1, and outer radius r_0, the rate of drug release can

be expressed as:

$$dM/dt=2\pi hK_d(C_1-C_2)/\ln(r_0/r_1) \quad 2\text{-}(9)$$

where K_d is the membrane/medium distribution coefficient (i.e., membrane permeability, $K_d=DK$ where D is the diffusion coefficient, and K the partition coefficient), C_1 is the drug concentration in the core, and C_2 is the drug concentration in the external medium. For a spherical reservoir of radius r_1, sorrrounded by a spherical membrane of radius r_0,

$$dM/dt=4\pi K_d(C_1-C_2)r_0r_1/(r_0-r_1) \quad 2\text{-}(10)$$

Assuming that the drug has the same solubility in the system core and in the external medium, the release for a sandwich or slab reservoir is described by

$$M_t= S_d K_d(C_1-C_2)t/l \quad 2\text{-}(11)$$

where M_t is the released amount of drug at time *t,* S_d is the releasing surface area, *l* is the thickness of the polymeric membrane [61].

2.3.2. Biodegradable matrices

Hopfenberg assumed that the rate of drug release from the erodible system is proportional to the surface area of the device which is allowed to change with time [67]. All mass transfer processes involved in controlling drug release are assumed to add up to a single zero-order process (characterized by a rate constant, k_0) confined to the surface area of the system. This zero-order process can correspond to a single physical or chemical phenomenon, but it can also result from the superposition of several processes, such dissolution, swelling, and polymer chain cleavage. A good example for systems Hopfenberg's model can be applied to is surface eroding polymer matrices where a zero-order surface detachment of the drug is the rate limiting release step. Hopfenberg derived the following general equation, which is valid for spheres, cylinders and slabs:

$$M_t/ M_\infty=1-(1-(k_0 t/C_0 a))^n \quad 2\text{-}(12)$$

M_t and M_∞ are the cumulative amounts of drug released at time t and at infinite time,

respectively; C_0 denotes the uniform initial drug concentration within the system; a is the radius of a cylinder or sphere or the half-thickness of a slab; n is a 'shape factor' representing spherical (n=3), cylindrical (n=2) or slab geometry (n=1).

Heller and Baker developed a mathematical model describing drug release from water-insoluble polymers that undergo hydrolytic backbone cleavage, during which the polymer chains are converted into small, water-soluble molecules [68]. They assumed that for polymer matrices undergoing bulk erosion, degradation can be described by first-order kinetics.

$$dM_t/dt=A/2 * (2 \cdot P_0 \cdot \exp(k \cdot t) \cdot C_0/t)^{1/2} \qquad 2\text{-}(13)$$

here, M_t is the cumulative absolute amount of drug released at time t; k is the first order rate constant; P_0 is the initial drug permeability and C_0 is the initial drug concentration within the system.

Table 2-1. Definitions of the terms used in nanostructured materials [4].

Terms	Definition
Cluster	A collection of units (atoms or reactive molecules) of up to about 50 units. Cluster compounds are such moieties surrounded by a ligand shell that allows isolation of a molecular species.
Colloid	A stable liquid phase containing particles in the 1-1000 nm range. A colloidal particle is one such 1-10000 nm sized particle.
Nanoparticle	A solid particle in the 1-1000 nm range that could be nanocrystalline, an aggregate of crystallites, or a single crystallite.
Nanostructured material	Any solid material that has a nanometer dimension; Three dimensions: Particles Two dimensions: Thin films One dimension: Thin wire Zero dimension: Quantum dot (A particle that exhibits a size quantization effect in at least one dimension.)

Table 2-2. Types of implant-tissue response [5].

Types	Tissue response	Example
Bioinert, (nontoxic and biologically inactive)	It has minimal interaction with its surrounding tissue. A fibrous capsule forms around a bioinert implant.	stainless steel, titanium, alumina, partially stabilized zirconia, and ultra high molecular weight polyethylene.
Bioactive, (nontoxic and biologically bioactive),	It interacts with the surrounding bone and the soft tissue. An interfacial bond forms.	synthetic hydroxyapatite, glass-ceramic A-W, and Bioglass.
Bioresorbable, (nontoxic and dissolves),	It dissolve (resorbed) slowly. The surrounding tissue replaces it.	tricalcium phosphate, Calcium oxide, calcium carbonate (coral),

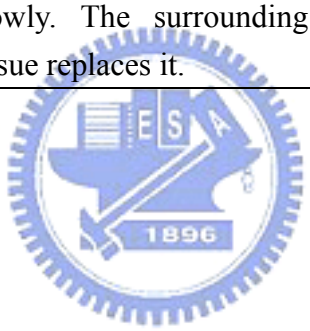

Table 2-3. Present uses of bioceramics [6].

Application	Material
Orthopedic load-bearing	Al_2O_3
Coatings for tissue ingrowth (Cardiovascular, orthopedic, dental and maxillofacial prosthetics)	Al_2O_3
Coatings for chemical bonding (Orthopedic, dental and maxillofacial prosthetics)	HA, Bioactive glasses, Bioactive glass-ceramics
Temporary bone space fillers	Tricalcium phosphate, Calcium and phosphate salts
Dental implants	Al_2O_3, HA, Bioactive glasses
Periodontal pocket obliteration	HA, HA-PLA composite, Trisodium phosphate, Calcium and phosphate salts, Bioactive glasses
Alveolar ridge augmentations	Al_2O_3, HA, HA-autogenous bone composite, HA-PLA composite, Bioactive glasses
Maxillofacial reconstruction	Al_2O_3, HA, HA-PLA composite, Bioactive glasses
Otolaryngological	Al_2O_3, HA, HA-PLA composite, Bioactive glasses
Percutaneous access devices	Bioactive glasses
Artificial tendon and ligament	PLA-carbon fiber composite
Orthopedic fixation devices	PLA-carbon fibers, PLA-CPC composites

Table 2-4. Name, abbreviations and formula of the calcium phosphate [11].

Ca/P	Abbreviation	Name	Formula
0.5	MCPM	Monocalcium phosphate monohydrate	$Ca(H_2PO_4)_2H_2O$
1	DCP	Dicalcium phosphate	$CaHPO_4$
1	DCPD	Dicalcium phosphate dihydrate	$CaHPO_42H_2O$
1	CPP	Calcium potassium phosphate	$CaKPO_4$
1	CPSP	Calcium potassium sodium phosphate	$Ca_2KNa(PO_4)_2$
1.5	α-TCP	Alpha tertiary calcium phosphate	α-$Ca_3(PO_4)_2$
1.5	β-TCP	Beta tertiary calcium phosphate	β-$Ca_3(PO_4)_2$
1.5	CDHA	Calcium deficient hydroxyapatite	$Ca_9(HPO_4)(PO_4)_5OH$
1.67	HA	Hydroxyapatite	$Ca_{10}(PO_4)_6(OH)_2$
2	TTCP	Tetracalcium phosphate	$Ca_4(PO_4)_2$
∞	--	Calcium oxide	CaO

Table 2-5. Source and composition of the commercialized bone cement [20].

Name and source	Powder				Liquid				
	PMMA	PBMA	BP	CM	MMA	BMA	DMPT	ETOH	HQ
Sulfix-60	79.618	8.84	0.836	9.834 ZrO_2	83.619	14.768	1.612 DMAPE	1.612	0.003
CERIM LT	87.0		3.0	10.0 $BaSO_4$	98.993		1.0	-	70-75 ppm
CEMEX RX	88.27		2.73	9.0 $BaSO_4$	99.10		0.90	-	75 ppm
ZIMMER Low viscosity	89.25		0.75	10.0 $BaSO_4$	97.25		2.75	-	65-85 ppm
ZIMMER Dough type	89.25		0.75	10.0 $BaSO_4$	97.25		2.75	-	65-85 ppm
Palacos	84.5		n.n.	15 ZrO_2	92			-	-
CMW 1	88.85		2.05	9.10 $BaSO_4$	98.215		0.816	0.945	0.002

PBMA: polybutyl-methacrylate; BP: benzoylperoxide; CM: contrast medium; MMA: methyl-methacrylate; BMA: butyl-methacrylate; DMPT: *N,N*-dimethyl-para-toluidine; DMAPE: dimethylamino-phenyl-ethanol; ETOH: ethanol; HQ: hydroquinone.

Table 2-6. Diffusion exponent (n) of the power law and drug release mechanism from polymeric controlled delivery system of different geometry [64, 65].

Diffusion exponent (n)			Drug release mechanism
Thin film	Cylinder	Sphere	
0.5	0.45	0.43	Fickian diffusion
0.5<n<1.0	0.45<n<0.89	0.43<n<0.85	Anomalous transport
1.0	0.89	0.85	Case-II transport

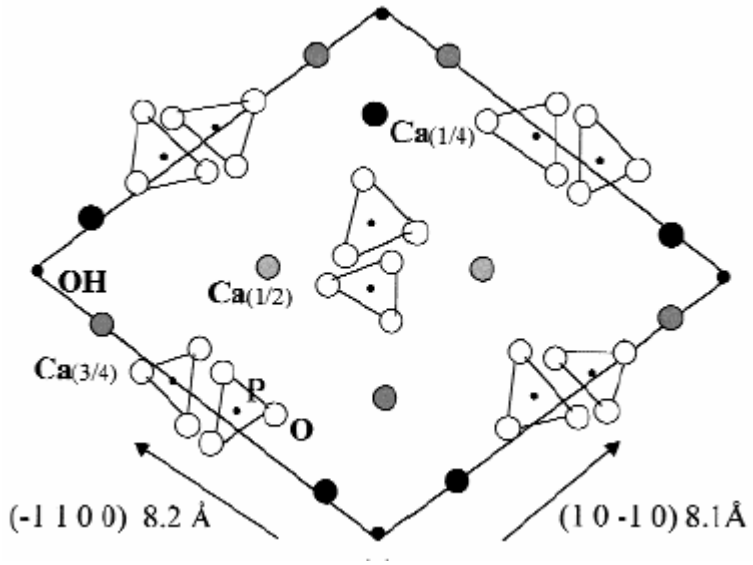

Figure 2-1 Structural model of hydroxyapatite with the [0001] as projection axis [16].

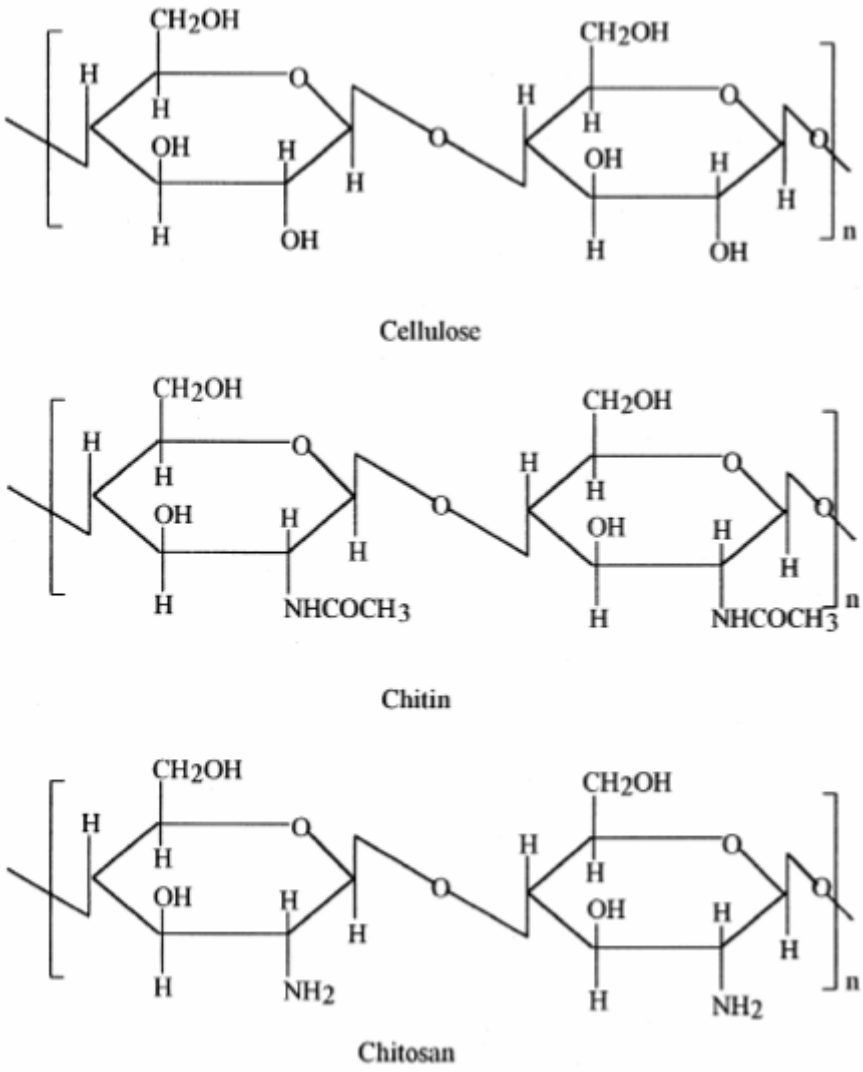

Figure 2-2. Structures of cellulose, chitin and chitosan [27].

CHAPTER 3

Influence of the Aspect Ratio of Bioactive Nano-fillers on Rheological Behavior of PMMA-based Orthopedic Materials

3.1. Introduction

Poly(methyl methacrylate), PMMA, has long been widely used as bone cement and orthopedic devices such as bone screw, pin, etc. The prime advantage of using the PMMA cement is that it is easily conformed to defective surrounds of any geometry. However, clinical practices revealed that the PMMA had several drawbacks such as weak bone-cement interface that renders PMMA prostheses more susceptible to fail after implantation [69-72].

Recently, the incorporation of bioactive reinforcement phase into PMMA offers an advantage to overcome those aforementioned deficiencies and moreover, improves mechanical integrity with the PMMA [73-75]. Among those reinforcement phases, bioceramic-based materials such as tricalcium phosphate (Ca/P = 1.5) and hydroxyapatite (Ca/P = 1.67) are most widely employed for clinical practices, simply because they exhibit considerably improved biological affinity and activity to surrounding host tissues when implanted [76-78]. Furthermore, both compositions are chemically similar to the mineral constituent of human hard tissue. However, bone mineral (natural biocrystal) has essentially a calcium-deficient apatitic structure with a Ca/P ratio of about 1.5, which is compositionally similar to tricalcium phosphates, $Ca_3(PO_4)_2$, (Ca/P = 1.5) and structurally similar to stoichiometric hydroxyapatite, $Ca_{10}(PO_4)_6(OH)_2$, (Ca/P = 1.67).

It is well known that the natural biocrystals with a needlelike or rodlike shape are well aligned along a specific direction with the polymer matrix, i.e. collagen, to form nature bone which exhibits better mechanical properties compared to individual components and those existing synthetic biomaterials. So far, several studies have been focused on the development

of nano-composites to simulate nature bone in apatite structure [79-82]. For example, Adriana. et al. developed a biomimetic process to control the alignment of nanoparticles in the nano-composites [79]. However, these methods could not be applied for the fabrication of medical devices with complex shape. On the other hand, a stress-induced process such as inject-molding or extrusion can be used for the alignment of nanoparticles in polymeric suspension under high shear rate. Although some investigations have been focused on the relationship between rheological behavior and nanoparticle structure of polymeric suspension in the nanocomposite mixtures [83-85], little information is available on the rheological properties of PMMA-HAp nano-composite with different aspect ratios of the nanoparticles for the fabrication of orthopedic parts like bone fixation devices.

Although Ti or C fibers can be incorporated into the PMMA to enhance the mechanical properties, it is more desirable if nano-metric calcium-deficient apatite crystals (hereafter termed CDHA) with pertinent aspect ratio, mimicking that of the mineral constitute in natural bone structure, can be introduced in the PMMA matrix. The improvement in both the biological affinity and mechanical properties of the resulting PMMA-CDHA composites is then expected. Therefore, nano-metric needle-like CDHA crystals, instead of Ti or C fibers, were synthesized and employed in this work to study the role of the aspect ratio of CDHA nano-needle crystals in the rheological behavior of the PMMA-CDHA mixture. As a first parts of the whole project, understanding of the rheological behavior of the PMMA-CDHA blend in this study should provide fundamental and valuable processing information in terms of solid content and aspect ratio of the reinforced phase as reported in this communication, for the fabrication of PMMA-based orthopedic devices by injection molding or alternative thermal molding process.

3.2. Experiment materials and methods

3.2.1. Synthesis of CDHA nano-particle

The calcium-deficient hydroxyapatite (CDHA) nano-particles with a Ca/P molar ratio of 1.5 were fabricated by co-precipitation method with $Ca(CH_3COO)_2$ and H_3PO_4 as Ca and P precursors, respectively. Prior to co-precipitation reaction, the pH value of H_3PO_4 solutions were kept above 12 by using NaOH solution. Subsequently, 0.001 wt% poly(acrylic acid) (PAA) (Aldrich Chemical, Mw 2000) was added into the alkalized H_3PO_4 solutions. In order to control the CDHA particle with different aspect ratios, three different adding rates of 5 ml/min, 30 ml/min, and 55 ml/min were used to drop $Ca(CH_3COO)_2$ aqueous solution (0.5M) into H_3PO_4 solution (controlled at 0.33 M) at 60°C [86]. During the titration process, the temperature deviation of each mixture was monitored and kept less than 3°C. After filtration and washing by acetone for several times, the precipitate dough was then mixed in 80 ml acetone to form three kinds of CDHA suspensions. The solid content in each CDHA-acetone suspension was determined by measuring the weight difference between before and after the removal of the diluting medium at 105°C.

3.2.2. CDHA-PMMA composite mixtures

Various volume from 5% to 15% CDHA nano-particles with different aspect ratios (AR=length of particle/width of particle) were dispersed in the PMMA-Acetone (PMMA: Aldrich Chemical Corp. Mw 13,000) polymer solution to form PMMA-CDHA composite. After stirring for 24 h, the CDHA-PMMA suspensions were dried to remove the diluting solvent and then subjected to heat treatment in vacuum oven for the removal of the residual solvent. After that, the CDHA-PMMA nanocomposite powders can be obtained after pulverization.

3.2.3. Rheometrical measurement

The rheological behavior of the mixtures with different concentrations of CDHA nanoparticles was examined at a working temperature of 240°C using capillary rheometry

(Schimadzu, CFT-500D). The specimens were first prepared into cylindrical shape of 10 mm x 10 mm dimensions via a uniaxial molding at a compressive pressure of 30 MPa at 160°C. The cylindrical specimen was then placed into the cavity die of the capillary rheometer. The capillary die has a size of 1 mm in diameter, located at the bottom of the cavity. After the sample was stabilized at the testing temperature of 240°C for several minutes, the specimen was compressed with a pre-determined uni-axial pressure.

In order to eliminate the entrance and end effect of the rheological data, both the first and final 1-mm region of the 10 mm-height specimens were excluded. In addition, the Rabinowitsch equation was also adopted for shear rate correlation due to wall effect. The relationship between shear stress(τ) and pressure drop along the specimen dimension can be determined with the use of Bagley model as follows [87],

$$\tau = \frac{PR}{4L} \qquad 3\text{-}(1)$$

where P, R and L represent the values of pressure drop, capillary radius and capillary length, respectively. The shear rate (γ) was determined by converting the ratio of the volume flow rate (F) to the capillary radius (R) through,

$$\gamma = \frac{4F}{\pi R^3} \qquad 3\text{-}(2)$$

The shear viscosity (η) was then determined by;

$$\eta = \frac{\tau}{\gamma} \qquad 3\text{-}(3)$$

Generally, three runs were conducted for each composition and aspect ratio to ensure the accuracy and the reproducibility of the rheological data. If needed, five runs were performed for more accurate results.

3.3. Results and discussion

3.3.1. Flow behavior

The XRD patterns in Figure 3-1 show that the synthetic powders can be indexed as a

calcium-deficient hydroxyapatite (CDHA) phase irrespectively of the addition rate. According to TEM observation, the morphology of the precipitate crystals exhibits needle-like geometry with different aspect ratios (L/d, length/diameter), ranging from 7, 10, to 17 for the addition rate of 5, 30, and 55 ml/min, respectively. (TEM photographs were not shown here.)

The flow behavior of the PMMA-CDHA mixtures can be characterized by a shear rate (γ)-viscosity (η) curve (derived simply from $\eta = K\gamma^{n-1}$), as shown in a log-log plot of Figure 3-2(a), 3-2(b) and 3-2(c) for CDHA nano-needles with AR = 7, 10, and 17, respectively. It is evidenced that the mixtures are shear-thinning character and the flow behavior of the mixtures is as a function of both AR and concentration of the nano-needles. The flow index n is generally falling in the range between 0.4 and 0.5 for the mixtures with 5 and 10% concentration of nano-needles. Even increasing CDHA concentration up to 15%, the difference in the flow index for the composition with the smallest AR [Figure 3-2(a)] is essentially much less pronounced over the range of solid concentration employed. This may indicate that the flow behavior as well as the suspension structure of the mixtures prepared with the nano-needles of the smallest AR is similar. Accordingly, this could be true for the nanoparticles with a lower AR below a certain solid loading where the interparticle interaction, including surface attraction or mechanical interlocking, may remain similar in magnitude.

On the other hand, for the compositions with larger AR, a smaller n value was observed at a 15% solid loading as revealed from Figures 3-2(b) and 3-2(c). While comparing to Figure3-2(a), a considerable reduction in the flow index (n), appearing at 15% loading, may suggest that the nano-particles with a higher AR should exert strong influence onto suspension structure and flow behavior. From those measured data in Figures. 3-2(b) and 3-2(c) for high-AR particles, it seems to indicate that at lower solid loadings, i.e., 5 and 10%, the interactions between the nano-needles should be not as significantly strong as that at 15%.

However, a particle network structure with more extensive entanglement with random distribution of the nano-needles should arise because of increasing solid loadings, i.e., 15% in

the current system. If this assumption in structural development is correct, then, we can speculate that the mixtures with solid loading as high as 15% may have an open network structure with voids between the closely-connect framework filled with polymer melt. With such an interconnect structure, the flowability of the polymer melt was then effectively retarded and a higher shear viscosity can be expected under an identical shear rate (or shear stress), leading to a higher-shear-dependent character than that at lower solid concentrations.

3.3.2. Yield strength

With the use of the Casson's model [88], Eqn. 3-(4), the yield strength of the mixtures can be obtained by extrapolating the straight lines obtained from the $\tau^{1/2}$ - $\gamma^{1/2}$ plot to zero shear rate.

$$\tau^{1/2} = \tau_y^{1/2} + c\,\gamma^{1/2} \qquad 3\text{-}(4)$$

where τ_y is the yield strength.

Figure 3-3 shows Casson's correlation for the mixtures with AR = 17, where straight lines for each solid loading can be obtained in Casson's plot. After extrapolating to zero shear rate, the τ_y was calculated and is also illustrated in the figure. It is observed that τ_y first increases slightly with increasing solid loading from 5% to 10%, but considerably increased at 15% loadings. Similar behavior is also observed for other mixtures, as illustrated in Figure 3-4. However, as expected, the τ_y at lower solid loadings, i.e., < 10%, does not show much difference for each category of AR, but the difference becomes more pronounced when the solid concentration is increased up to 15%.

The yield strength is merely a direct indication of the strength of the particle network within the matrix, which has been well recognized due to net attractive interaction. For high-aspect-ratio particles, mechanical interlocking between neighboring particles should play some role. In a previous investigation [89], Liu experimentally verified that the yield strength is correlated linearly with the Van der Waals potential between two identical spheres; however,

the near-surface potential should remain identical for particles with various geometries. Furthermore, it turns out to be more pronounced for smaller particles because the particle-to-particle separation (λ) is getting smaller for nanometric dimension by [89];

$$\lambda = \frac{4}{3} r \frac{\Phi_m - \Phi}{\Phi} \qquad 3\text{-}(5)$$

where Φ_m is the maximum solid loading of a given mixture system, r is the particle radius, and Φ is the solid faction of the mixture. For particles with high aspect ratio such as needlelike geometry, Eqn. 3-(5) may be suitable only when the needlelike particles are well aligned with parallel configuration and λ_{rod} obtained from Eqn. 3-(5) is approximated as the needle-to-needle distance, as schematically illustrated in Figure 3-5. λ is proportional to particle radius (r) and the decreased solid fraction (Φ). The resulting Van der Waals potential is increased proportionally with both decreased r of the particles and increased solid fraction of the mixture. Therefore, an enhanced yield strength is expected.

However, real network structure in the mixtures, when first prepared, is far from being idealized and simplified as depicted in Figure 3-5 but randomly oriented. This gives complexity upon a quantitative analysis due to the increase in the randomness and geometry of the dispersed particles. One of the most commonly seen phenomena is a direct physical contact of the needlelike particles spreading over the entire mixture volume. Once it happens, mechanical interlocking with enhanced friction, except the attractive potential, between needles is thus reasonably expected. If this occurs, then the mechanical friction force should increase because of more "contact points" due to the introduction of higher fractions and/or higher aspect ratio of the nano-needles.

Further analysis of the frictional force could be feasible but not the primary focus of this paper. Therefore, the variation of suspension structure in terms of particle packing efficiency seems able to provide clues for better understanding on rheological behaviors. It is conceivable that the interparticle friction, stemming from the physical "contact" of the needles

in this communication, should directly affect the efficiency of particle packing. This means that a maximum solid fraction (Φ_m) should be achievable and inversely proportional to the density of the contact points. Since only when particles are physically separated from each other in the mixture suspension, effective volume in the suspension for further deformation is available, permitting a higher maximum loading to be attained. However, whilst particles are closely packed with each other by physical contact, the effective space is then diminished and no deformation can be detected, restricting the development toward higher level of Φ_m.

Therefore, the estimation of the maximum loading in a given mixture is able to provide physically meaningful evidence for better understanding the interlocking effect in this nanocomposite system. To estimate the maximum fraction, Liu recently proposed a simple two-parameter model that is useful to predict Φ_m for a number of suspension systems with precision [90]. Here, we employ the model, having an analytical form:

$$1 - \eta^{-1/2} = a\,\Phi + b \qquad 3\text{-}(6)$$

where Φ_m can be determined via the slope (a) and intercept (b) in $(1 - \eta^{-1/2})$ - Φ plot by:

$$\Phi_m = \frac{1-b}{a} \qquad 3\text{-}(7)$$

As expected, Figure 3-6 shows a linear relationship according to Eqn. 3-(6), but surprisingly, the correlation is well suitable for high-aspect-ratio nanoparticles, although it was originally derived from sphere model.

The Φ_m obtained is also described in Figure 3-6 for nanoparticles with different aspect ratios. It is evidenced that an increase in aspect ratio causes a decrease in packing efficiency, resulting in a lower Φ_m. This further substantiates that the packing efficiency of the nano-needles is considerably retarded with the increased aspect ratio. In other words, for high-aspect-ratio nanoparticles, percolation of the particle can be easily reached with lower solid fraction than that of particles with low aspect ratio. Based on this argument, it is reasonable to believe that as aforementioned, a huge number of physical contacts between

nano-needles do give considerable yield strength to the mixtures and accordingly, mechanical interlocking associated with the rising effect of frictional force is largely expected.

3.3.3. Aspect ratio-dependent suspension property

By plotting the Φ_m in terms of AR (symbolized as ξ), Figure 3-7 shows dependence of maximum solid concentration on the aspect ratio of the CDHA particles, where an extra point (arrow indicated) was derived from sphere suspension (AR = 1). A sigmoidal behavior (solid line) was clearly observed. Although the data point at AR = 1 is borrowed from other well-characterized system [90], it is generally believed that a randomly close packing of spherical particles with a relative packing density of ~0.64 can be attainable under infinite shear. A steeper transition in the sigmoidal curve can be found with the aspect ratio (ξ) in the range between 7 and 10. This is suggestive of an existing critical aspect ratio (ξ_c), above which the suspension structure may be considerably altered because of poorer packing efficiency. To determine the ξ_c, a simple 3rd-order polynomial equation in Eqn. 3-(8) was employed for curve fitting (dash curve in Figure 3-7). Although the curve-fitting is not matched very well with the experimental data, the fitted curve still shows good consistence with the data in the important aspect-ratio (ξ) range of 7 to 10. Therefore, the transition point can be further derived by double differentiating Eqn. 3-(8) in terms of ξ, and a value of 8.8 was calculated while solving the differentiated form of Eqn. 3-(8) at $d^2\Phi m/d\xi^2 = 0$.

$$\Phi_m = 0.0952\ \xi^3 - 2.512\ \xi^2 + 13.753\ \xi + 52.664 \qquad 3\text{-}(8)$$

This value at ξ_c = 8.8 seems in agreement with a preceding observation of the Φ_m determined in Figure 3-6, suggesting that the resulting particle packing efficiency is substantially retarded when the used nano-needles have an aspect ratio greater than 8.8 in the current system. Furthermore, this phenomenon becomes more pronounced when the solid loading reaches (and above) 15%. The poorer particle packing efficiency due to the influence of the particle aspect-ratio is then believed because of the increased density of physical

contacts between the nano-needles. It can be then reasonably expected for a significant increase in the frictional force among the contact nano-needles. As further evidenced from a correlation between the aspect ratio and yield strength, as shown in Figure 3-8, where a considerable increase in the yield strength can be found when the particle aspect-ratio is increased from 7 to 10 for 15% of solid loading.

Therefore, it is clear that above a certain solid loading, the aspect ratio of the particles turns into a dominant factor on the variation of suspension structure and corresponding yield behavior. It is more interesting to note that the critical aspect ratio, for the first time so far as we know, in current mixture can be semi-empirically determined via a simple mathematic treatment.

In this work, the use of capillary rheometry instead of dynamic rheometry for the characterization of the rheological properties of the PMMA-CDHA blends does provide more realistic flowing behavior of the melting suspension under the operation of injection molding or thermal extrusion process. The influence of the nano-metric CDHA crystals on the rheological behaviors of the blend allows the nano-sized CDHA particles dispersed in the nano-composites to be optimized in terms of aspect ratio and loading of the nano-CDHA under sufficient shear rate. However, the effect of the stress-induced alignment of the nano-sized CDHA particles on the mechanical properties of the resulting composite will be reported separately.

3.4. Conclusion

Calcium-deficient hydroxyapatite nano-needles with different aspect ratios were prepared and incorporated into poly(methyl methacrylate) to form nanocomposite mixtures. The rheological properties and suspension structure of the mixtures were characterized with respect to the particle aspect ratio. Some conclusions can be summarized as follows.

(1) The influence of particle aspect-ratio on packing efficiency is significant and a critical value of the aspect ratio was determined to be 8.8.

(2) With increasing the aspect ratio, especially above the critical value, the nano-needles result in an extensive contact between the particles upon which a poorer packing efficiency, higher yield strength and poorer flowability of the mixture suspension can be observed.

(3) The maximum solid loadings of nano-CDHA particles with aspect ratio 7, 10, and 17 were determined to be 28%, 31%, and 57%, respectively.

(4) Rheological behavior of the PMMA-CDHA mixture as functions of solid loading and aspect ratio of the CDHA nanoparticles provides not only optimal design of nanoparticles in the polymeric suspension but also optimized conditions for the fabrication of PMMA-CDHA-based orthopedic devices.

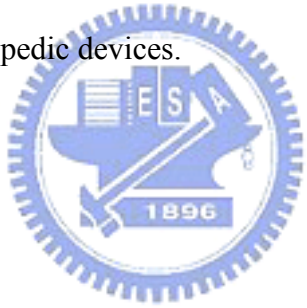

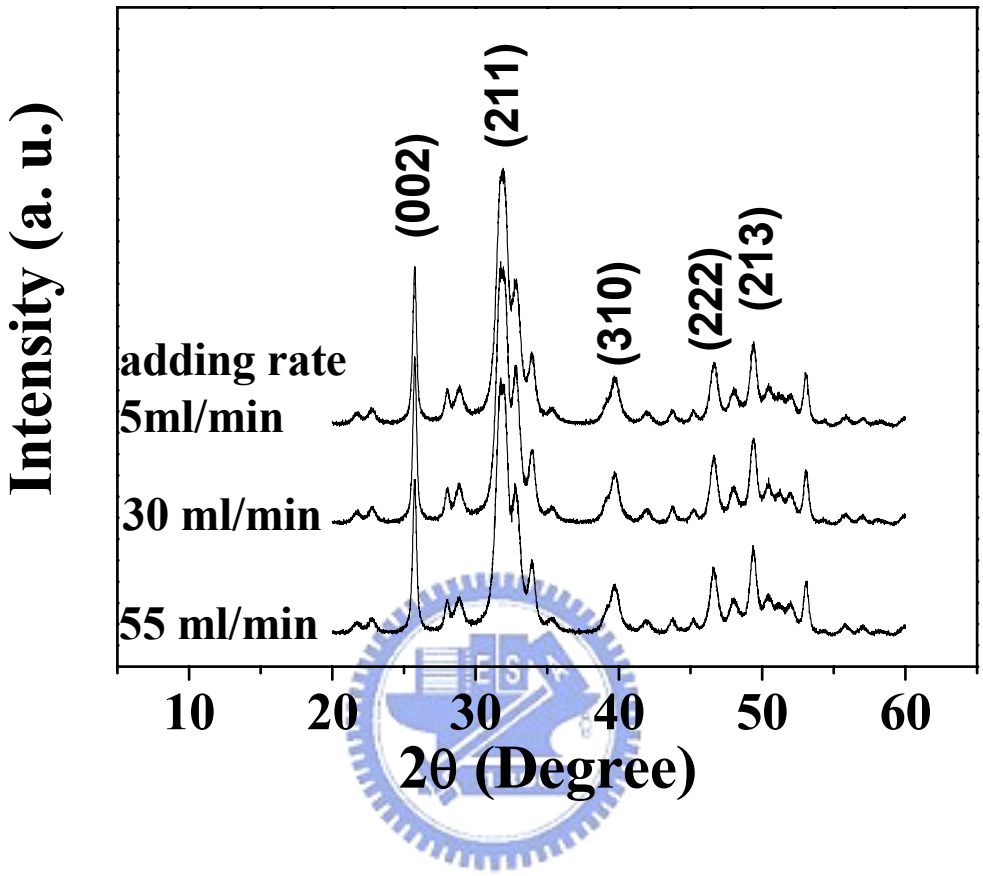

Figure 3-1. X-ray diffraction patterns of the calcium phosphate powders prepared with various addition rates.

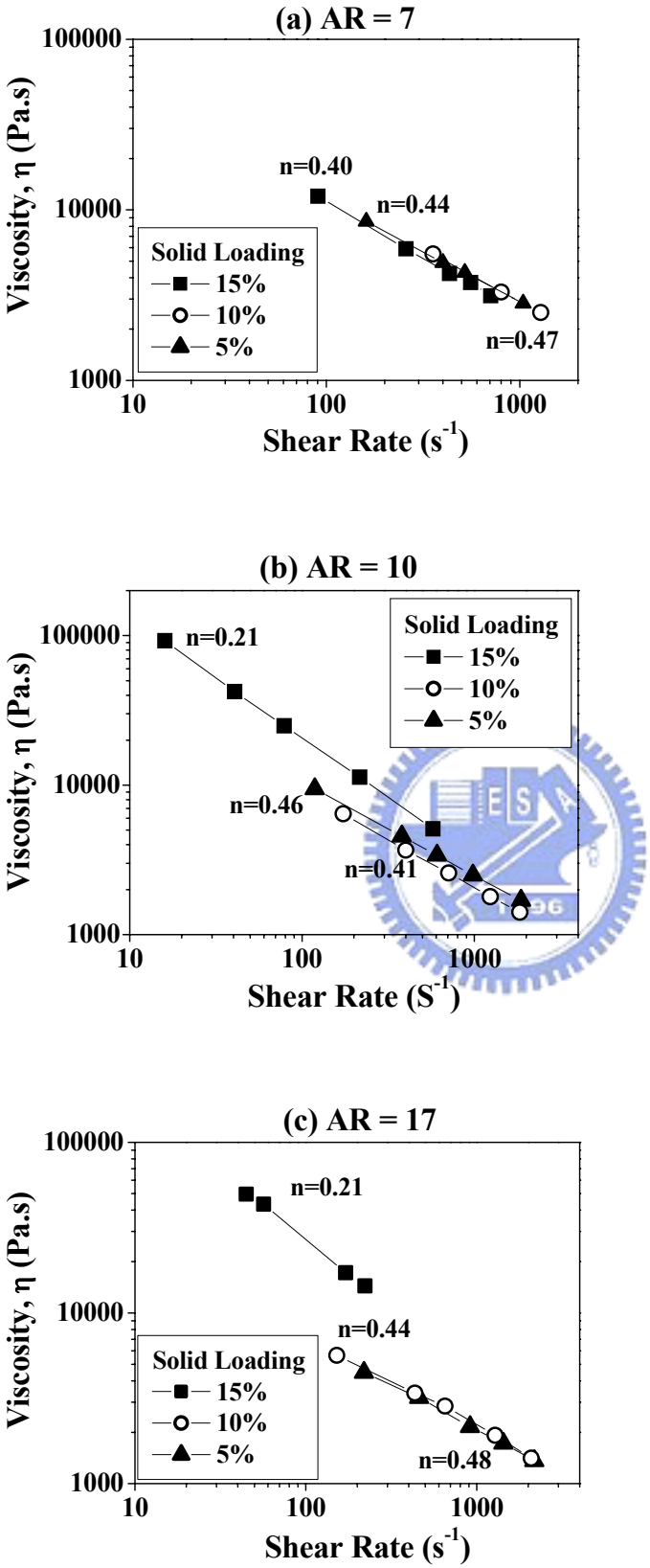

Figure 3-2. Shear rate-shear viscosity relationship for CDHA-PMMA mixtures with nano-needles of different aspect ratio.

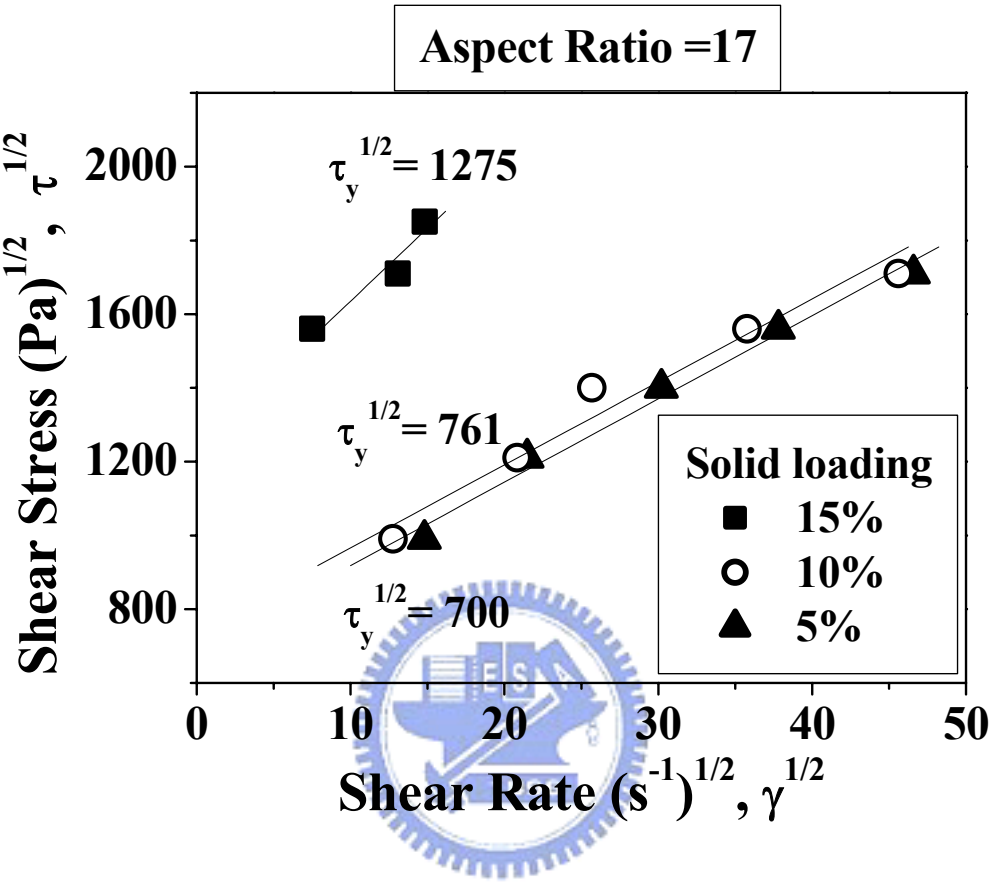

Figure 3-3. Casson's correlation for the mixtures with AR = 17, corresponding yield stress can be obtained by extrapolating the straight line at zero shear rate.

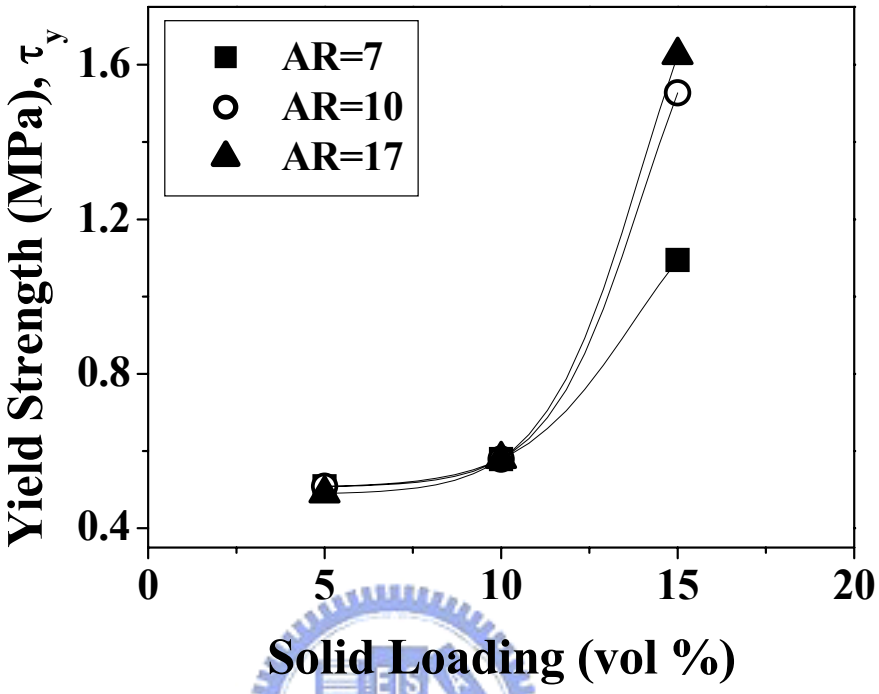

Figure 3-4. Yield stress of the CDHA-PMMA mixtures increases with solid concentration, and a considerable increase in the yield stress was observed for CDHA of higher aspect ratio.

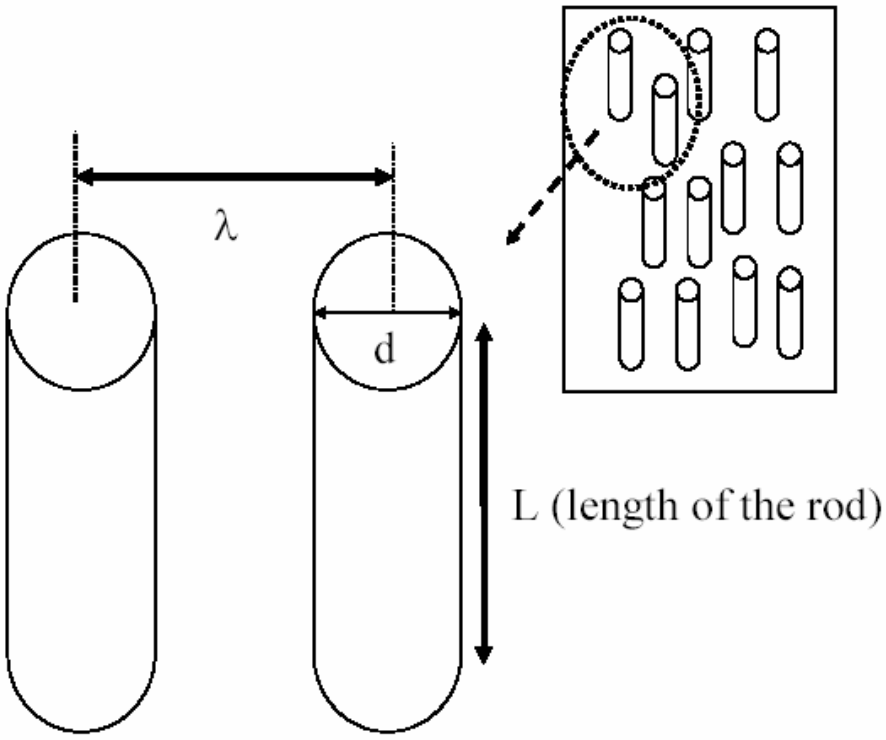

Figure 3-5. Dimensional configuration between two nano-needles with an interparticle distance of λ. Upper right is a schematic drawing of a given volume of the nano-needle mixture.

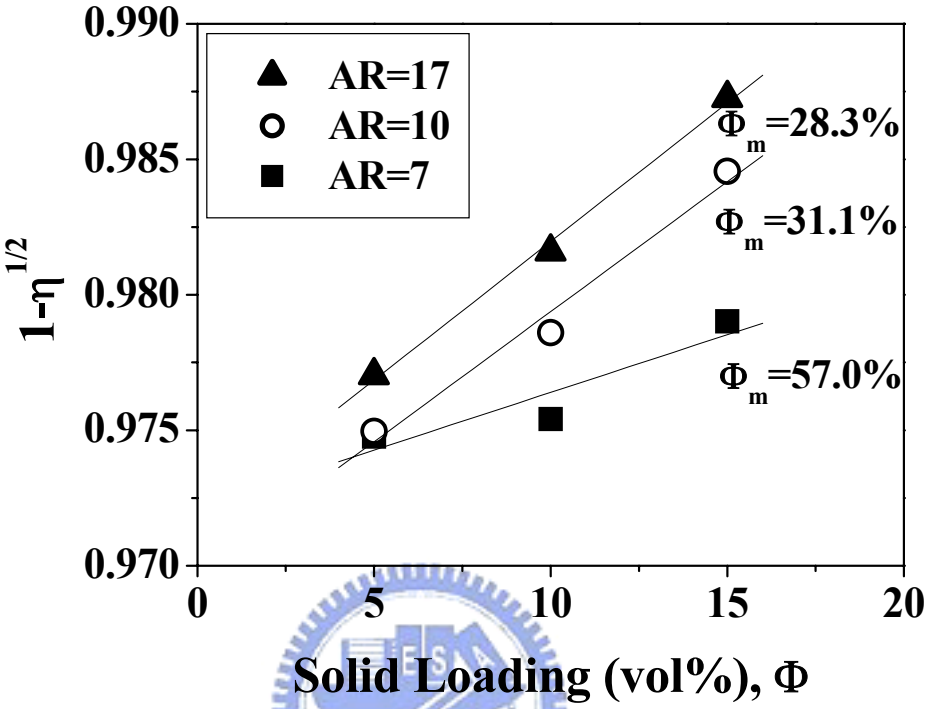

Figure 3-6. Maximum solid load (Φ_m) of the CDHA-PMMA mixtures under investigation can be determined via an extrapolation of the linear ($1-\eta^{-1/2}$) - ϕ correlation at $1-\eta^{-1/2} = 1$. A corresponding AR value of the mixtures is also indicated.

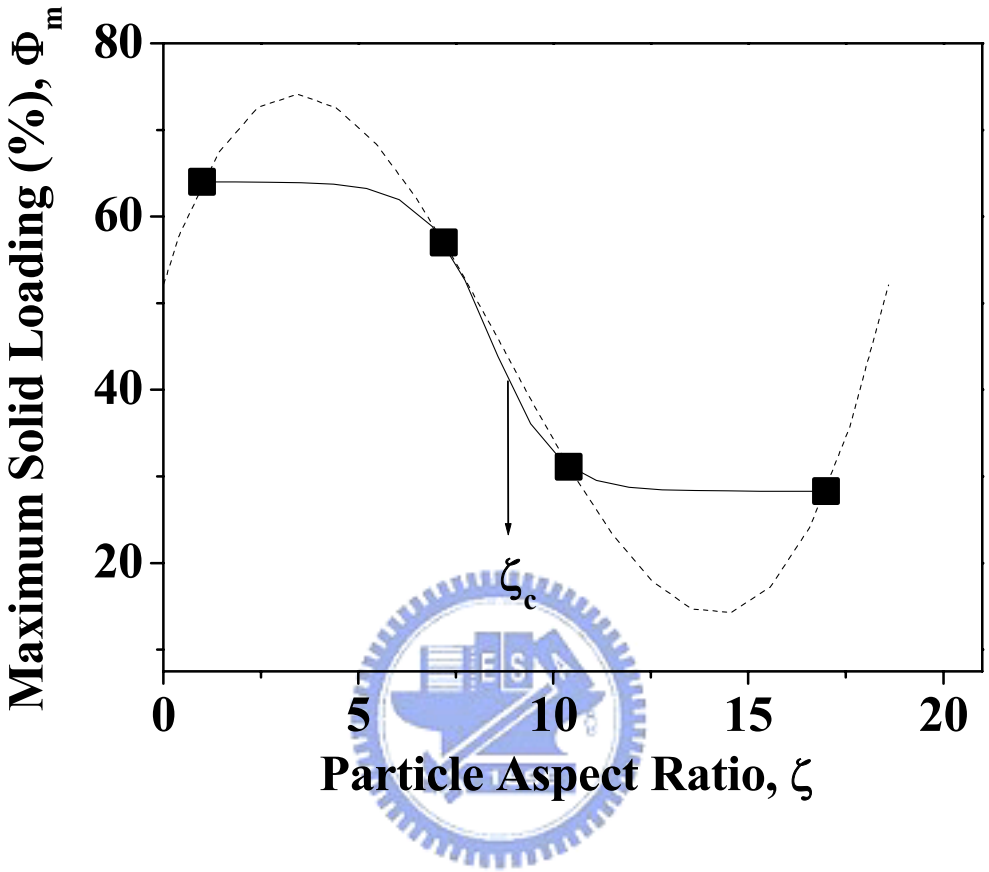

Figure 3-7. showing dependence of maximum solid concentration on the aspect ratio of the CDHA particles, where a sigmodal behavior was clearly observed. A simple 3rd-order polynomial Equation was employed for curving fitting (dash curve), which facilitates estimation of the deflection point, i.e., critical aspect ratio, ξ_c, in the sigmodal correlation.

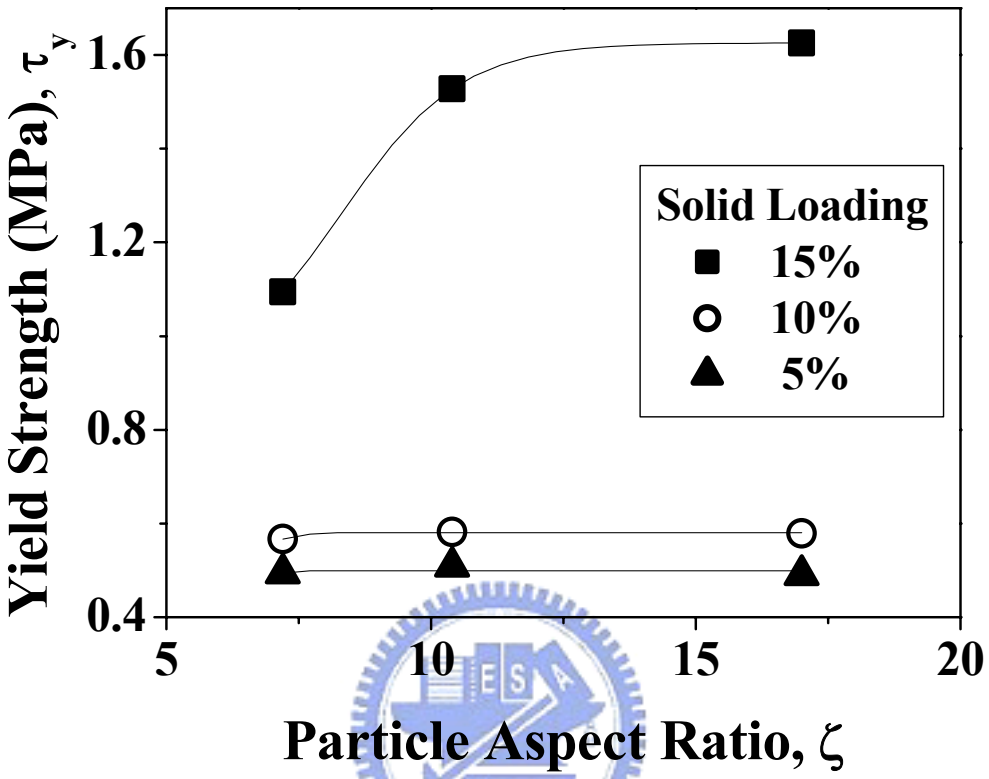

Figure 3-8. The variation of the yield strength of the CDHA-PMMA mixtures as a function of particle aspect ratio at different solid loads, where the influence of particle dimension becomes more pronounced only when solid load reaching 15%.

CHAPTER 4

BSA-loaded Calcium-deficient Hydroxyapatite Nano-carriers for Controlled Drug Delivery

4.1. Introduction

Hydroxyapaite (HA), having a chemical formula $Ca_{10}(PO_4)_6(OH)_2$, is a naturally occurring inorganic materials that has been a mineralized tissue of bones and teeth in humans and vertebrates. HA has been well-recognized as it is an excellent biocompatible and bioactive material for a number of clinical demands in the areas of orthopedics and dentistry for the past several decades. The use of HA as adsorbent for biomolecules has also attracted a great deal of attention over the years, because HA has long been recognized as having excellent affinity to biological substances, such as collagen, proteins, enzymes, cells, and viruses [91, 92].

Incorporation of active agents or drugs by physical absorption within porous HA-based implants has been frequently reported for orthopedic uses [93-95]. However, low efficiency of drug encapsulation due to limited surface area has remained an issue to be resolved. On the other hand, the inconsistency of therapeutical effect of different drugs may encounter when a multiple drug administration is operated, whereas sequential release and simultaneous release of multiple drugs are hardly properly controlled by the same carrier to, for instance, enhance osteogenesis and suppress antibiotic resistance, respectively [96-98]. These drawbacks seem to be easily overcome by the use of micro-carriers or nano-carriers delivering antibiotics and growth factors with controlled release kinetics regulated by different synthetic process. Ijntema et al. employed HA microcrystals as micro-carriers to load BSA of 5-10 wt% and concluded that it would be a step ahead if the apatitic crystals are able to carry higher amount of the active agents for a variety of biomedical purposes such as drug delivery, orthopedics

and dentistry [99]. Furthermore, it is particularly critical for those areas where a higher dosage of drugs with relatively small amount of the carrier is required.

Very recently, there has been growing interest in nano-crystals as carriers for bioactive agents. Ueno et al. employed nano-sized $CaCO_3$ as carrier for sustain release of betamethasone phosphate [100]. Matsumoto et al. investigated the influence of protein concentration and synthetic temperature on the protein release from HA nano-carrier [101]. However, studies on the release mechanism of protein-loaded nano-carriers through the manipulation of synthesis are rarely found in the literature but very important.

The apatite crystal often used to carry drugs or proteins has regularly a stoichiometric composition, i.e., Ca/P = 1.67, in the literature. However, mineralized apatite in humans and vertebrates is essentially non-stoichiometric, i.e., Ca/P < 1.67, or more specifically, a calcium-deficient hydroxyapatite, i.e., CDHA. Therefore, it is technically important to simulate the synthesis of CDHA nano-crystals in the presence of active agent. As the main concern of this communication, BSA was employed as a model protein to further understand the loading efficiency and release behavior of the BSA in CDHA nano-carriers. Therefore, the influences of synthetic solution pH and processing variation on the incorporation of BSA molecules with CDHA were systematically investigated. In addition, in order to gain better understanding on the interfacial structure between BSA and CDHA, nano-structure at BSA-CDHA interface was further explored by high resolution transmission electron microscopy (HR-TEM) and electron energy loss spectroscopy (EELS). The subsequent release behaviors of the resulting BSA-loaded CDHA nano-particles were explored and correlated with the synthesis scheme proposed in this investigation.

4.2. Experiment materials and methods

4.2.1. BSA-loaded CDHA synthesis

0.25M $Ca(CH_3COO)_2$ solution and 0.16M H_3PO_4 solution were used as precursors of Ca

and P to prepare CDHA nano-particles, respectively. The molar ratios of Ca to P were fixed at 1.5 and bovine serum albumin (BSA, Aldrich, A-7638) was selected as candidate protein in this study. A BSA aqueous solution of 1500 μg/ml was prepared by dissolving BSA powder into distilled water for each synthesis process. For in-situ synthetic process A, BSA solution was dropped into H_3PO_4 solution maintained at pH7.5, pH8.5 and pH9.5 by the addition of NaOH solution (1 M) and the samples were named as A-7.5, A-8.5 and A-9.5, respectively (see Table 4-1). Subsequently, $Ca(CH_3COO)_2$ solution was dropwisely added into the above solution to form suspensions. On the other hand, in order to understand the importance of synthesis sequence on the BSA-loaded CDHA nano-particles, BSA solution was first mixed with $Ca(CH_3COO)_2$ solution instead of H_3PO_4. After that, H_3PO_4 was added into the solution to form suspensions. The samples were named as B-7.5, B-8.5 and B-9.5. For comparison, ex-situ synthetic process was also prepared. CDHA powder was first prepared at pH 7.5 and dispersed in DI water. The obtained suspension was then mixed with the BSA solution in the range of pH from 7.5 to 9.5, namely as sample C-7.5, C-8.5 and C-9.5. For all the synthetic processes, the suspensions were filtered off and the resulting precipitates were then washed with phosphate-buffered solution (PBS buffered with HCl at pH6.8) and DI water for 3 times for further characterization.

4.2.2. Characterization

The relative amount of the BSA associated with the CDHA nano-particles was determined using thermogravimetric analysis, TGA (Perkin Elmer), with a heating rate of 10^oC/min. Crystallographic phase of the BSA-loaded CDHA powders was identified by X-ray diffractometer (M18XHF, Mac Science, Tokyo, Japan), at a scanning rate of 4^o 2θ per min over a range of 2θ from 20^o to 60^o. Fourier transform Infrared (FT-IR) spectra were recorded on a spectrometer (Model 580, Perkin–Elmer) using a compressed pellet of about 1 mm thick prepared by a mixture of 100mg of KBr and 1mg of the BSA powders. The FT-IR spectra

were taken with a resolution of 4.00 cm^{-1} in the range of 4000-400 cm^{-1} and were averaged from 128 scans. Microstructure observations were performed using a Philips Tecnai 20 (Holland, The Netherlands) transmission electron microscope operated at 200 keV and equipped with a Gatan image filter (GIF, Model GIF-2000) for EELS analysis. EELS spectra were obtained with an energy resolution of 1 eV (zero-loss peak) and an energy dispersion of 0.2 eV per channel.

4.2.3. Release test

Bovine serum albumin-loaded CDHA nano-particles (0.15g) were dispersed in 10ml buffer solution buffered with NaOH and $C_6H_8O_7$ at pH 6 with a stirring rate of 100 rpm at 37^oC. The BSA release test was carried out by taking 0.1 ml of the buffer solution and 2ml of bicinchoninic acid solution (Sigma, bicinchoninic acid protein assay kit, BCA-1 and B9643) for each juncture. UV-visible spectroscopy (Agelent 8453) was used for the characterization of absorbance peaks at 562 nm to determine the BSA concentration through the use of a pre-determined standard concentration–intensity calibration curve.

4.3. Results and discussion

4.3.1. Material characterization

Figure 4-1 shows the FT-IR spectra of the BSA-loaded nano-particles. The IR spectra of pure BSA and CDHA are also shown for comparison. The spectrum of BSA exhibited an apparent absorption band at 1654 cm^{-1} assigned to amide I, C=O stretching mode, 1540 cm^{-1} assigned to amide II, N-H bending mode and 1384 cm^{-1} assigned to amide III, C-N stretching mode and N-H bending mode. The spectrum of the pure CDHA presents the characteristic absorption band at 1640 cm^{-1} assigned to molecular water, 1092 and 1040 cm^{-1} assigned to P-O stretching mode, and 602 cm^{-1} and 563 cm^{-1} assigned to O-P-O bending mode. For in-situ process (A, B), the band at 1652 cm^{-1} was likely due to the overlap of 1654 cm^{-1} and 1640

cm^{-1}, suggesting that all the CDHA powders are associated with BSA. These broad, featureless ν_3 PO_4^{3-} bands at 1092-1040 cm^{-1} in both samples of A-9.5 and B-9.5 also suggest that the resulting crystals exhibit poorly-crystalline structure. It was noted that for all synthetic conditions, no significant red shift of carboxylate band (1338 cm^{-1}) was detected in the final CDHA-BSA composite powders, indicating no chemical bonding between surface Ca^{2+} of the CDHA and COO^-(BSA) was observed in the BSA-loaded CDHA powder [102].

Three possible mechanisms can be adapted to explain the interaction between the CDHA and BSA molecules. The first mechanism can be of Ca-bridging: This charge-transfer bonding was reported by Ellingsen [103], considering that acid proteins bind to the P-sites of the HA particles through O^--Ca^{2+}-COO^- (Ca-bridging). The P-site is a negatively-charged site formed by six oxygen atoms of phosphate of the ***ab*** crystal plane of the HA [104]. Similar behavior can be applied to the CDHA nano-crystals currently synthesized. The second one can be operated through the electrostatic interaction between the positive Ca^{2+} and COO^-(BSA): This has been also reported by Liou [105] who suggested that there is an intermediate complex between COO^- and CDHA. This complex can be formed via the electrostatic interaction between the negative COO^- on BSA molecule and positive Ca^{2+} on the C-sites of CDHA surface. Kandori [104] indicated that the C-sites were located on the crystal planes that are perpendicular to ***a***-axis and ***b***-axis of apatite crystal. These C-sites were developed as a result of the calcium ions on the CDHA surface, thus making positive charges to attract COO^- groups of BSA molecules. The third one is based on the formation of acetate salt which is an intermediate product between calcium ions and COO^-(BSA) after synthesis, or more specifically, a BSA-bonding Ca ion. However, both Ca-bridging and BSA-bonding Ca ions can not further react with $(PO_4)^{3-}$ and/or $(HPO_4)^{2-}$ to form CDHA nano-crystals in the solution. Therefore, once it (Ca-bridging and/or BSA-bonding Ca ions) occurred, a lower production yield of CDHA formation than those pre-designed (theoretical) can be observed. This is further evidenced in Figure 4-2, where about 15% of the Ca ions were associated with the

BSA, thus a CDHA production yield ratio (i.e., the ratio of real to theoretical production yield) of 85% was attained at the $Ca(CH_3COO)_2$ concentration of 0.25 M (i.e., The corresponding ratio of Ca^{2+} to amino acid residue was calculated as 3.16 and shown in the second Y-axis of Figure 4-2). As the concentration of $Ca(CH_3COO)_2$ was further decreased (i.e., the corresponding ratio of Ca^{2+} to amino acid residue was decreased), a decreased CDHA yield ratio was observed. This suggests that an interaction takes place between the BSA molecules and Ca ions via Ca-bridging or BSA-bonding Ca ions. However, as mentioned before, no red shift of carboxylate band at 1338 cm^{-1} was observed for all BSA-loaded CDHA samples. Therefore, it is inferred that Ca-bridging plays an important role between BSA molecules and CDHA crystals.

Figure 4-3 shows the X-ray diffraction (XRD) patterns of the BSA-loaded CDHA nano-powders. Two major characteristic diffraction peaks could be obtained for all the powdered samples: one closed at 2θ of ~ 26^o and the other broad one at ~32^o. According to ICDD No. 46-0905, it can be indexed as a poorly crystalline calcium-deficient apatite structure. No considerable difference in those characteristic diffraction peaks was discerned for both synthetic sequences outlined above. This may suggest that the presence of the BSA during the synthesis of the CDHA does not give pronounced influence on the structural development of the CDHA nano-crystals.

4.3.2. BSA incorporation with CDHA

Figure 4-4a shows the HR-TEM nanostructure of sample B-9.5 (in-situ process) and corresponding color-enhanced image is illustrated in Figure 4-4b. As it can be seen, the nanostructure of the BSA-CDHA hybrid may be divided into 4 regions as indicated with different colors. In the region A, the lattice fringes with parallel to (100) CDHA were clearly observed in the long needle-like crystallites, indicating a well-crystallized region. The region B, i.e., the layer nearest to the highly crystalline inner layer, is formed with a lattice

development strongly affected by the nearest region of highly-order structure. The region B is a result of "growth inhibition". In other words, much poor crystallization was observed [106]. As the crystal continuously grows, the effect of BSA molecule, becomes stronger in distributing the deposition of Ca-P materials, and in a certain case, conjugate as a complex and integrate into "outer area of the lattice" (the so-called BSA-CDHA complex), resulting in an amorphous region C. However, from its nanostructure, the crystallization is prohibited, and this may be caused by, possibly, a regulation of lattice mismatch resulting in somewhat "gradient crystallinity". The outer region D can be considered as a transition region from BSA-CDHA complex to absorption BSA. An adsorbed BSA layer is essentially tangled with the underlying CDHA-BSA complex (region C).

It was also found that both nano-sized CDHA crystal and BSA-loaded CDHA samples prepared via the ex-situ process were more susceptible to electronic beam bombardment than that prepared via in-situ process, thus causing radiolysis under HR-TEM analysis [107]. This probably reveals that different extent of interaction exists between CDHA and BSA for in-situ and ex-situ processes, which could be further explored via derivative thermogravimetry (DTG) analysis as shown in Figure 4-5. For in-situ processes of A-9.5 and B-9.5, a broad band at 400^{o}C were detected, which is probably attributed to the thermal decomposition of the BSA-CDHA complex. Due to the incorporation of BSA molecules into regions C and D through electrostatic force (C sites) and/or Ca-bridging (P-sites), a higher thermal decomposition temperature was observed for BSA-CDHA complex compared to that of pristine BSA (350^{o}C). For the sample prepared in a lower pH value (A-7.5 and B-7.5), this band at 400^{o}C was not only detected but also the other strong band at 350^{o}C was detected. The latter band can be primarily attributed to the thermal decomposition of adsorbed BSA molecules. The adsorption of BSA onto CDHA nano-crystals can be considered as a type of pseudo-Langmuir adsorption [104]. In other words, a number of the BSA layers are adsorbed on CDHA surface which are not tightly bound with CDHA crystals. Therefore, thermal

decomposition temperature of adsorbed BSA molecule is close to that of pristine BSA. However, the band at 350 °C was not detected for both samples of A-9.5 and B-9.5, which is probably due to the fact that the outer-layered BSA molecules are easily eluted in the solution with a higher pH value upon synthesis [91]. In contrast, for the samples prepared via ex-situ processes, only a band at 350°C was observed. This reflects that no strong interaction exists in the interface of the BSA molecules and CDHA crystals for the samples prepared via ex-situ process.

The TEM images in Figures 4-6(a) and (c) show that the BSA-loaded CDHA nano-crystals synthesized in different conditions present needle-like morphology with dimensions of 4-12 nm in diameter and 40-70 nm in length. The particle size was measured from the TEM images and each datum was averaged from at least 10 TEM photographs. Furthermore, it was observed that crystal morphology was changed with an increase of solution pH for the in-situ processes (A and B). The dependence of the solution pH value on the aspect ratio of CDHA nano-crystals is further illustrated in Figure 4-7(a). It is interesting to note that the resulting BSA-loaded CDHA nano-crystals derived from the higher pH solution (A-9.5 and B-9.5) showed a smaller aspect ratio compared to that synthesized at a lower pH solution (A-7.5 and B-7.5). Such a preferential growth in the solution at a lower pH can be correlated with preferential adsorption. It means that more BSA should be adsorbed onto the C-sites of the CDHA nano-crystals at a lower pH value, which causes considerable preferential inhibition effect on the growth of nano-crystals along the ***ab*** axis, resulting in a high aspect ratio [108]. In contrast, at a higher solution pH, O^{-}-Ca^{2+}-COO^{-} (Ca-bridging) is prominent due to the stability of $(PO_4)_3^{-}$. Therefore, crystal growth of in both C-sites and P-sites are inhibited, resulting in a lower aspect ratio. Moreover, it is known that the conformation of protein could be more linear (un-folding) in the solution with strong base and ionic strength [109]. The resulting unfolding BSA molecules and/or amino acid residues strongly attracted Ca^{2+} through the formation of Ca-bridging [110], which kinetically lead to

the inhibition growth on the P-sites of CDHA crystals at the earlier crystallization stage. Therefore, the aspect ratio for nano-carriers prepared via the in-situ process at higher pH is reduced.

The corresponding amount of the BSA uptake by the CDHA particles (after calibration by subtracting water content) determined from the TGA is shown in Figure 4-7(b). Obviously, a lower pH resulted in a higher BSA incorporation, and as high as 17.5 wt% of the BSA associated with the CDHA was detected, which is about 75% higher than that reported in the literature [99]. In contrast, since the isoelectric point (IEP) of CDHA and BSA is around 7 and 4.7, respectively [111, 112]. It is then expected that the electrostatic repulsive force between the BSA and CDHA nano-crystal becomes dominant for a solution with a higher pH (9.5) compared to that with a lower pH (7.5). Therefore, an increase in solution pH resulted in a decreased amount of BSA.

Considerable differences in the amount of the BSA uptake associated with the CDHA at pH 9.5 can be seen from Figure 7(b), where the CDHA carries a higher amount of the BSA from the ex-situ process (C-9.5) than that from the in-situ processes (A-9.5 and B-9.5). This may be explained by the aspect ratio of the CDHA carries, as illustrated in Figure 7(a) which showed the aspect ratio of the nano-carriers prepared via the ex-situ process (C-9.5) was higher than that prepared via the in-situ process (A-9.5, B-9.5). The CDHA nano-particles with a higher aspect ratio indicates a higher population of the positively-charged C-sites for BSA adsorption and therefore, the total effective areas of adsorption sites (C-site) are much larger for the high aspect-ratio nano-particles compared to that of low aspect-ratio nano-particles per unit weight. If the above argument is correct, then, it is conceivable to realize that the ex-situ CDHA carries higher amount of the BSA than those in-situ CDHA at pH 9.5. However, at pH 7.5, the preferential growth along ***c***-axis for carriers prepared via in-situ process (A-7.5, B-7.5) resulted in a larger aspect ratio compared to that prepared via ex-situ process (C-7.5). Consequently, in contrast to that at pH 9.5, a higher amount of BSA

(about 10 wt%) was detected in the in-situ CDHA than the ex-situ CDHA at pH 7.5.

4.3.3. Controlled BSA release

The BSA release profiles of the BSA-loaded CDHA nano-crystals are shown in Figure 4-8. It was found that samples prepared from ex-situ processes (C-7.5 and C-9.5) showed a pronounced bursting behavior for the initial time period of 8 hours during which BSA were nearly entirely released. The bursting release of BSA can be assigned to the desorption of BSA molecules which are not tightly bound with CDHA surface. In contrast, although the BSA-loaded CDHA nano-crystals prepared from the in-situ processes (A-7.5, B-7.5) showed bursting release behaviors in the initial time period, a slow release was then followed, suggesting a two-stage release mechanism. The BSA release behavior in the initial stage is similar to that of the samples prepared ex-situ process. This busting release could be assigned to the desorption of BSA molecules which were not strongly interacted with CDHA crystals. The release profile in the second stage may be attributed to the BSA molecules which have been incorporated into CDHA crystals (BSA-CDHA complex). This slow release may result from the dissolution of CDHA crystal, which will be further discussed later. However, as the BSA-loaded CDHA nano-crystal was prepared from in-situ process with a higher solution pH value (A-9.5 and B-9.5), only a single-stage slow release profile was detected, which may be also attributed to the release of incorporated BSA from BSA-CDHA complex.

Moreover, as shown in Figure 4-6, it was found that a considerable reduction in the dimension of ***c***-axis was observed after release test for particularly the CDHA nano-crystals prepared via in-situ process. This observed size reduction may suggest that the dissolution of the CDHA nano-crystals is highly anisotropic with respect to the crystal plane of the CDHA particles. This result is further supported by HR-TEM shown in Figure 4-4(b), where P-sites were rich in amorphous region C causing higher ***c***-axis dissolution rate compared to both ***a*** and ***b*** axes. If the above argument is correct, it is conceivable to realize that crystal dissolution

in ***c***-axis is responsible for the slow release of incorporated BSA from BSA-CDHA complex [106]. Moreover, in order to explore the difference in the release profiles between samples A-9.5 and B-9.5, electron energy loss spectroscopy (EELS) was employed to explain subtle variation in the local structure of nano-scale regions. As shown in Figure 4-9, the excitation counts of Ca $L_{2,3}$-edges with energy-loss ranging from 340 to 360 eV were smaller for A-9.5 than those for B-9.5. According to the Fermi golden rule of quantum mechanics [113], a structural disorder presents a lower excitation count peak in electron-energy loss near-edge structure (ELNES). This may suggest that the crystallinity of A-9.5 is poorer than that of B-9.5, which subsequently results in the higher release (also dissolution) rate of sample A-9.5.

It can then be concluded that the release profile was first dominated by BSA desorption, followed by a slow release controlled by crystal dissolution. Although the nature of the interaction between BSA and CDAH is not fully understood at present, this study suggests that the resulting release profile permits a design of the CDHA nano-crystal as nano-carrier for drug release.

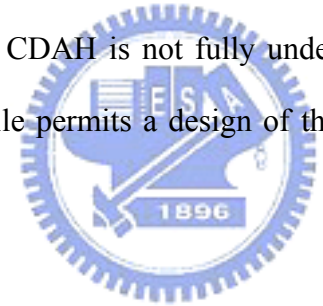

4.4. Conclusion

In summary, the amount of BSA uptake was dependent on the solution pH and processing variation, i.e., in-situ and ex-situ synthetic schemes. Moreover, both synthetic process and pH value upon synthesis significantly altered the drug release behaviors of BSA-loaded CDHA nano-crriers. It is feasible to employ the CDHA nano-carrier to load protein, such as acid growth factor and acid protein-drug conjugation, as component of bone substitutes or as a reinforced filler together with a pre-designed drug release function for particular therapeutic effect.

Table 4-1. Synthetic conditions of the BSA-CDHA nano-carriers.

Process	Adding sequence	pH range	Sample name
In-situ process A	H_3PO_4→BSA→$Ca(CH_3COO)_2$	7.5	A-7.5
		8.5	A-8.5
		9.5	A-9.5
In-situ process B	$Ca(CH_3COO)_2$→BSA→H_3PO_4	7.5	B-7.5
		8.5	B-8.5
		9.5	B-9.5
Ex-situ process C	CDHA→BSA	7.5	C-7.5
		8.5	C-8.5
		9.5	C-9.5

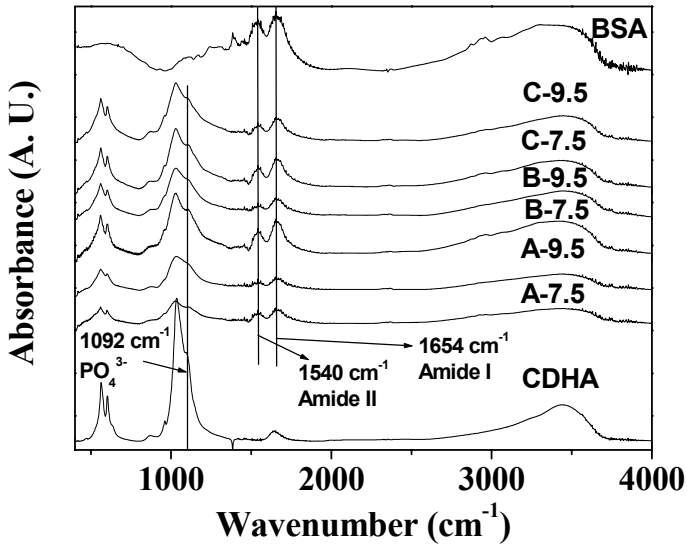

Figure 4-1. FT-IR spectra of the nano-carriers synthesized in different conditions.

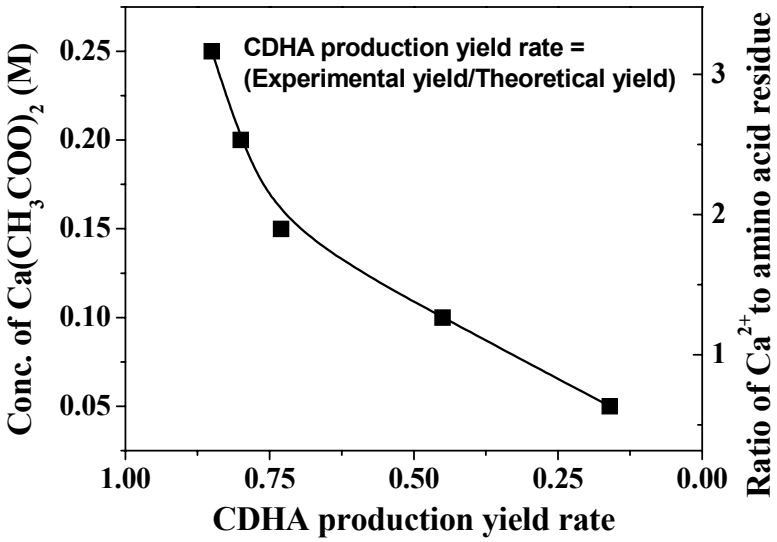

Figure 4-2. Dependence of $Ca(CH_3COO)_2$ concentrations on the CDHA production yield rate. The corresponding ratio of Ca^{2+} to amino acid residue was calculated and shown in the second Y-axis.

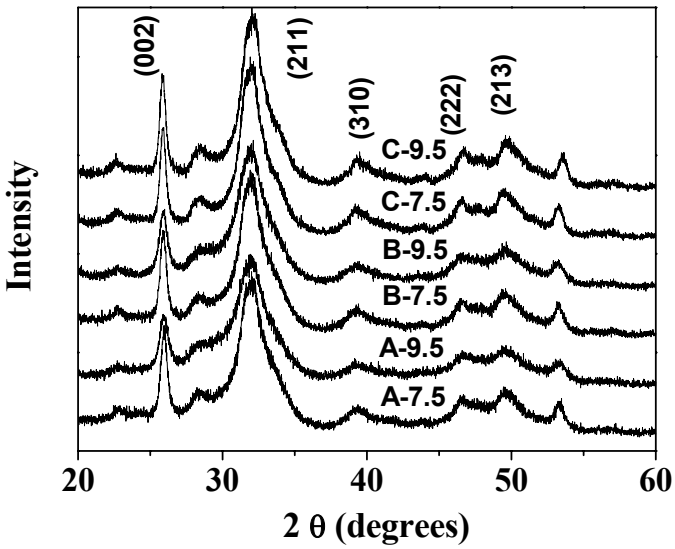

Figure 4-3. XRD patterns of the BSA-loaded CDHA nano-carriers synthesized in different condition.

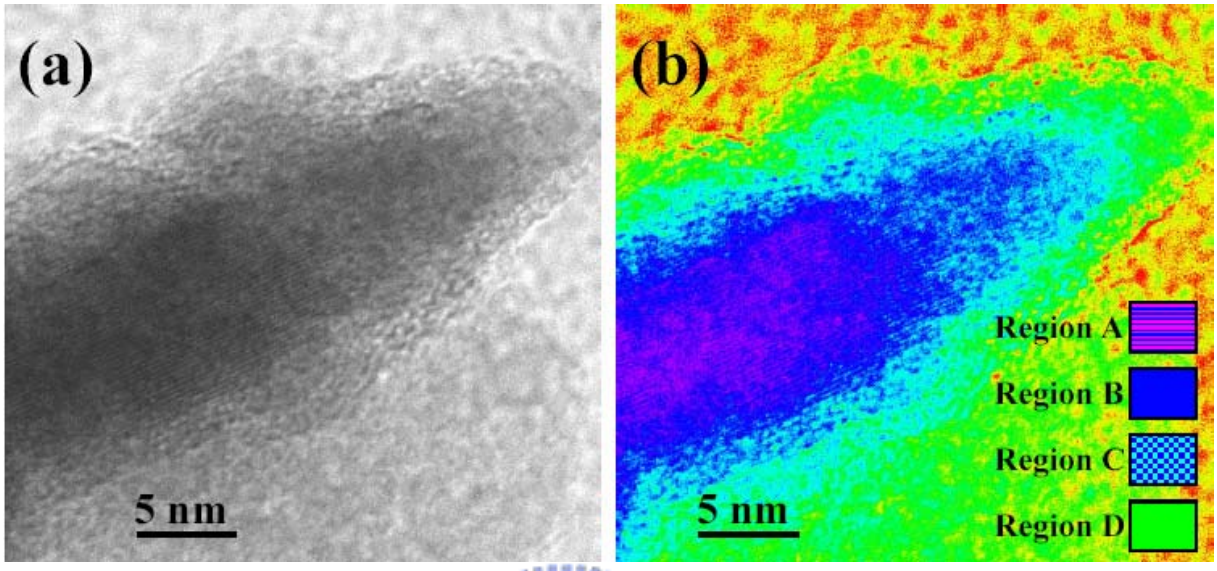

Figure 4-4. (a) HR-TEM photograph of the BSA-loaded CDHA nano-carriers prepared through in-situ processes at pH=9.5, (b) Corresponding color-enhanced image of (a).

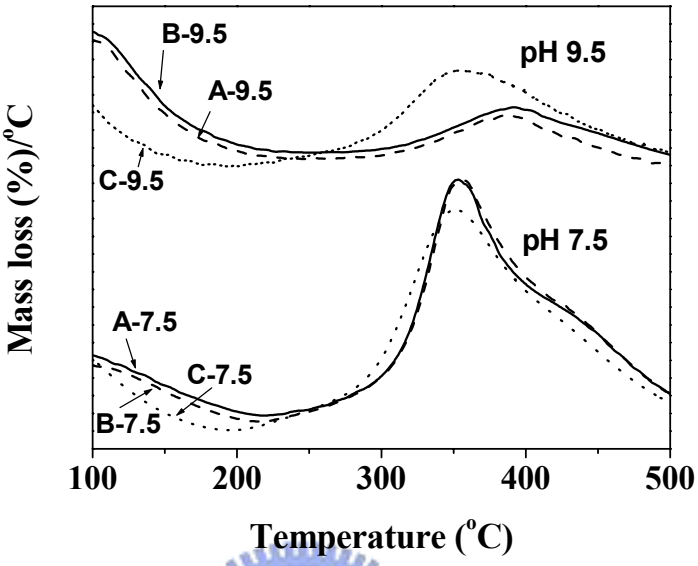

Figure 4-5. DTG curves of the BSA-loaded CDHA nano-carriers synthesized in different conditions.

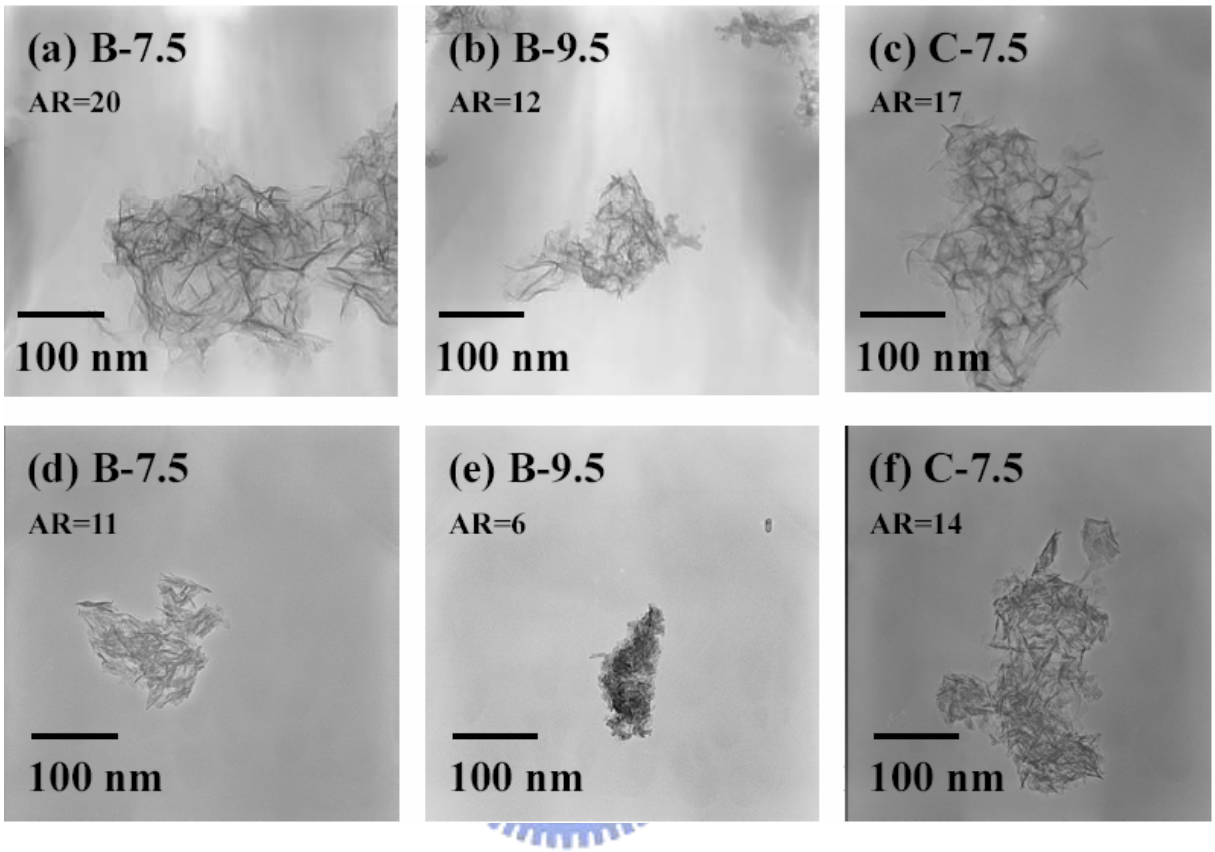

Figure 4-6. TEM micrographs of the BSA-loaded CDHA nano-carriers prepared through different processes, (a)-(c) showing the effect of processing variation on morphology and size of CDHA nano-crystals before release test, (d)-(f) showing a further reduction in both aspect ratio and size of the CDHA nano-crystals after release test compared to that before the test. The aspect ratios were measured from the TEM images and each datum was averaged from at least 10 TEM photographs.

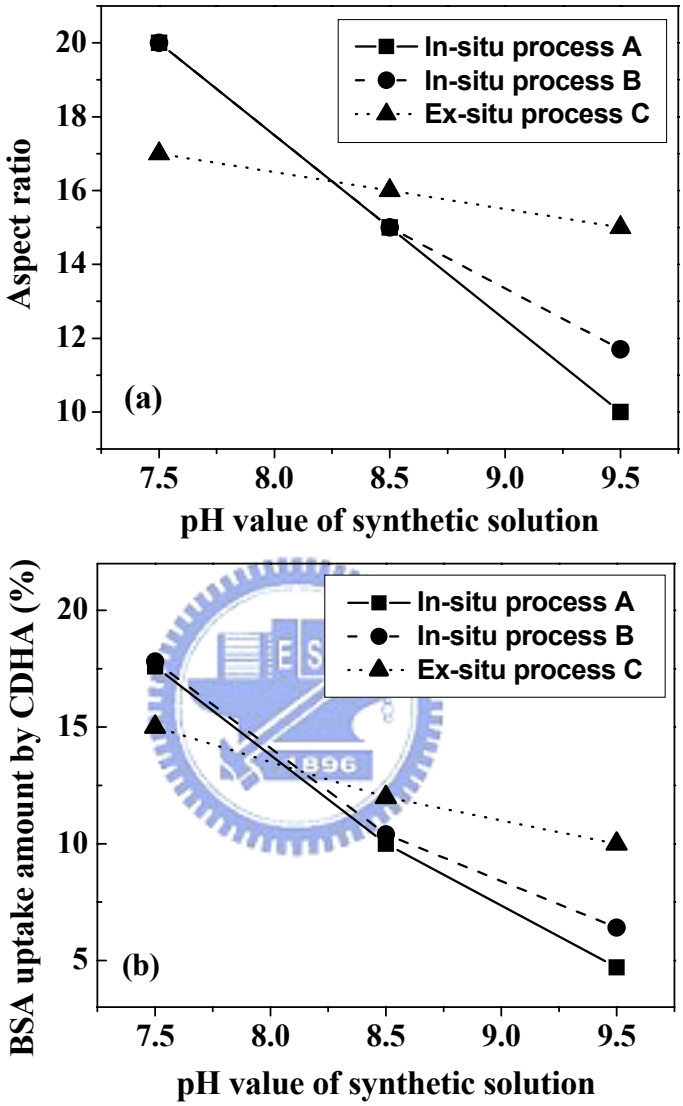

Figure 4-7. Dependence of the pH value of synthetic solution on the (a) aspect ratio of CDHA crystal, (b) amount of BSA uptake by CDHA nano-crystal.

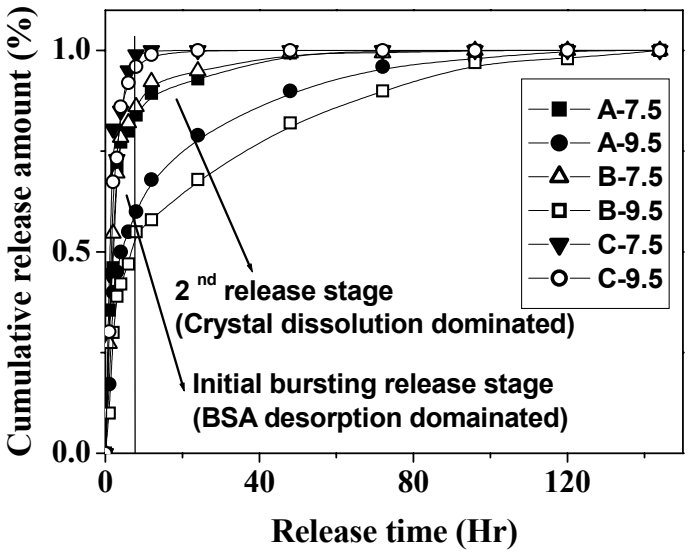

Figure 4-8. BSA release profiles of the BSA-loaded CDHA nano-carriers synthesized in different conditions.

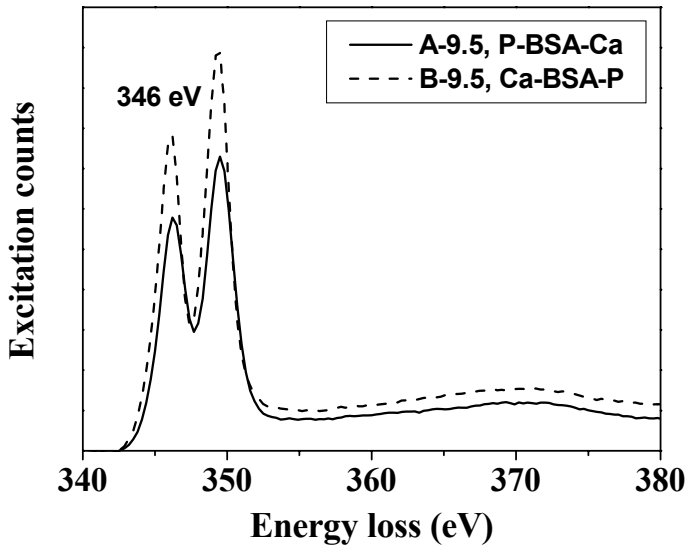

Figure 4-9. ELNES spectra near the Ca $L_{2,3}$-edge of BSA-loaded CDHA nano-carriers prepared through in-situ processes at pH=9.5.

CHAPTER 5

Drug Release Behaviour of CDHA/Chitosan Nanocomposites-Effect of CDHA Nanoparticles

5.1. Introduction

Chitosan (CS) has been widely used as a scaffolding material in tissue engineering [58], orthopedic implants [114] and drug delivery vehicles [115] for many years because of its low price and outstanding characters, such as osteoconductivity, biodegradability, and biocompatibility. Nevertheless, chitosan lacks sufficient mechanical strength, which restricts its uses for load-bearing applications, especially in orthopedics. Many studies have attempted to improve its mechanical strength by incorporating calcium phosphate bioactive ceramic such as hydroxyapatite (HA, $Ca_{10}(PO_4)_6(OH)_2$) and β-tricalcium phosphate (β-TCP, $Ca_3(PO_4)_2$) [116, 117]. However, natural bone mineral has essentially a calcium-deficient apatitic structure (Ca-deficient hydroxyapatite, CDHA) with a Ca/P ratio of about 1.5, which is compositionally similar to tricalcium phosphates (Ca/P = 1.5) and structurally similar to stoichiometric hydroxyapatite (Ca/P = 1.67). Therefore, CDHA is considered to be a candidate material with respect to both mechanical reinforcement and biological activity for orthopedic application.

The key to success in using macroporous implantable devices for osteogenesis is not only the suitable matrix with sufficient bioactivity and mechanical strength for osteogenic progenitor cells, but also the sustained release of antibiotics and growth factors to eliminate infection and insure osteoblast differentiation, respectively [115, 118]. Up to now, many studies have been done for the influence of hydroxyapatite nanoparticles on the mechanical properties of CS/HAp nanocomposites for orthopedic use [57, 119]. However, the role of

CDHA nano-crystals in drug release behaviour of chitosan-based composite has rarely been found in the literature. In order to enhance the therapeutic efficiency of a bioactive agent via manipulating its release profiles, it is necessary to explore the effect of CDHA nano-crystals on the drug release mechanism of the CS-based polymeric matrix.

Generally, drug release kinetics of polymeric drug delivery system is usually characterized by membrane permeability (P) and diffusion exponent (n), which are employed to describe the release behaviours of reservoir (membrane) systems and the diffusion mechanism for monolithic (matrix) systems, respectively [61]. Furthermore, both indexes in polymer-based materials are strongly dependent on crystallinity, plasticization, glass transition temperature (T_g) and swelling of the polymer vehicle, which are also affected by the presence of nanofillers [120-122]. Most researchers found an increase in T_g as a function of nanofiller content [123, 124]. On the contrary, a decrease in T_g with increase in nanofiller was also reported [122, 125]. Furthermore, the influence of filler on resulting crystallinity of the polymeric phase has not been consistently reported. Some reported that the nanofiller acted as a nucleation agent to enhance the crystallinity of semi-crystalline polymer [121]. However, some suggested that the nanofiller could retard the evolution of crystalline structure within the polymeric domains of the composite [126]. These arguments arise due to various extents of polymer-filler interaction in different composite systems [126, 127]. In order to classify the role of polymer-filler interaction in the drug release behaviours of CDHA/CS nanocomposites, the in-situ preparation process was employed and expected to enhance polymer-filler interaction to alter the diffusion mechanism of CDHA/chitosan composite [128].

In this work, with the aim of studying the role of polymer-filler interaction in the drug release behaviours of CDHA/CS nanocomposites, in-situ incorporation of CDHA nanoparticles, i.e. CDHA synthesized in the presence of chitosan, was employed. For comparison, ex-situ synthetic process was also used. In other words, CDHA nanofiller was

synthesized first and then added into the chitosan solution. Membrane permeability and diffusion exponent of CDHA/CS nanocomposites with various CDHA contents were systematically investigated to explore the influence of CDHA nanofillers on the drug release behaviour and the corresponding release mechanism.

5.2. Experiment materials and methods

5.2.1. CDHA/CS nanocomposite membrane preparation

In this study, the CDHA/CS nanocomposite membranes with various CDHA contents were prepared via in-situ and ex-situ processes to characterize the influence of nanofiller and polymer-filler interaction on drug delivery behaviour. CS with 215 kD molecular weight and 80% degree of deacetylation was supplied by Aldrich-Sigma. CS solution of 1% (w/v) was first prepared by dissolving CS powder in 10% (v/v) acetic acid solution. For ex-situ processes, CDHA nanoparticles were first synthesized by mixing $Ca(CH_3COO)_2$ aqueous solution with H_3PO_4 aqueous solution. The pH value was kept at 7.5 by the addition of NaOH solution (1M). The un-reacted precursors in the resulting CDHA suspension were removed by repeated precipitation and distilled-water (DI water) washing for three times. The resulting CDHA/DI water suspension was added into the CS solution to form CDHA/CS suspension. For the in-situ process, H_3PO_4 aqueous solution (0.16M) was first added into the CS solution, and $Ca(CH_3COO)_2$ aqueous solution (0.25M) was then added into this mixture solution. The pH value was also kept at 7.5 by adding NaOH solution (1M). The composite membranes with the volume ratios of CDHA/CS controlled at 95/5, 90/10, 70/30 and 50/50 for both in-situ and ex-situ processes (see Table 5-1). Subsequently, these CDHA/CS suspensions were poured into Petri dish to form CDHA/CS membranes after drying at room temperature for 7 days.

5.2.2. Material characterization

The volume ratio of CDHA/CS was confirmed by thermogravitational analysis (TGA, Perkin Elmer). The crystallographic phase of CDHA/CS composites were identified by X-ray diffractometer (XRD, M18XHF, Mac Science, Tokyo, Japan). The morphology of both composite membranes and CDHA nano-crystals was observed by using scanning electron microscopy (SEM, Hitachi S4000) and transmission electron microscopy (TEM, JEOL-2000FX). Dynamic mechanical analysis (DMA) was performed using a TA Instruments 2980 dynamic mechanical analyzer from -130^{o}C to 210^{o}C with a frequency of 1 Hz and a heating rate of 2 ^{o}C/min.

5.2.3. Determination of diffusion exponent for drug-loaded matrix system

Vitamin B_{12} (Sigma, V-2876) is a water-soluble agent with low molecular weight (1355Da), small molecular size and negligible interaction with CDHA, thus is a suitable model drug for our system. It should be incorporated into the CDHA/CS matrices in advance for diffusion exponent determination. The preparations of drug-loaded matrix membranes were similar to the above-mentioned process (Section 5.2.1). Before membrane drying, vitamin B_{12} was added into those CDHA/CS suspensions. The subsequent drying process was also the same as the above-mentioned process (Section 5.2.1). These composite membranes were put into phosphate-buffered solution (PBS, pH 7.4) for release test. The release medium was withdrawn for each juncture and replaced with equivalent volume of fresh buffer. UV-visible spectroscopy (Agelent 8453) was used for the characterization of absorption peak at 361 nm to determine the amount of vitamin B_{12} released via the use of pre-determined standard concentration-intensity calibration curve. The diffusion exponent (n) of non-porous material can be determined by plotting Log(M_t/ M_∞)-Log(t) curve and the use of Eqn. 5-(1):

$$(M_t/M_\infty) = kt^n \qquad 5\text{-}(1)$$

where M_t is the amount of drug released at time t, M_∞ is the amount of drug released at equilibrium state, k is a constant and n is the diffusion exponent related to the diffusion

mechanism.

5.2.4. Determination of permeability of membrane system

The permeation tests were performed by the use of side-by-side diffusion cell. Vitamin B_{12} aqueous solution (90 ml) of 0.02% (m/v) was added into the donor cell as the model drug. The same volume of PBS was added into the receptor cell. Drug-free composite membrane was fixed between the two half-cells. The amount of vitamin B_{12} permeated was determined using UV-Visible spectroscopy for each juncture. Membrane permeability of polymeric film can be determined using Eqn. 5-(2) [129]:

$$\text{Ln}\ (1-C_t/C_0)= -(2ADH/V)= -(2AP/V) \qquad 5\text{-}(2)$$

where C_t is the solution concentration in the receptor cell at time t, C_0 is the initial solute concentration of the donor cell, V is the volume of each half-cell, A is the effective area of permeation, D is the diffusion coefficient, H is the partition coefficient, and P is the membrane permeability (P = D*H). The slope of the plot of $-((V/2A)\ \text{Ln}\ (1-C_t/C_0))$ versus t is membrane permeability. The apparent partition coefficient (H) of vitamin B_{12} for nanocomposite/aqueous medium was determined as follows [130]. Drug-free CDHA/CS nanocomposite (10 mg) was immersed in the release medium until equilibrium state. The wet weight (W) was recorded. The nanocomposite was then immersed in 10 mg of vitamin B_{12}-containing medium. Partition coefficient (H) was determined from the initial (C_0) and equilibrium (C_e) concentrations of vitamin B_{12}-containing mediums by Eqn. 5-(3):

$$H=10(C_0-C_e)/WC_e. \qquad 5\text{-}(3)$$

5.3. Results and discussion

5.3.1 Material characterization

Figure 5-1 shows the cross-sectional area (fracture surface) of those composite

membranes. For the in-situ process (Figures 5-1(a), 1(b) and 1(c)), it can be found that most of the membranes were non-porous with dimple-like fractured surface except for the sample In-situ 50 (Figure 5-1(d)), which is probably caused by plastic deformation. The number of dimples decreased and the dimple size increased with increasing CDHA content. By contrast, for the ex-situ process, the membranes became porous when the CDHA amount exceeded 30% (Figure 5-1(f)). It is attributed to agglomeration of the incorporated CDHA nanoparticles that could be observed for the sample prepared via the ex-situ route and evidenced by TEM as shown in Figure 5-2. These agglomerates could be the favorable sites for the nucleation of voids upon drying. Therefore, in this work, data of Ex-situ 30 and Ex-situ 50 were excluded due to their macro-porous structure, which could not comply with the fundamental hypothesis of Eqn. 5-(1) and 5-(2) in the forthcoming analysis [61].

Figure 5-3 shows the XRD patterns of CDHA, CS and CDHA/CS nanocomposites. One major peak at 2θ~21^{o} and two minor peaks at 2θ~26^{o} and 32^{o} appeared in both samples In-situ 10 and Ex-situ 10. According to the ICDD No. 39-1894 and No. 46-0905, the major peak and two minor peaks can be identified as semi-crystalline chitosan and poorly crystalline CDHA, respectively. It indicated that CDHA/CS composites could be synthesized through both in-situ and ex-situ processes. Furthermore, it was found that the crystallinity of CS was decreased with increasing CDHA content, which is probably caused by the well-dispersed CDHA nano-crystals which act as point defects in the chitosan matrix [125]. In addition, Strawhecker et al. also reported that strong polymer-filler interaction could change the molecular conformation of polymer chain in the vicinity of filler and simultaneously gave rise to the formation of localized amorphous regions [126]. This accounts for considerable inhibition of the crystallinity development of chitosan crystals and this retardation becomes more pronounced when the CDHA content exceeds 30 wt%.

Figure 5-4 shows the TGA curves of CDHA/CS nanocomposite membranes prepared via the in-situ process. The TGA curve of Ex-situ 10 was similar to that of In-situ 5 (not shown).

Thermal decomposition of pure chitosan without cross-link was clearly observed from 150°C to 250°C, which is attributed to the cleavage of hydrogen bonding [131]. However, no thermal decomposition region was observed for both In-situ 30 and In-situ 50. Furthermore, it was found that as the pure chitosan membrane was fully cross-linked by sodium tripolyphosphate (sTPP), its TGA curve was very similar to that of both In-situ 30 and In-situ 50. This result suggests that the CDHA acts as a cross-linking medium with chitosan, which is attributed to the electrostatic attraction between $(PO_4)^{3-}$ moieties (from CDHA) and protonated amino groups (NH_3^+) in chitosan molecules. This filler-polymer attraction force stabilizes the polymer chain network via the cross-linking operation. The degree of cross-link could be quantified by calculating the weight loss of the composite membranes with respect to the weight loss of pure chitosan in the range from 150°C to 250°C and the results are shown in Figure 5-5(a). As can be seen, when the incorporated CDHA was below 10%, the degree of cross-link increased almost linearly with CDHA content; above that, the correlation tended to become constant. This observation could be accounted for by assuming that all the NH_3^+ groups in chitosan molecules are fully occupied by interaction with the surface phosphate groups of the CDHA nanoparticles and under such a full occupation, no further sites are available for cross-link. On the other hand, for the sample with 10% CDHA, the degree of cross-link of the composite membrane prepared via the in-situ process was higher than that synthesized via the ex-situ process. It is then reasonable to believe that in-situ synthesis offers more nucleation sites (i.e., filler-polymer interaction sites), resulting in better dispersion of the CDHA nanoparticles in the chitosan matrix (Figure 5-2). Under this condition, the well-dispersed CDHA nano-crystals provide higher cross-link density (degree) with chitosan than that of the agglomerated CDHA nano-crystals prepared via the ex-situ process.

5.3.2 Diffusion exponent of drug-loaded matrix system

Diffusion exponent (n), as defined in Eqn. 5-(1), can be employed to determine release kinetics and diffusion mechanism for polymeric matrix drug delivery systems (DDS) [132, 133]. As revealed in Figure 5-5(a), the exponent n was strongly affected by the synthetic process and concentration of the nanofiller. It was observed that the n values of the membranes synthesized through the in-situ process were higher than those through the ex-situ process. This, according to previous argument, is probably due to the stronger filler-polymer interaction (short-range interaction) between well-dispersed CDHA crystals and CS side groups, as well as chain-chain interaction (long-range interaction) in highly cross-linked network particularly for the in-situ route. This assumption is further supported by DMA curves shown in Figure 5-6. It is known that for semi-crystalline polymers, short-range interaction in the side group causes a shift of β-transition to the higher temperature region. Long-range interaction in backbone causes the α-transition to be broadened or even the peak to disappear [121, 122, 125]. These two phenomena were both observed in the DMA curves for sample In-situ 10. It suggests that well-dispersed CDHA nanoparticles, i.e., in-situ route, provide greater extent of interaction with the chitosan and reduce more effectively the molecular relaxation rate of chitosan molecules, i.e., restricted relaxation. This restriction of molecular relaxation is believed to affect drug diffusion within the nanocomposites and result in an increase in exponent n, indicating that drug release shifts from a diffusion-controlled towards swelling-controlled mechanism [133].

Hongbin et al. reported a coarse-grained domain relaxation model for depicting the restricted relaxation behaviour in the nanocomposite system according to the nature of polymer-filler interaction [124]. The polymer chains around the filler can be classified into three regions: Domain I (slow relaxation region in the vicinity of filler), Domain II (fast relaxation region in the central areas among neighboring fillers), and Domain III (normal relaxation region in the bulk matrix). This model supports that α-transition peak with a lower peak height assigned to Domain III could be observed for sample Ex-situ 10 (Figure 5-6)

because the total volume of Domain III is increased with the agglomeration of CDHA nanofillers in the CS matrix. Therefore, restricted molecular relaxation in the membrane prepared via the ex-situ process is not as prominent as that prepared via the in-situ process. Therefore, the diffusion exponent of the CDHA/CS membranes is lower for that synthesized through the ex-situ processes than that through the in-situ synthesis, as further confirmed in Figure 5-5(a).

The effect of CDHA content on diffusion exponent is illustrated in Figure 5-5(a). For pure CS, n was close to 0.5, indicating a Fickian diffusion kinetics. Incorporating the CDHA nanoparticles into CS matrices caused an increased n, which is well explained in terms of the coarse-grained domain relaxation model. Increasing the concentration of CDHA gives rise to an increase in polymer-filler interaction, leading to an increased volume of Domain I, and at the same time, a decrease in the volume of Domain II and Domain III. This indicates that the extent of restricted relaxation is increased when the concentration of CDHA increases. Therefore, when the CDHA was added up to 10%, exponent n was rapidly increased to 0.7 for the nanocomposite prepared via the in-situ process, indicating a transition from diffusion control to swelling control. Furthermore, from experimental findings, when the CDHA was increased from 10% to 30%, the volume for Domains II and III were largely replaced by Domain I and tended to approach a saturated level. The n value then became relatively constant when the CDHA content exceeded 30%. Interestingly, this phenomenon reveals that the effect of CDHA content on diffusion exponent n is very similar to that of CDHA content on the degree of cross-link. This also implies a possible correlation of diffusion exponent with the degree of cross-link. Figure 5-5(b) shows the resulting dependence, where a linear correlation with R^2 as high as 0.98 was obtained. It indicates that the degree of cross-link within the matrix due to the incorporation of CDHA nanoparticle affects profoundly the drug diffusion exponent.

5.3.3 Permeability of membrane system

The effect of CDHA content on the permeability and partition coefficient of the membrane prepared through the in-situ process is illustrated in Figure 5-7. It was found that the partition coefficient was slightly decreased with increasing CDHA content because the incorporated CDHA does not dissolve the model drug. It suggests that the diffusion coefficient (D) becomes the dominant item for membrane permeability (P=D*H). The membrane permeability was decreased with the incorporation of CDHA from 0% to 10%. However, further increase in the CDHA from 10 to 30% caused an increase in the permeability, which became more pronounced when the CDHA content was higher than 30%. These results may be explained as follows. The degree of cross-link and the length of diffusion path increase with the incorporation of CDHA nanofillers, leading to a decrease in diffusion coefficient. Therefore, the membrane permeability of CDHA/CS nanocomposite decreased with increasing CDHA content. On the contrary, the crystallinity decreased as CDHA was incorporated into the chitosan matrix as evidenced in Figure 5-3. The CDHA nanoparticles retard the crystallization of chitosan, thus making the resulting chitosan more amorphous, which in turn increases the diffusion coefficient of the chitosan matrix [134]. Therefore, the influence of the CDHA on the chitosan diffusion coefficient is essentially a compromise between degree of cross-link and crystallinity. As the CDHA content was increased to over 30%, the decrease in crystallinity of the chitosan became dominant. In addition, a further addition of CDHA causes the agglomeration of nanoparticles as observed in sample In-situ 50, which may further induce the formation of microcracks between the CDHA phase and the chitosan matrix as a result of increased rigidity or more specifically, voids within the CDHA agglomerates. Either microcracks or voids could act as effective diffusion paths, which cause a significant increase in permeability, as observed in sample In-situ 50.

Figure 5-7 also shows the influence of synthetic processes on membrane permeability.

For the CDHA content of 5% and 10%, the permeability of composite membranes was lower for the in-situ route than that via the ex-situ process. This is probably due to better dispersion of the CDHA nanoparticles for samples prepared by the in-situ process, resulting in more efficient physical barriers. A higher degree of cross-link (Figure 5-5(a)), compared with the ex-situ synthesis, also provides inhibition to the resulting diffusion coefficient.

According to the aforementioned argument, it is possible to manipulate the release profile by selecting suitable values of n and P through incorporating various contents of CDHA. Take 5%, 30% and 50% for example, the resulting drug release profiles for vitamin B_{12} from the matrix membranes are illustrated in Figure 5-8. A near-zero order release profile with rapid release rate was observed for the 50% (In-situ 50) matrix membrane samples (with n=0.72, P=8.9 * 10^{-4} cm^2/h, H=0.096, D=9.3 * 10^{-3} cm^2/h); however, a near-zero order release profile with moderate release rate was achieved for the 30% ones (with n=0.71, P=3.4 * 10^{-4} cm^2/h, H=0.103, D=3.5 * 10^{-3} cm^2/h). It suggests that D value could be altered drastically without changing the n value for CDHA amount ranging from 30% to 50%. Compared with In-situ 30, In-situ 5 had a relative long-term release (with n=0.6, P=3.7 * 10^{-4} cm^2/h, H=0.112, D=3.7 * 10^{-3} cm^2/h), whose D value was close to that of In-situ 30.

Recently, sequential release of growth factor has been reported because of its potential in enhancing wound healing and osteogenesis [135]. In addition, using combination antibiotic therapy to decrease antibiotic-resistance has been investigated [97, 136]. Therefore, it is feasible to design a bone substitute consisting of CDHA/CS composite loaded with multiple drugs for either simultaneous release or sequential release via regulating the amount of CDHA nano-phase [137]. Compared with existing conventional approaches to manipulating drug release kinetics (i.e., molecular weight, crystallinity, amount of cross-linking agents), this study provides a relatively simple, precise and controllable synthetic methodology for manipulating release kinetics. In this work, in order to clarify the effect of filler-polymer on drug release kinetics, vitamin B_{12} was selected as the model drug because of its small

molecular weight, as well as negligible drug-filler and drug-polymer interaction. Unfortunately, a variety of bioactive agents with a wide range of drug-filler interaction, drug-polymer interaction and molecular weight may be therapeutically inconsistent or possibly interacted adversely in the same carrier materials, which merits further investigation.

5.4. Conclusion

In conclusion, an orthopedic implant material consisting of chitosan and CDHA with drug delivery function has been studied. It was found that both the amount of CDHA incorporated and the synthetic process altered significantly the extent of filler-polymer interaction, which influences strongly the diffusion exponent and permeability of CDHA/chitosan nanocomposites. Hence, CDHA nanocrystal could concurrently play the roles as bioactive nanofiller and drug-release regulator. This study may provide valuable information for a better design of chitosan-based orthopedic devices with improved bioactivity and controlled drug release function.

Table 5-1: Synthetic conditions of the CDHA/CS nanocomposites.

Processes	CDHA content	Composite code
In-situ processes	5%	In-situ 5
H_3PO_4→CS→$Ca(CH_3COO)_2$	10%	In-situ 10
	30%	In-situ 30
	50%	In-situ 50
Ex-situ processes	5%	Ex-situ 5
CS→CDHA	10%	Ex-situ 10
	30%	Ex-situ 30
	50%	Ex-situ 50

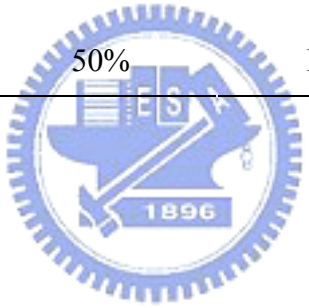

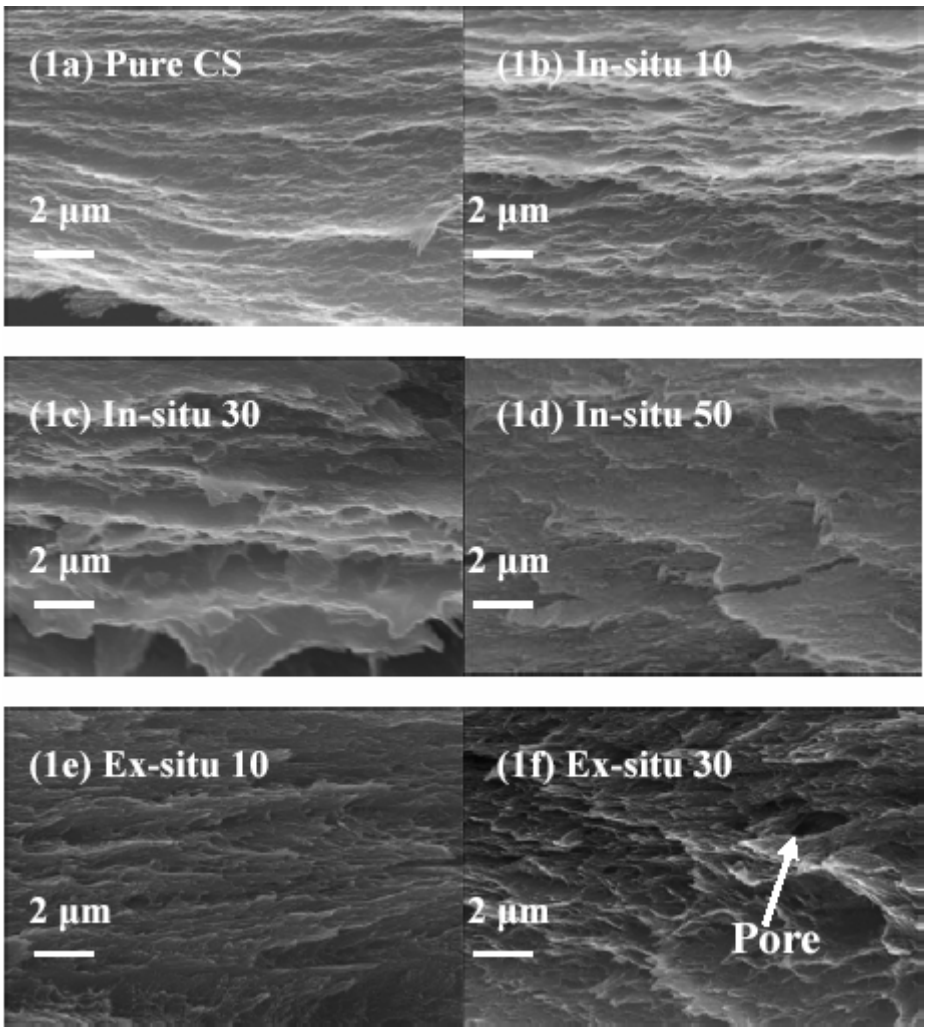

Figure 5-1. Selective SEM micrographs (cross-section) of CDHA/CS nanocomposite membranes.

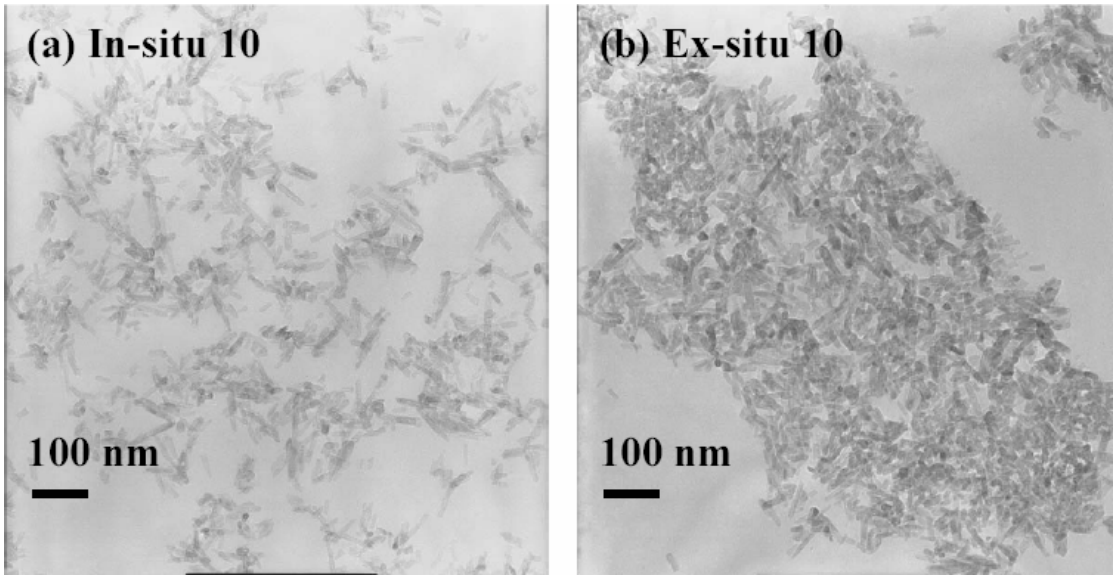

Figure 5-2. Selective TEM micrographs of CDHA/CS nanocomposite membranes.

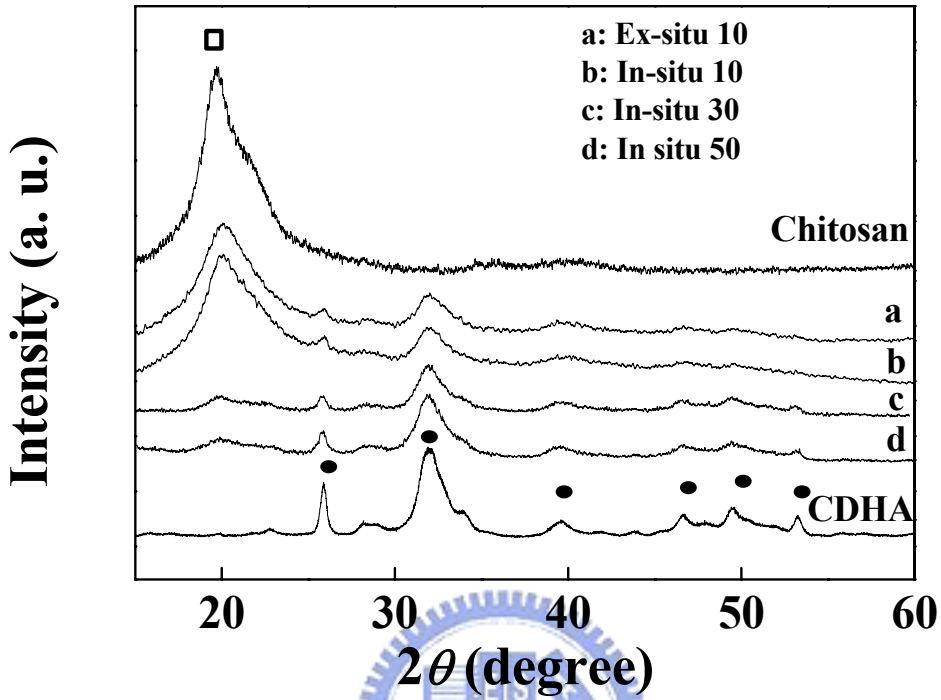

Figure 5-3. XRD patterns of CS, CDHA and CDHA/CS nanocomposites.

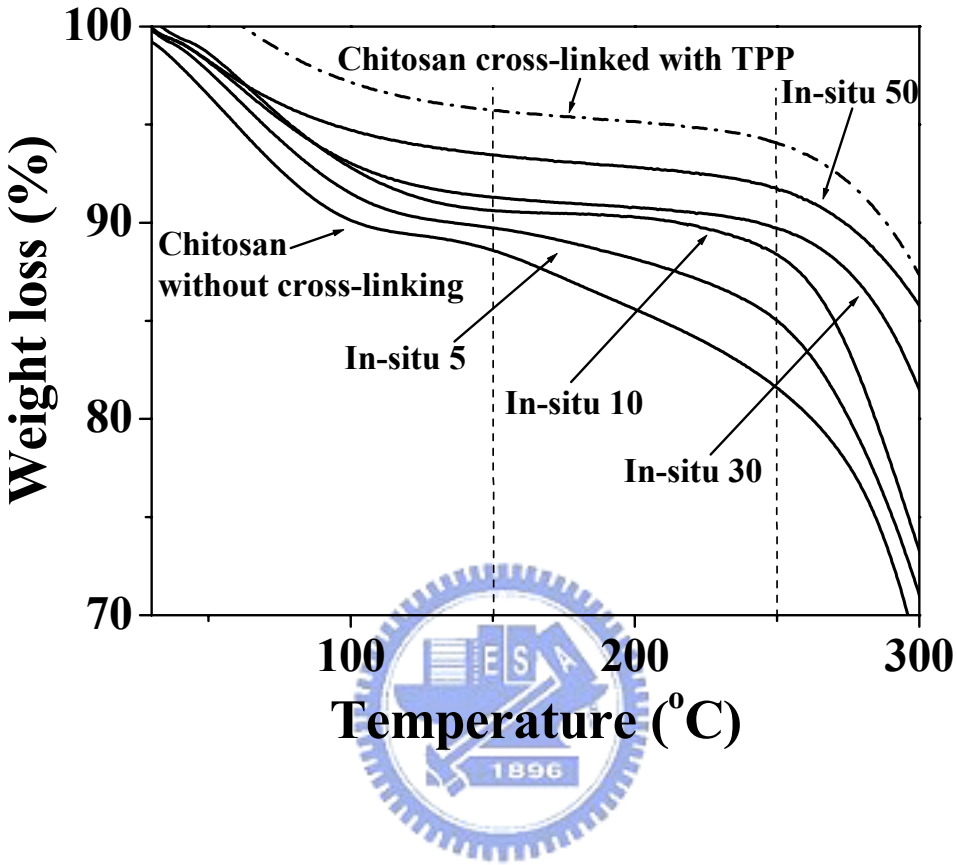

Figure 5-4. TGA curves of sTPP cross-linked chitosan and CDHA/CS nanocomposite membranes prepared via in-situ process.

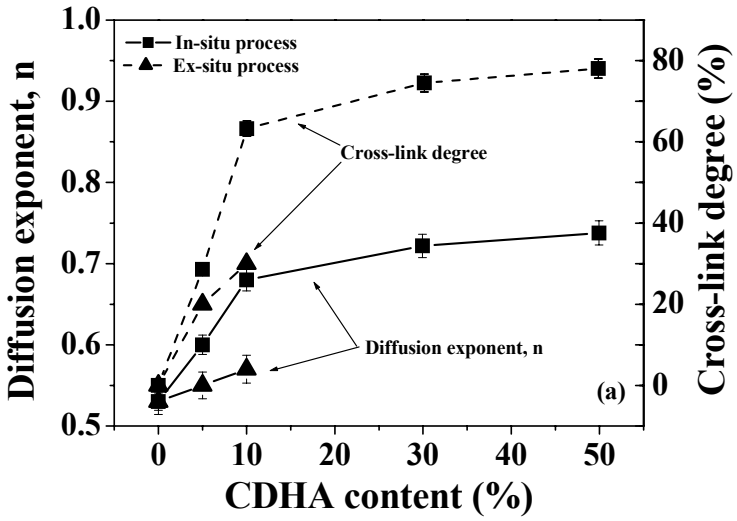

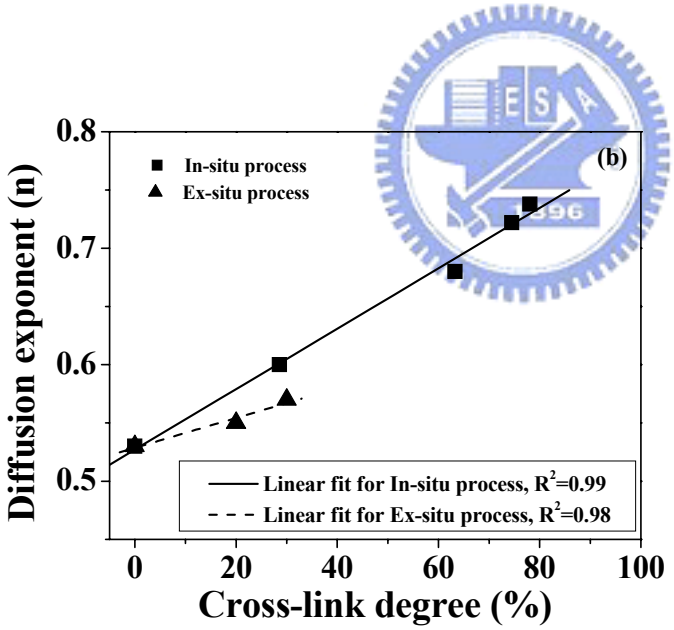

Figure 5-5(a). Dependences of synthetic processes and amount of CDHA on the degree of cross-link and diffusion exponent of nanocomposite membranes. 5(b). Dependences of degree of cross-link on the diffusion exponents of nanocomposite membranes.

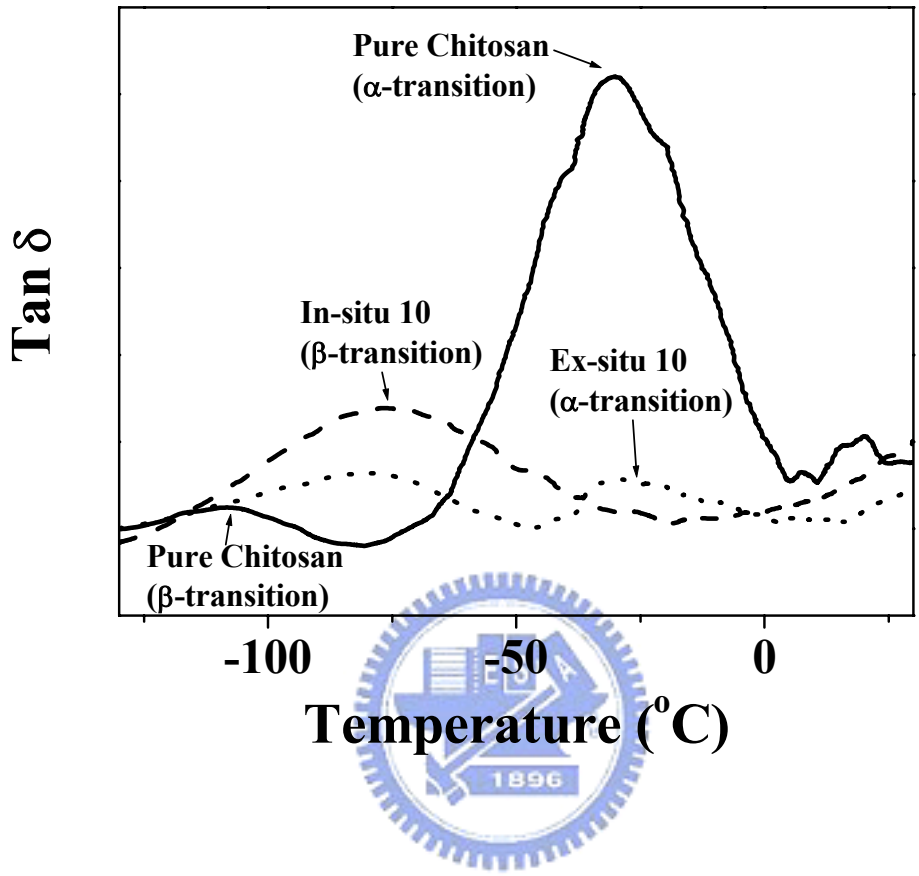

Figure. 5-6. DMA curves of chitosan and CDHA/CS nanocomposite membranes with CDHA content of 10%.

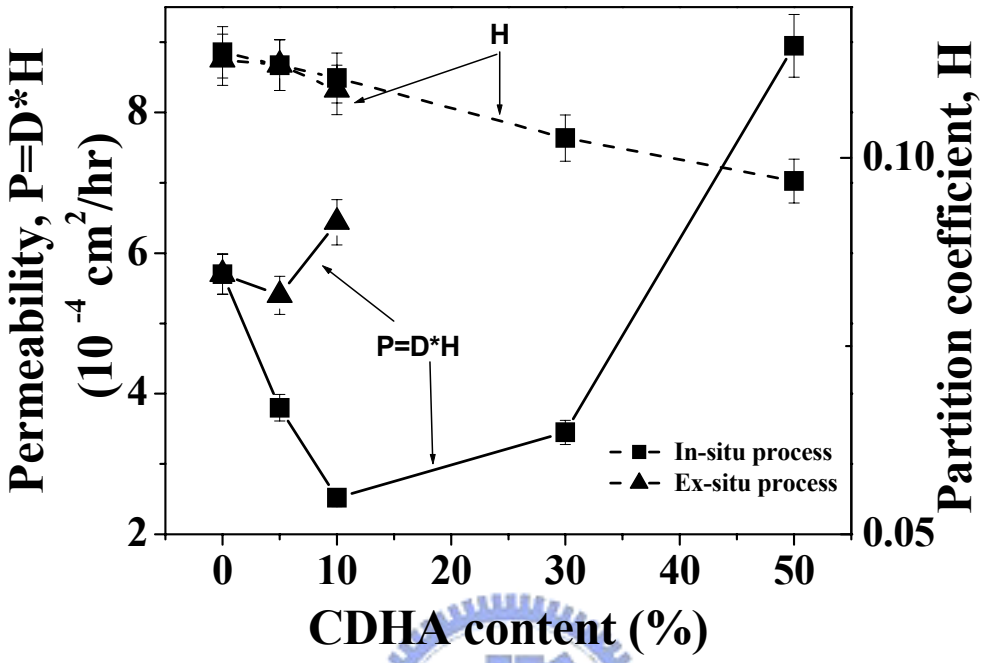

Figure 5-7. Dependences of synthetic processes and CDHA content on the permeability (P) and partition coefficient (H) of CDHA/CS nanocomposite membranes.

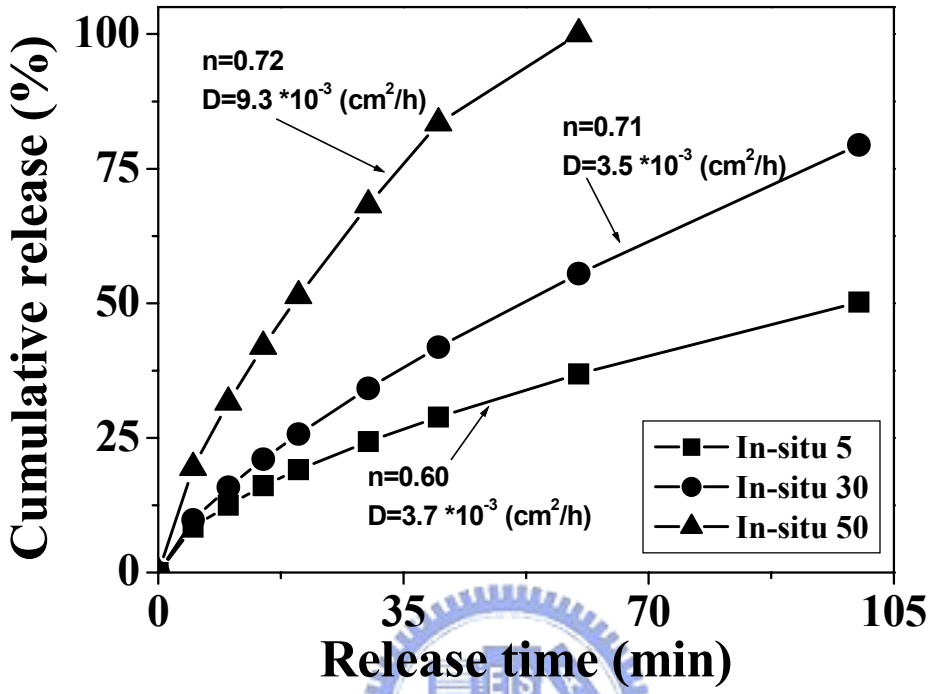

Figure 5-8. Release profiles of CDHA/CS nanocomposite matrix membranes.

CHAPTER 6

Synthesis and Characterization of Amphiphatic Carboxymethyl-hexanoyl Chitosan Hydrogel: Water-retention Ability

6.1 Introduction

In recent years, much attention has been focused on chitosan (CS) hydrogels for wound dressing, cartilage tissue engineering and drug-loaded implants owing to its glycosaminoglycan-like structure and outstanding characters such as biodegradability and low price [52, 138-140]. However, insufficient swelling ability in neutral physiological condition, poor solubility in organic solvents, and lack of amphiphatic nature have limited its uses. Therefore, a number of chitosan derivatives have been developed over the years in order to improve desirable properties, thus enhancing its bio-applicability [141, 142].

For the occlusive films used in wound healing, it has been reported that healing under a wet environment is faster than that under a dry environment [143, 144]. In addition, hydrogel-based scaffold in a highly swollen state has been used for delivering cell with bioactive agents [145]. Therefore, it is beneficial to employ chitosan derivatives with excellent water-absorption ability and water-retention ability in neutral physiological condition for both burn-dressing and cell encapsulation application [146]. On the other hand, an increase in hydrophobicity of drug-loaded hydrogel is required to improve drug transport across the buccal mucosa and to enhance the encapsulation efficiency for many amphiphatic bioactive agents such as vancomycin and ibuprofen [52]. Therefore, it is necessary to develop a chitosan-based hydrogel with high encapsulation efficiency of bioactive agents with a wide range of hydrophilic/hydrophobic nature, to replace currently employed hydrophilic or hydrophobic polymeric matrices [131, 147-149]. On this base, amphiphatic

carboxymethyl-hexanoyl chitosan (NOCHC) bearing hydrophilic and hydrophobic substitutions was synthesized for the first time and expected to possess excellent water-absorption ability and water-retention ability in neutral condition, as well as high encapsulation efficiency for the therapeutic agent with partial hydrophobicity.

In general, the water-absorption ability and water-retention ability (deswelling behavior) are determined by the intermolecular interactions in water solution such as hydrogen bonding, hydrophobic and electrostatic interactions, which depends on macromolecular structure and the state of water [150, 151]. It is known that the state of water in hydrophilic polymer can be classified into three types: (i) non-freezable bound water with tight water-polymer interaction, (ii) freezable bound water with loose water-polymer interaction, (iii) free (freezable) water without water-polymer interaction [150]. Various approaches have been proposed to explore the relationship between water-polymer interaction and water mobility in hydrogels [152, 153]. However, it remains unclear whether the hydrophobic hexanoyl group influences the water state, water-absorption and deswelling behaviors of amphiphatic hydrogel.

This study investigates systematically the influence of the substitution of the carboxymethyl and hexanoyl groups on water-absorption ability and deswelling kinetic of the NOCHC. In addition, ibuprofen (IBU) was employed as a partially hydrophobic model drug to further understand its loading efficiency in the NOCHC hydrogel since the therapeutic effect (modulation of tissue perfusion) of IBU on burns has been reported [154]. This study is expected to provide fundamental understanding on the amphiphatic NOCHC hydrogel used for biomedical, drug delivery, and cosmetic application requiring super-swelling or super water-retention properties.

6.2. Experiment materials and methods

6.2.1. Materials

Chitosan (Mw = 215,000 g · mol^{-1}, deacetylation degree = 85%-90%) was supplied from Aldrich-Sigma. Ibuprofen was purchased from Aldrich-Sigma (I4883).

6.2.2. Synthesis of NOCC and NOCHC

NOCHC was synthesized via selecting *N,O*-carboxymethyl chitosan (NOCC) as a starting precursor because its skeletal structure favored the formation of hyaluronic acid-like structure [146]. The synthesis of NOCC with various degrees of substitution has been reported in many studies [155]. In brief, 5 g of chitosan were suspended in isopropanol (50 ml) at room temperature while being stirred for 30 minutes. The resulting suspension was gently mixed with 12.5 ml of NaOH solution at different concentrations for controlling the degree of substitution. The mixture containing NaOH of 10M was mixed with 7 g of chloroacetic acid to prepare NOCC sample with low degree of carboxymethyl substitution. The mixtures containing NaOH of 13.3M were mixed with 7g and 25g of chloroacetic to prepare the NOCC sample with medium and high carboxymethyl substitutions, respectively. These three resulting suspensions were stirred for 30 minutes and heated to 60°C for 4 hours, followed by filtration, washing by methanol solution and drying. The obtained chitosan derivates with low, medium and high degree of carboxymethyl substitutions were named as NOCC-1, NOCC-2 and NOCC-3, respectively. NOCC-2 and NOCC-3 were selected as starting precursors for the synthesis of NOCHC because it is hard to dissolve NOCC-1 in neutral water to achieve a homogeneous synthesis. Each of the NOCC samples (2 g) was dissolved in distilled water (50 ml) while being stirred for 24 hour. These resulting solutions were mixed with methanol (50 ml), followed by the addition of hexanoyl anhydride at concentration of 0.1M, 0.3M and 0.5M for the NOCHC samples with low, medium and high hexanoyl substitution, respectively. After the reaction time of 12 hours, the resulting solutions were collected by dialysis membrane after dialysis with ethanol solution (25% v/v) for 24 hour. The obtained ethanol/water (volume ratio = 3:2)-soluble chitosan derivates were named as NOCHC.

NOCHC samples with various carboxymethyl and hexanoyl substitution degrees were named and shown in Table 6-1. For subsequent material characterization, chitosan-derived solutions of 1.3% (w/v) were prepared by dissolving obtained derivates in DI water. These solutions were then cross-linked with various amounts of genipin (molecular structure is shown in Scheme 6-1(a)) solution (1% w/v) to prepare hydrogels with same degree of cross-linking (constant amino residue/genipin ratio).

6.2.3. Material characterization

Proton nuclear magnetic resonance spectroscopy (^{1}H-NMR) spectra were used to confirm the sites and degrees of substitution recorded by NMR spectrometer (Varian unityinova 500) at 270 MHz. Attenuated total reflectance Fourier transformed infrared spectroscopy (ATR-FTIR) spectra were recorded on a spectrometer (Bomem DA8.3, Canada) using a film type sample (4 cm * 0.5 cm). The ATR-FTIR spectra were taken with a resolution of 2 cm^{-1} in the range of 4000-400 cm^{-1}. The state of water was characterized by a differential scanning calorimeter (DSC, Perkin Elmer instrument) [156]. Each dried sample was weighed in an aluminum pan, followed by the addition of various amounts of water into the sample pan. Samples were quenched from room temperature to 213 K and conditioned at 213 K for 10 minutes prior to the DSC test. DSC curves were then obtained by reheating the sample to 300 K at a scanning rate of 10 K min^{-1}. The maximum content of non-freezable bound water ($W_{nf,max}$) could be determined by detecting the endothermic peak assigned to the first-order phase transformation of water in the samples with various contents of water. The endothermic peak of freezable bound water is not detected until a critical amount of water is added to the sample. The critical amount of water is defined as $W_{nf,max}$, which is correlated with the number of tight water binding sites.

6.2.4. Moisture absorption and retention test

The characterization of water-absorption ability was measured following the report of Chen et al. [146]. Briefly, the samples were dried in vacuum chamber with P_2O_5 for 24 hours prior to the moisture absorption test which was carried out by putting the sample in an incubator with relative humidity of 40% and 70% at 20°C for 48 hours. Water-absorption ability (W_c) was determined by the percentage of weight change of the dry sample:

$$W_c(\%)=100\% * (W_w-W_d)/W_d \quad 6\text{-}(1)$$

where W_w and W_d are the weights of the sample after and before the absorption test. Saturated water-absorption ability ($W_{c,sat}$, equilibrium swelling ratio) was also determined by Eqn. 6-(1) and measured after putting the samples in DI water (pH=7) at 20°C for 48 hours.

The water-retention ability was evaluated by measuring water mobility during dynamic deswelling test [157]. Fully swollen hydrogels were placed in desiccators containing silica gel at 37°C and removed from desiccators at regular intervals for weighing. The weights of fully swollen hydrogels (W_{wet}), hydrogels at each juncture (W_t), and dry sample (W_{dry}) were recorded. The deswelling profile could be presented by plotting (M_t/M_0)-time curves, where M_0 is the initial amount of water in polymer ($M_0=W_{wet}-W_{dry}$), and M_t is the amount of water remaining in the polymer at any given time ($M_t=W_t-W_{dry}$).

6.2.5. Drug encapsulation efficiency

Ibuprofen was employed as a partially hydrophobic model drug (molecular structure is shown in Scheme 6-1(b)). Ibuprofen-loaded monolithic films (matrix films) prepared by chitosan derivates were obtained using the film-casting method. In brief, chitosan/acetic acid solution, NOCC/DI water solutions and NOCHC/ethanol/DI water solutions with pH values of 7.0 were adjusted by NaOH solution (1M), followed by mixing these polymeric solutions with saturated IBU/DI solution and genipin solution to form IBU-loaded polymeric solutions (IBU concentration: 1.2 mg/ml). Subsequently, those drug-loaded polymeric solutions were poured into Petri dish to form drug-loaded matrix films after cross-linking and drying at 50°C

for 2 days. In order to calculate the real encapsulation efficiency, these genipin-crosslinked matrix films were rinsed with ethanol solution for 30 seconds followed by measuring the amount of IBU rinsed out to ethanol solution (L_2) determined by UV-visible spectroscopy (Agelent 8453) at 264.4 nm through the use of pre-determined standard concentration-intensity curve. The IBU encapsulation efficiencies (E) could be determined by Eqn. 6-(2)

$$E=(L_1-L_2)/L_1 *100\% \quad 6\text{-}(2)$$

where L_1 is the initial loading amount of IBU incorporated.

6.3. Results and Discussion

6.3.1. Synthesis of NOCHC

Carboxymethyl-hexanoyl chitosan was synthesized using NOCC as the starting precursor. Upon substitution reaction, a hydrogen atom on the amino group or hydroxyl group can be replaced by the hexanoyl group. Figure 6-1 shows the molecular structure and the ^{1}H-NMR spectrum of NOCHC-2B. The chemical shift at 3.2 and 3.9 ppm was probably assigned to the proton of the segment with low molecular weight due to the acidic process with mild heating. The chemical shift at 1.9 and 2.9 ppm was assigned to the protons on the acetyl group and C2 position (H-2), respectively. In addition, the ring protons (H-3 to H-6) are considered to be resonated at 3.6-4.0 ppm. Moreover, the chemical shifts at 4.2 and 4.4 ppm were designated to the protons of -N-CH_2-CO- (*N*-position) and -O-CH_2-CO- (*O*-position) of NOCHC, respectively. On the other hand, the chemical shifts at 0.7 ppm (-CH_3), 1.1 ppm (-$C_\delta H_2$-), 1.2 ppm (-$C_\gamma H_2$-), 1.5 ppm (-$C_\beta H_2$-) and 2.2 ppm (-CO-$C_\alpha H_2$-) were assigned to the protons on the hexanoyl group. This demonstrates hexanoyl substitution replaced some of the amino and hydroxyl sites of the *N,O*-carboxymethyl chitosan. The method for determining the degree of carboxymethyl substitution has been described in the

literature and the result is shown in Table 6-1 [155]. The degree of hexanoyl substitution was determined by Eqn. 6-(3) and shown in Table 6-1.

DH = ((integrated area at 0.75 ppm, $-CH_3$)/(integrated area at 2.9 ppm, ^1H)) * 1/3 6-(3)

where DH is the substitution degree of the hexanoyl group at amino sites.

6.3.2. Moisture absorption test

The influence of carboxymethyl substitution on W_c (moisture-absorption ability) and $W_{nf,max}$ (maximal non-freezable water amount) values under the environment with various degrees of relative humidity (RH) is shown in Figure 6-2. Under low humidity (RH = 40%), the value of W_c was decreased with increasing degree of carboxymethyl substitution. This phenomena was also observed for $W_{nf,max}$ which is related to the number of tight water-binding sites, suggesting that W_c is closely correlated with the number of tight water-binding sites. In other words, water-binding site is the dominant factor for W_c under low humidity condition and decreased with increasing degree of carboxymethyl substitution. This is due to the fact that the samples with high carboxymethyl substitution favored the formation of intermolecular hydrogen bonding (polymer-polymer interaction), resulting in a structure with fewer tight water-binding sites (water-polymer interactions). This is further evidenced by the ATR-FTIR spectra shown in Figure 6-3. The characteristic peaks at 1730 cm^{-1} for the samples NOCC-2 and NOCC-3 were assigned to the carboxymethyl dimmer ($O=COH^{\cdots}O=COH$), suggesting an intermolecular interaction. Moreover, as compared with unmodified chitosan, it was found that the amide I characteristic peaks (1635 cm^{-1}) of samples NOCC-2 and NOCC-3 shifted significantly to lower wavenumber (red shifts δ= 20 cm^{-1}), which was due to the formation of intermolecular hydrogen bonding between the amide group and carboxylic group ($O=CNH_2^{\cdots}O=COH$) in the modified chitosan. This hydrogen bonding is stronger than that in un-modified chitosan (amide resonance H-bonding: $O=CNH_2^{\cdots}O=CNH_2$) because the dipole moment of an N-H bond is smaller than that of an

O-H bond [158]. These strong intermolecular bonds reduced the number of tight water-binding sites (water-polymer interaction), resulting in the lowest water-absorption ability detected for the sample with the highest degree of carboxymethyl substitution (NOCC-3) under low humidity. However, the W_c of sample NOCC-3 was significantly enhanced when hexanoyl substitution was introduced (NOCHC-3A), as shown in Figure 6-4. This agrees with the finding that $W_{nf,max}$ of sample NOCHC-3A was significantly higher than that of sample NOCC-3. This implies that the number of tight water-binding sites increased with the incorporation of hexanoyl groups because it could inhibit the formation of intermolecular hydrogen bonding (i.e., $O{=}CNH_2\cdots O{=}COH$, $O{=}COH\cdots O{=}COH$) in NOCC, which is further evidenced by the ATR-FTIR spectra shown in Figure 6-3. The red shift for amide I characteristic peak observed for samples NOCHC-2A and NOCHC-3A was of a lesser extent than that for samples NOCC-2 and NOCC-3, respectively. Additionally, characteristic peaks at 1723 cm^{-1} assigned to carboxymethyl dimmer were broadened and shifted to higher wavenumber region for samples NOCHC-2A and NOCHC-3A. These two findings in the ATR-FTIR spectra suggest that the intermolecular hydrogen bonding in sample NOCC was inhibited to a certain extent (H-bonding inhibition effect) as the hexanoyl group was introduced, resulting in extensive water-polymer interactions and higher water-absorption ability under condition of low relative humidity.

Under medium relative humidity (RH=70%), as shown in Figure 6-2 and Figure 6-4, it was found that W_c values were not significantly altered with increasing carboxymethyl and hexanoyl substitutions. In addition, W_c values, for all samples, were larger than the corresponding $W_{nf,max}$ but much lower than $W_{c,sat}$. Under this condition, the water-absorption ability was mainly determined by the hydration volume (i.e., the amount of freezable bound water occupying the hydration layer) of hydrophilic group, implying that the tight water-binding sites is not the only dominant factor. Therefore, the W_c value was less sensitive to the degrees of carboxymethyl and hexanoyl groups under medium relative humidity.

For the fully-swollen condition, the $W_{c,sat}$ value (i.e., equilibrium swelling ratio) was significantly decreased with increasing carboxymethyl substitution as shown in Figure 6-2. This can be ascribed to the fact that the intermolecular volume for free water was drastically reduced by the intermolecular electrostatic attraction (between COO^- and NH_3^+) and the above-mentioned intermolecular hydrogen bonding. Therefore, a higher $W_{c,sat}$ value was obtained for the un-modified chitosan compared with those samples with high carboxymethyl substitution (NOCC-2 and NOCC-3). However, as shown in Figure 6-4, the $W_{c,sat}$ values of samples NOCC-2 and NOCC-3 were significantly enhanced as the hexanoyl group was introduced (NOCHC-2A and NOCHC-3A). This is attributed to the fact that the formation of electrostatic attraction and intermolecular hydrogen bond in NOCC was inhibited by the hexanoyl groups (NOCHC), which enlarge significantly the intermolecular volume for free water as further evidenced by DSC test and it will be discussed later. Consequently, $W_{c,sat}$ values were significantly enhanced for NOCHC compared with NOCC. However, as the hexanoyl substitution was further increased, the above-mentioned H-bonding inhibition effect is compensated by hydrophobic interaction which acts as an intermolecular interaction and reduces the intermolecular volume for free water [159]. Therefore, the $W_{c,sat}$ value was slightly decreased with increasing hexanoyl substitution.

6.3.3. Moisture retention characterization

The deswelling behavior of fully-swollen hydrogel can be illustrated by plotting (M_t/M_0) versus time (t) as shown in Figure 6-5(a). The deswelling kinetics of hydrogels investigated in this study could be characterized by further plotting (M_t/M_0)-$t^{1/2}$ curves (Figure 6-5(b)) using Eqn. 6-(4) derived simply from Higuchi's model [63]:

$$M_t/M_0 = -kt^{1/2} + 1 \qquad 6\text{-}(4)$$

where M_0 is the initial amount of water in polymer, M_t is the amount of water remaining in the polymer at any given time, and k is a constant.

Figure 6-5(b) shows that a linear (M_t/M_0)-$t^{1/2}$ curve of the sample NOCC-3A exhibited a one-stage profile which can be fitted to Higuchi's model, suggesting that the water release followed a diffusion control mechanism. In order to further understand the deswelling mechanism, the state of water in hydrogel was characterized by the DSC test. It is known that the state of water and its corresponding DSC curve can be classified into three types: (i) non-freezable bound water (where the DSC endothermic peak of water cannot be detected), (ii) freezable bound water (endothermic peak of water is much lower than 4.8°C), (iii) free (freezable) water (endothermic peak of water is close to 4.8°C) [156]. DSC curves of the samples with high carboxymethyl substitution (0.5) measured at W_c=200% are shown in Figure 6-6. A heavily overlapped band (solid line) was observed and could be divided into three peaks (dash lines) using the Lorentzian curve-fitting procedure. In Figure 6-6(a), the endothermic peak of free water was not observed for the NOCC-3 hydrogel even under fully-swollen state. Instead, the endothermic peaks at 1.3°C and bellow assigned to freezable bound water were observed. Hence, it is reasonable to believe that the single release (deswelling) stage of sample NOCC-3 is mainly due to dehydrated-evaporation of freezable bound water. By contrast, Figure 6-5(b) shows that sample NOCHC-3A exhibited a two-stage profile, suggesting the state of water in sample NOCHC-3A was significantly different from that in sample NOCC-3 as previously described. This assumption is further supported by DSC curves shown in Figure 6-6(b), the peak III of sample NOCHC-3A was very close to 4.8°C, revealing that the NOCHC-3A hydrogel contained free water at and above W_c =200%. On the other hand, the peaks II and III were assigned to freezable bound water. Hence, it is reasonable to believe that the first and second release stages of sample NOCHC-3A are mainly due to dehydrated-evaporation of free water and freezable bound water, respectively. This demonstrates that the hexanoyl group played an important role in affecting free water. However, as the hexanoyl substitution was further increased (NOCHC-3B), the peak III shifts

towards low temperature (Figure 6-6(c)). It implies that the intermolecular volume for free water was decreased with further increasing hexanoyl substitution.

An interesting finding can be seen in Figure 6-5(b) that the diffusion coefficient of free water released from sample NOCHC-3A was lower than that of freezable bound water released from sample NOCC-3. This means that the "bound" water has a faster diffusion rate compared with that of the "free" water through a given medium. This unusual result is probably attributed to a so-called "hydrophobic effect" under which water becomes more structured and less mobile in the vicinity of the hydrophobic group [160]. Hence, the diffusion coefficients of water molecules from sample NOCC-3 was higher than that from sample NOCHC-3A upon deswelling. This also implies that the water-retention ability of NOCHC is much better than that of NOCC.

6.3.4. Drug encapsulation efficiency

The influence of both carboxymethyl and hexanoyl substitutions on the encapsulation efficiencies of IBU within the samples are displayed in Figure 6-7. The encapsulation efficiency of NOCC was lower than that of pristine chitosan. It is probably due to the electrostatic attraction forces between COO^- (from IBU) and NH_3^+ (from chitosan) and becomes more pronounced when the NH_3^+ groups are richer in pristine chitosan than in its modified version, i.e., NOCC. On the other hand, IBU encapsulation efficiency was significantly enhanced when part of the amino groups in NOCC were substituted by the hexanoyl groups. It was ascribed to an increasing hydrophobicity of the polymer with the substitution of the hexanoyl group. On this base, it was believed that the critical micelle concentration (CMC) of IBU in polymeric solution was increased. Thus, IBU tended to be dissolved in the NOCHC polymeric solution in the form of molecules rather than micelles [161]. IBU in molecular form after encapsulation could increase drug-polymer electrostatic attraction such as IBU-COO^-…NH_3^+-polymer together with drug-polymer hydrogen bonding

including IBU-COOH···O=COH-polymer and IBU-COOH···O=CNH_2-polymer, and this results in a higher miscibility of IBU in NOCHC solutions and matrices. Consequently, encapsulation efficiencies of IBU in NOCHC-2A and NOCHC-3A were significantly higher than those in NOCC-2 and NOCC-3, respectively. Moreover, as shown in Figure 6-7, for the NOCHC samples with medium degree of carboxymethyl substitution (NOCHC-2A and NOCHC-2B), the encapsulation efficiency was increased with increasing hexanoyl substitution because the hydrophobicity of sample NOCHC-2B is higher than that of sample NOCHC-2A. However, for the samples with a high degree of carboxymethyl substitution (NOCHC-3A and NOCHC-3B), the hexanoyl group did not affect drug encapsulation efficiency in a considerable manner because the amino group was proportionally decreased for the sample with a high degree of carboxymethyl and hexanoyl substitution (NOCHC-3B). Thus, the binding sites between IBU and polymer were mainly contributed by carboxymethyl substitution (IBU-COOH···O=COH-polymer) rather than the amino group alone. Therefore, although hydrophobicity of NOCHC-3B was higher than that of NOCHC-3A, the difference in encapsulation efficiency between NOCHC-3A and NOCHC-3B was not pronounced. This suggests that the influence of carboxymethyl and hexanoyl groups on drug-polymer bonding sites is not independent of each other. The interaction between these two factors can be further evidenced from Figure 6-7. For samples with the same degree of hexanoyl substitution, drug encapsulation efficiency was significantly enhanced with increasing carboxymethyl substitution. This phenomenon can be explained as a result of the presence of hexanoyl substitution that could enhance drug-polymer interaction which is favorable for the formation of intermolecular hydrogen bonding between the drug molecule (in terms of COOH moiety) and the non-ionized substitutions in polymer chains, i.e. COOH and NH_2 groups. Accordingly, drug encapsulation efficiency for samples NOCHC-2A and NOCHC-2B (medium COOH) were lower than those for HNAOCC-3A and NOCHC-3B (high COOH). It suggested that the

carboxymethyl group played an important role in affecting IBU encapsulation efficiency on the premise that the hexanoyl group was present.

6.4. Conclusion

Amphiphatic hydrogel derived from chemically-modified chitosan was successfully synthesized through bearing both carboxymethyl and hexanoyl substitutions. Water-absorption ability decreased with increasing substitution of the carboxymethyl group but was significantly increased with the introduction of the hexanoyl group because it altered the number of water-binding sites and the state of water under low humidity and the fully-swollen condition, respectively. Moreover, compared with NOCC, NOCHC also demonstrated enhanced water-retention ability. It is feasible to employ NOCHC hydrogel as a novel and potential amphiphatic carrier to effectively encapsulate and deliver numerous amphiphatic drugs, such as vancomycin and naproxen, for cell encapsulation or wound dressing material with excellent water-retention ability and pre-designed drug release function for enhanced therapeutic efficacy.

(a) genipin **(b) ibuprofen**

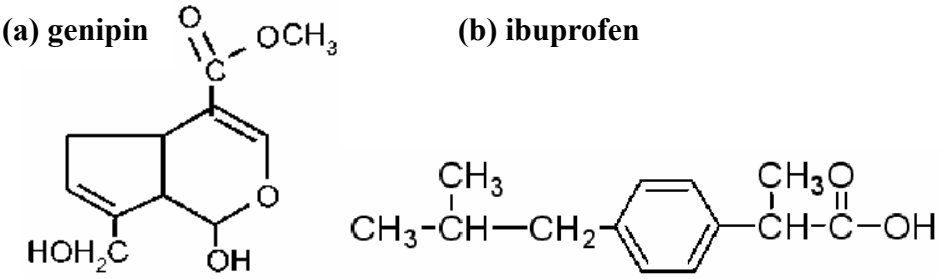

Scheme 6-1. Molecular structures of (a) genipin and (b) ibuprofen.

Table 6-1: Sample name and corresponding estimation of substitution degree by 1H-NMR.

	Degree of substitution	
	Carboxymethyl group	Hexanoyl group
Chitosan	0	0
NOCC-1	0.06	0
NOCC-2	0.32	0
NOCHC-2A	0.32	0.259
NOCHC-2B	0.32	0.461
NOCC-3	0.50	0
NOCHC-3A	0.50	0.264
NOCHC-3B	0.50	0.483

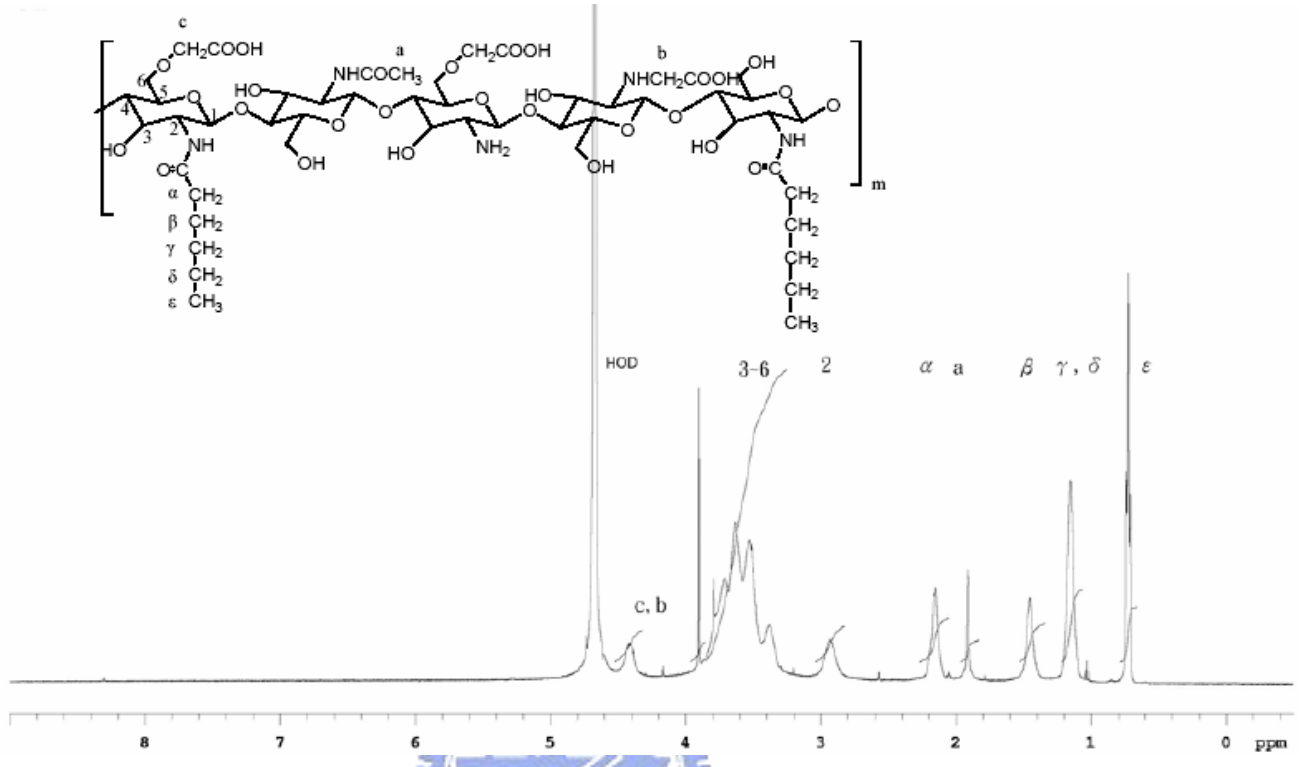

Figure 6-1. ^{1}H-NMR spectrum of sample NOCHC-2B.

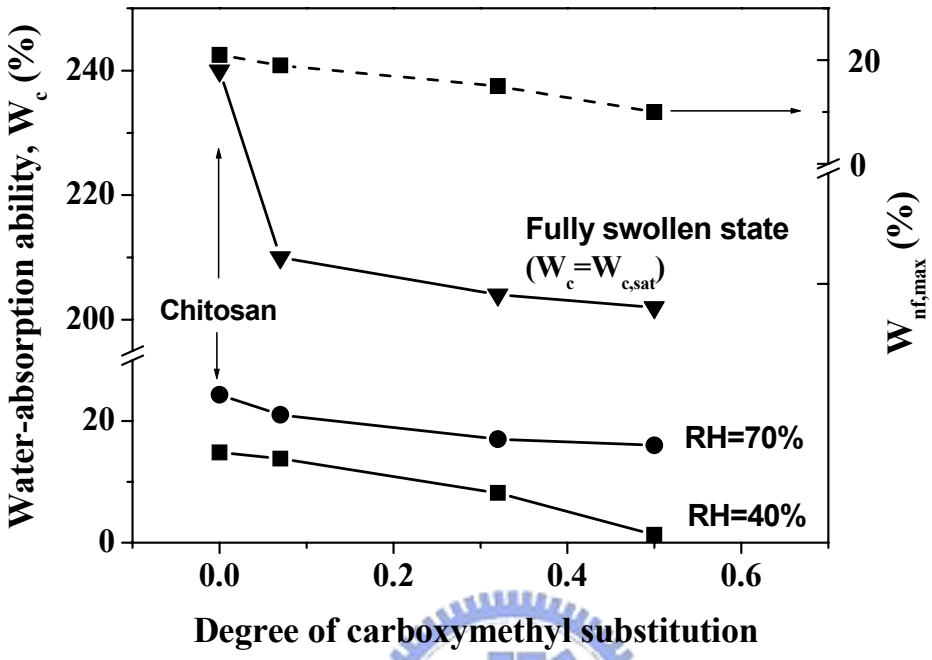

Figure 6-2. Dependence of carboxymethyl substitution on water-absorption ability (W_c, solid line) and maximal non-freezable water amount ($W_{nf,max}$, dash line).

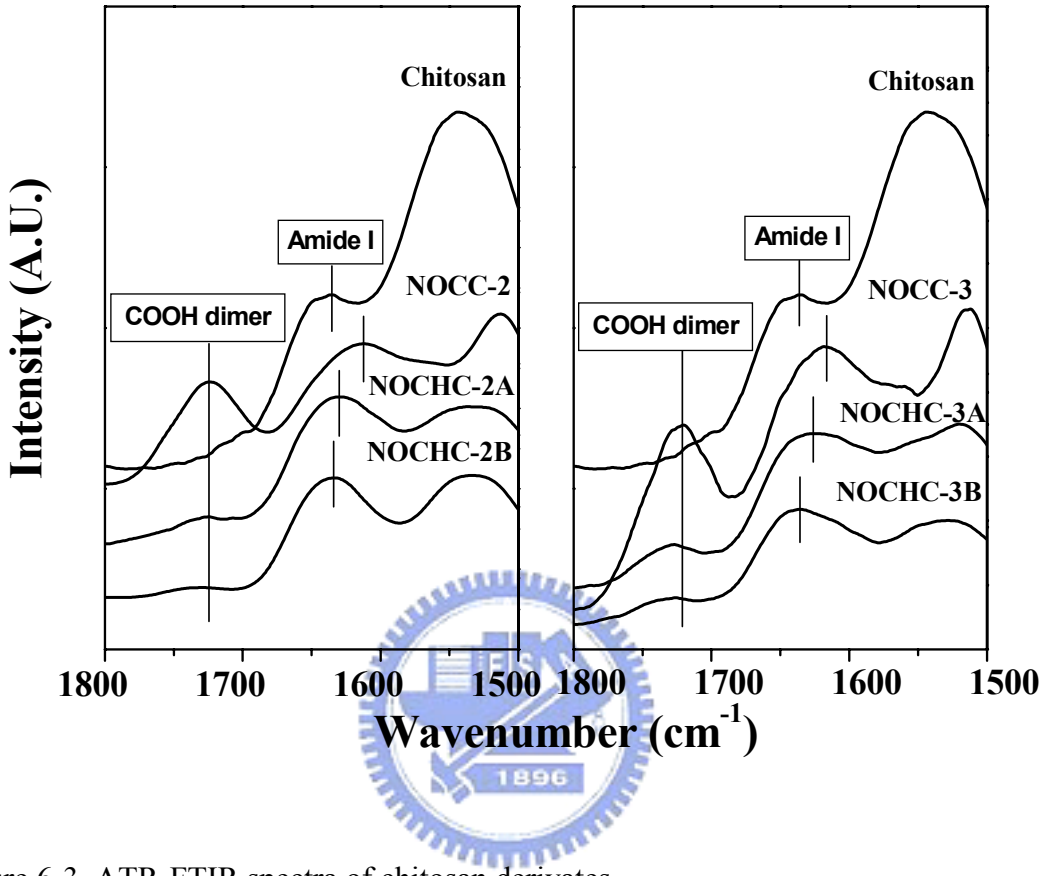

Figure 6-3. ATR-FTIR spectra of chitosan derivates.

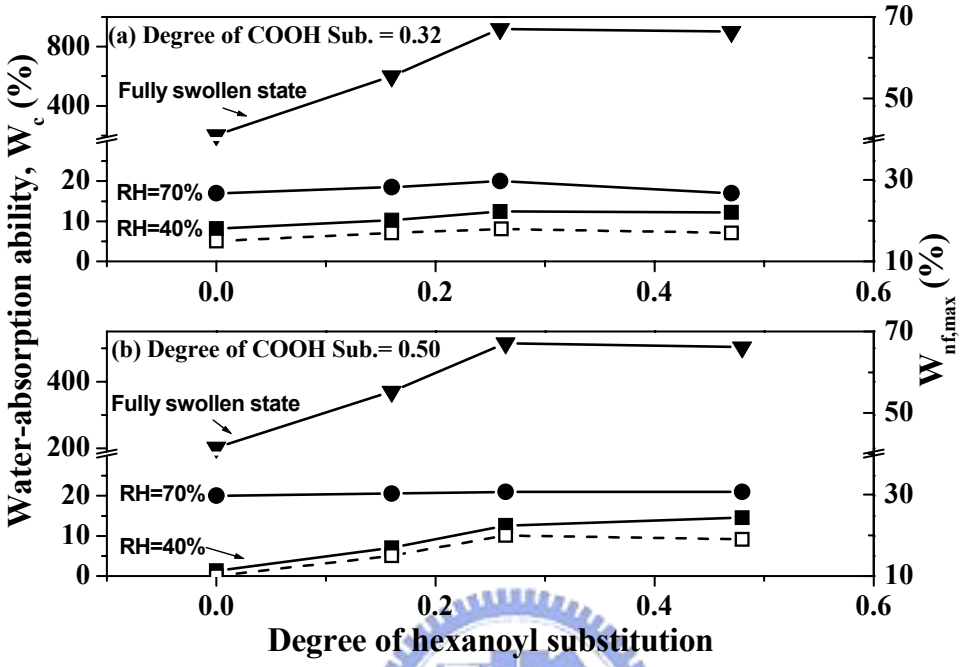

Figure 6-4. Dependence of hexanoyl group on water-absorption ability (W_c, solid line) and maximal non-freezable water amount ($W_{nf,max}$, dash line).

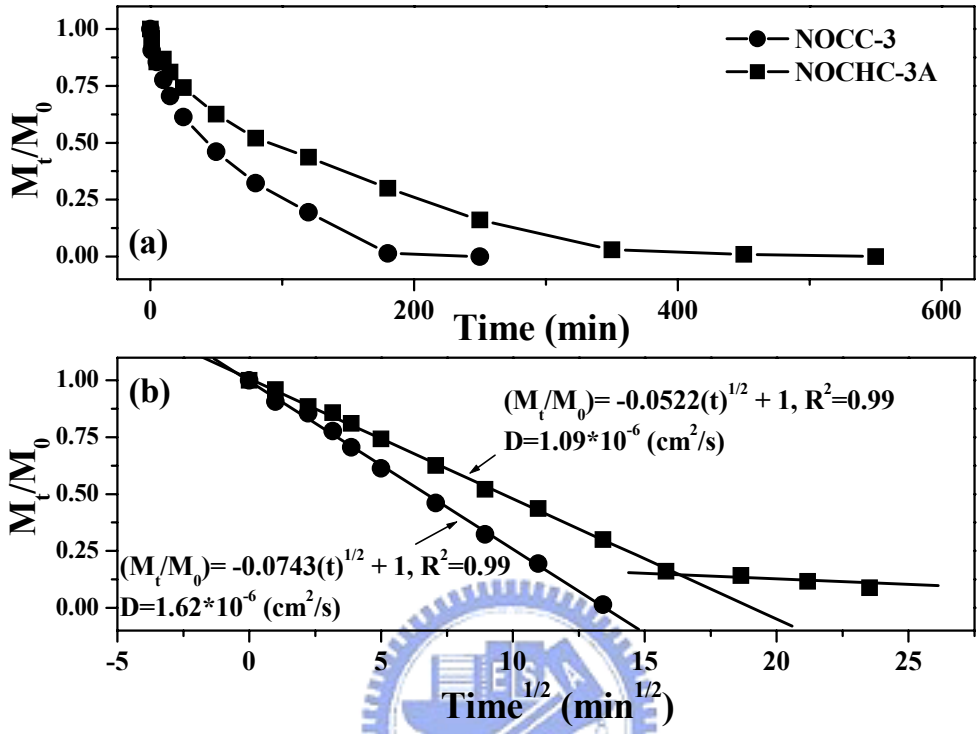

Figure 6-5. Deswelling profiles of samples NOCC-3 and NOCHC-3A.

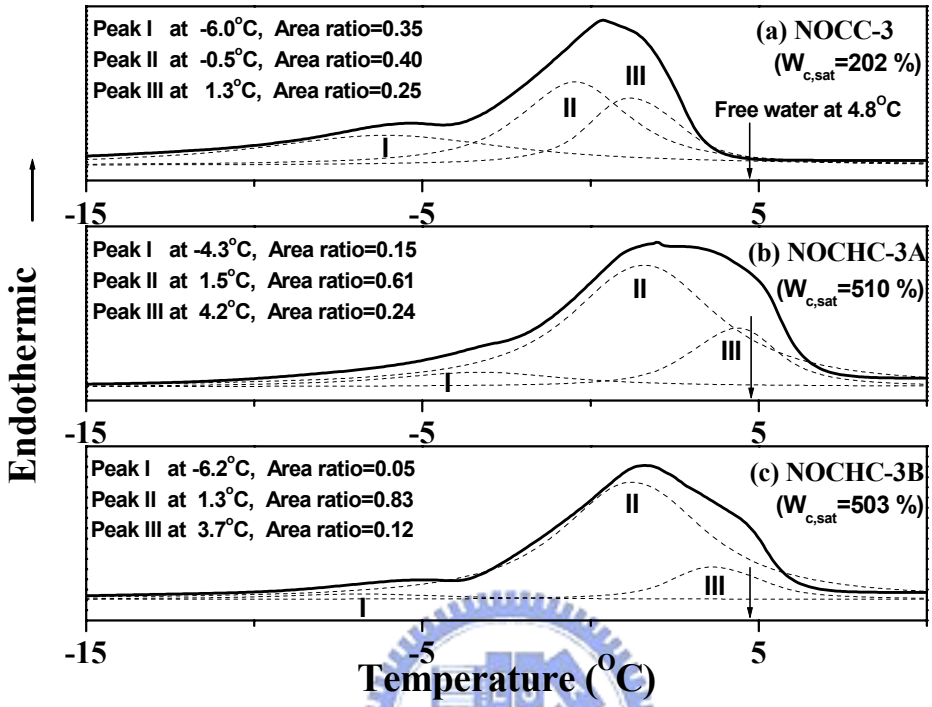

Figure 6-6. DSC curves of chitosan derivates (carboxymethyl substitution degree =0.5) measured at W_c = 200%. Dash lines represent the curve fitting by Lorentzian curve-fitting procedure.

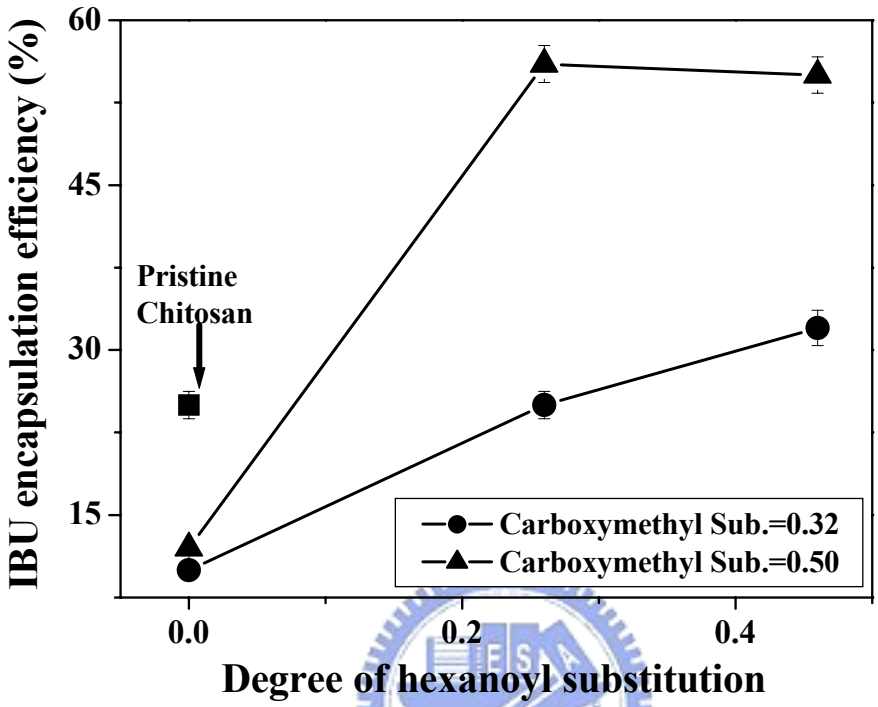

Figure 6-7. Dependences of degrees of carboxymethyl and hexanoyl substitution on ibuprofen encapsulation efficiency.

CHAPTER 7

Synthesis and Characterization of Amphiphatic Carboxymethyl-hexanoyl Chitosan Hydrogel: pH-sensitivity and Drug Release Behaviors

7.1. Introduction

In recent years, much attention has been focused on chitosan (CS) hydrogels for wound dressing, cartilage tissue engineering and drug-loaded implants owing to its glycosaminoglycan-like structure and outstanding characters such as biodegradability and low price [139, 140, 162]. However, insufficient swelling ability in neutral physiological condition, poor solubility in organic solvents, and lack of amphipathic nature have limited its uses. Therefore, a number of chitosan derivatives have been developed over the years in order to improve desirable properties, thus enhancing its bio-applicability [52, 141, 142].

N,O-carboxymethyl chitosan (NOCC) is a pH-sensitive and water-soluble chitosan derivate with excellent water-retention ability and water-absorption ability because carboxymethyl substitution favored the formation of hyaluronan-like structure [143, 144]. However, low encapsulation efficiency of water-insoluble agents has limited the NOCC hydrogel to be utilized widely because many amphipathic bioactive agents, such as doxorubicin and ibuprofen, are preferable to be dissolved in water-miscible organic solvent and encapsulated in amphipathic matrices [145]. Moreover, for the hydrogel-based drug delivery system applied to muccal route administration, it is known that an increase in hydrophobicity of drug-loaded hydrogel improves drug transport across the buccal mucosa [147]. On this base, carboxymethyl-hexanoyl chitosan (NOCHC) bearing both carboxymethyl and hexanoyl groups was synthesized for the first time and expected to possess excellent

pH-sensitive property, water-absorption ability in neutral condition, as well as high encapsulation efficiency for the therapeutic agent with partial hydrophobicity.

In previous chapter, the influences of carboxymethyl and hexanoyl substitutions on water-absorption ability and water-retention ability have been reported [163]. This study is stressed particularly on the influence of carboxymethyl and hexanoyl subsitutions on the pH-sensitive property of the resulting amphipathic hydrogel. In addition, ibuprofen (IBU, a non-steroidal antiinflammatory drug with amphipathic nature and its therapeutic effect on burns has been reported [146]) was employed as a model drug to further investigate its loading efficiency and release behavior in the NOCHC hydrogel. Taking the advantage of the ligand substitution, the resulting amphipathic hydrogel is expected to have a higher sensitivity to environmental pH varation, and its controlled hydrophilicity/hydrophobicity allows the resulting hydrogel capable of encapsulating therapeutically active agents of different nature such as hydrophilic, lipophilic, and amphiphilic drugs, for medical uses.

7.2. Experiment materials and methods

7.2.1. Materials

Chitosan (M_w = 215,000 g · mol^{-1}, deacetylation degree = 85%-90%) was supplied from Aldrich-Sigma. Ibuprofen was purchased from Aldrich-Sigma (I4883).

7.2.2. Synthesis of NOCC, NOCHC and NOCPC

NOCHC was synthesized via selecting *N,O*-carboxymethyl chitosan (NOCC) as a starting precursor. The synthesis of NOCC with various degrees of substitution has been described in section 6.2.2. The obtained chitosan derivatives with medium and high degree of carboxymethyl substitutions were named as NOCC-2 and NOCC-3, respectively. Each of the NOCC samples (2 g) was dissolved in distilled water (50 ml) while being stirred for 24 hour. These resulting solutions were mixed with methanol (50 ml), followed by the addition of

hexanoyl anhydride at concentration of 0.3M and 0.5M for the NOCHC samples with two degrees of hexanoyl substitution. NOCPC was obtained by the addition of palmitic anhydride instead of hexanoyl anhydride. After the reaction time of 12 hours, the resulting solutions were collected by dialysis membrane (Aldrich-Sigma, D6191) after dialysis with ethanol solution (25% v/v) for 24 hour. The obtained ethanol/water (volume ratio = 3:2)-soluble chitosan derivates were named as NOCHC and NOCPC. Samples with various carboxymethyl, hexanoyl and palmityl substitution degrees were named and shown in Table 7-1. For subsequent material characterization, chitosan-derived solutions of 1.3% (w/v) were prepared by dissolving obtained derivates in DI water. These solutions were then cross-linked with various amounts of genipin (molecular structure is shown in Scheme 7-1(a)) solution (1% w/v) to prepare hydrogels with same degree of cross-linking (constant amino residue/genipin ratio).

7.2.3. Material characterization

Proton nuclear magnetic resonance spectroscopy (^{1}H-NMR) spectra were used to confirm the sites and degrees of substitution recorded by NMR spectrometer (Varian unityinova 500) at 270 MHz. Attenuated total reflectance Fourier transformed infrared spectroscopy (ATR-FTIR) spectra were recorded on a spectrometer (Bomem DA8.3, Canada) using a film type sample (4 cm * 0.5 cm). The ATR-FTIR spectra were taken with a resolution of 2 cm^{-1} in the range of 4000-400 cm^{-1}. The state of water was characterized by a differential scanning calorimeter (DSC, Perkin Elmer instrument), which has been described in section 6.2.3.

7.2.4. Cytotoxicity test and cell attachment test

The cytotoxicity tests were performed by elution method following ISO 10993-5 standards. Fibroblast cells (L929) were cultured in the Dulbecco's modified eagle's medium (DMEM) containing 10% of fetal bovine serum and plated at a density of 2* 10^5 cells/well in

a 24-well plate at 37°C in 5% CO_2 atmosphere. After 24 hours of culture, the medium was replaced by extract fluids which were obtained by placing the NOCHC hydrogel (0.2 g/ml of culture medium) in cell culture medium at 37°C for 24 hours. In addition, the cells cultured in medium and in the medium containing dimethylsulphoxide (DMSO, Conc.=5%) at the same condition for 24 hours acting as negative and positive control, respectively. The adherent cells were trypsinized, centrifuged and re-suspended for vital cell counting by a hemacytometer combined with an inverted phase contrast microscope. For the cell attachment test, fibroblast cultures were prepared from the covering menings of the brain of Wistar rats. Cells were seed onto 6-well plate which was coated the NOCHC hydrogel. In addition, the culture onto the plate without coating at the same condition acting as a control group. After 24 hours of culture, The adherent cells were observed by an inverted phase contrast microscope.

7.2.5. Characterization of swelling ratio

The samples for swelling test were dried in vacuum chamber with P_2O_5 for 24 hours prior to the swelling test which was carried out by putting the sample in solution with various pH values (from pH=1 to 10) at 20°C for 48 hours. Swelling ratio (W_S) under equilibrium state was determined by Eqn. 7-(1):

$$W_S = (W_w - W_d)/W_d \qquad 7\text{-}(1)$$

where W_w and W_d are the weights of the sample after and before the swelling test.

7.2.6. Drug encapsulation efficiency and release test

Ibuprofen was employed as a partially hydrophobic model drug (molecular structure is shown in Scheme 7-1(b)). Ibuprofen-loaded monolithic films (matrix films) prepared by chitosan derivates were obtained using the film-casting method. In brief, chitosan/acetic acid solution, NOCC/DI water solutions and NOCHC/ethanol/DI water solutions with pH values of 7.0 were adjusted by NaOH solution (1M), followed by mixing these polymeric solutions

with saturated IBU/DI solution and genipin solution to form IBU-loaded polymeric solutions (IBU concentration: 1.2 mg/ml). Subsequently, those drug-loaded polymeric solutions were poured into Petri dish to form drug-loaded matrix films after cross-linking and drying at 50^{o}C for 2 days. In order to calculate the real encapsulation efficiency, these genipin-crosslinked matrix films were rinsed with ethanol solution for 30 seconds followed by measuring the amount of IBU rinsed out to ethanol solution (L_2) determined by UV-visible spectroscopy (Agelent 8453) at 264.4 nm through the use of pre-determined standard concentration-intensity curve. The IBU encapsulation efficiencies (E) could be determined by Eqn. 7-(2)

$$E=(L_1-L_2)/L_1 *100\% \qquad 7\text{-}(2)$$

where L_1 is the initial loading amount of IBU incorporated. The IBU release test was then carried out by putting the above-mentioned IBU-loaded membrane (~50 mg) in the quartz cuvette containing release medium (50 ml) with constant rotary-shaking at 37 ^{o}C. The release medium (phosphate-buffered solution, pH 7.4) was withdrawn for each juncture and replaced with an equial volume of fresh buffer. UV-visible spectroscopy (Agelent 8453) was used for the characterization of absorption peak at 264.4 nm to determine the released amount of ibuprofen through the use of pre-determined standard concentration-intensity calibration curve. The drug release profile was presented by plotting (M_t/M)-t curve, where M_t is the amount of drug released at time t, M is the amount of drug released at equilibrium state.

7.3. Results and Discussion

7.3.1. In vitro cytotoxicity test.

The cell viability of the newly synthesized carboxymethyl-hexanoyl chitosan is shown in Figure 7-1. As observed, no significant statistical difference ($p>0.05$) in survival cell population was detected between the negative control and NOCHC samples. However, all samples were significantly different ($p<0.05$) from the positive control. In addition, the degree

of hexanoyl substitution did not affect the number of vital cells. These preliminary results indicate that carboxymethyl-hexanoyl chitosan did not show any sign of cytotoxicity in vitro.

Figure 7-2 shows the cell morphology on the 6-well plates (a), NOCHC-2A immobilized plates and (b) NOCHC-2B immobilized plates after cell seeding for 24 h. The result indicates that cells extensively and randomly spread with spindle morphology on the non-coating well surface while all the cells on the NOCHC-2A surface remain round morphology. This is probably due to the the brush-like hydration layer of the plate coated with NOCHC-2A. Hence, compared with the plate without coating, the hydrophilicity was enhanced and the electrostatic attraction between plate and cell was inhibited for the plate coated with NOCHC. However, as the degree of hexanoyl substitution was increased (NOCHC-2B), the amount of adherent cells was slightly increased because the hydrophobic interaction between hexanoyl group and cell membrane could favor the formation of initial cell contact.

7.3.2. pH sensitive behaviors

The influences of carboxymethyl group on the pH-sensitivity of chitosan derivates are shown in Figure 7-3. As it can be seen, both samples NOCC-2 and NOCC-3 showed a similar pH sensitivity with a transition (i.e., the minimum swelling ratio) in the range from pH 7 to 8 which was due to the electrostatic attraction between COO^- and NH_3^+. When the pH value was below and above the transition point, the swelling ratio was increased due to the electrostatic repulsion caused by $NH_3^+ \cdots NH_3^+$ and $COO^- \cdots COO^-$, respectively. On the other hand, the influence of hexanoyl group on the swelling ratio under the condition of various pH values is also shown in Figure 7-3. It was found that the swelling ratios of NOCHC-2A and NOCHC-3A were higher than those of NOCC-2 and NOCC-3, respectively. In general, the swelling behaviors are determined by the intermolecular interactions such as hydrogen bonding, hydrophobic and electrostatic interactions, which depends on macromolecular structure and the state of water [150, 151]. Therefore, the influences of hexanoyl substitution

on macromolecular structure and the water state of the chitosan derivatives were characterized by ATR-FTIR and DSC tests to clarify the role of hexanoyl substitution in swelling ratio.

The ATR-FTIR spectra are shown in Figure 6-3. As compared with unmodified chitosan, it was found that the amide I characteristic peaks (1635 cm^{-1}) of samples NOCC-2 and NOCC-3 shifted significantly to lower wavenumber (red shifts δ= 20 cm^{-1}). This was ascribed to the formation of intermolecular hydrogen bonding between the amide group and carboxylic group ($O=CNH_2\cdots O=COH$) in NOCC because this hydrogen bonding is stronger than that in un-modified chitosan (amide resonance H-bonding: $O=CNH_2\cdots O=CNH_2$) since the dipole moment of an N-H bond is smaller than that of an O-H bond [158]. Interestingly, the red shift for amide I characteristic peak observed for samples NOCHC-2A and NOCHC-3A was of a lesser extent than that for samples NOCC-2 and NOCC-3, respectively. Additionally, the characteristic peaks at 1723 cm^{-1} assigned to carboxymethyl dimmer were broadened and shifted to higher wavenumber region for samples NOCHC-2A and NOCHC-3A. These two findings in the ATR-FTIR spectra suggest that the intermolecular hydrogen bonding (i.e., $O=CNH_2\cdots O=COH$, $O=COH\cdots O=COH$) in sample NOCC was inhibited to a certain extent (H-bonding inhibition effect) as the hexanoyl group was introduced.

The above-mentioned H-bonding inhibition effect can be further evidenced via exploring the influence of hexanoyl substitution on the water state of the samples with the same water-absorption ratio (W_C = 2), which was characterized by DSC test and shown in Figure 6-6. As it can be seen, a heavily overlapped band (solid line) was observed and could be divided into three peaks (dash lines) using the Lorentzian curve-fitting procedure. In Figure 6-6(a), all endothermic peaks were much lower than 4.8°C, indicating free water was not observed for the NOCC-3 hydrogel even under fully-swollen state (W_C=2, which is almost equal to the W_S value of NOCC-3). However, as shown in Figure 6-6(b), the peak III of sample NOCHC-3A was very close to 4.8°C, revealing that the NOCHC-3A hydrogel contained free water at and above W_C=2. This result together with the ATR-FTIR result

demonstrate that the intermolecular volume for free water was increased with the introduction of hexanoyl substitution because it inhibited the intermolecular bonding (polymer-polymer interaction). On this base, the swelling ratio of samples NOCC-2 and NOCC-3 were significantly enhanced as the hexanoyl group was introduced (NOCHC-2A and NOCHC-3A). Furthermore, once the intermolecular H-bonding (i.e., $O=CNH_2\cdots O=COH$, $O=COH\cdots O=COH$) were inhibited by the hexanoyl substitution, the electrostatic repulsion ($NH_3^+\cdots NH_3^+$ and $COO^-\cdots COO^-$) became the dominant role of intermolecular interactions while pH value was less than 2 and larger than 9. In addition, the electrostatic repulsion force was not inhibited in the presence of hexanoyl substitution because the formation of electrostatic force is unlike hydrogen bonding which needs a specific distance and angle. Therefore, a more prominent pH-sensitivity behavior was observed for the NOCHC samples compared with those NOCC samples with the same degree of carboxymethyl substitution. Moreover, this phenomenon became more pronounced while amino group was substituted by a longer side-chain (NOCPC) as shown in Figure 7-4. The swelling ratios of NOCPC at low and high pH values were much higher than those of NOCHC-3A.

7.3.3. Drug release behaviors.

Figure 7-5 illustrates the IBU release profiles from NOCHC films. It was found that NOCHC samples with carboxymethyl substitution of 0.3 (NOCHC-2A and NOCHC-2B) showed a pronounced bursting behavior in the first 2 hours during which 83% of IBU were released, followed by a near zero-order release behavior. In contrast, NOCHC samples with carboxymethyl substitution of 0.5 (NOCHC-3A and NOCHC-3B) showed a fast release behaviors following Higuchi model in the initial time period, a subsequent near zero-order release was followed. The IBU released in the first stage was assigned to the IBU molecules which did not tightly interact with polymer chains. Therefore, a faster release rate was detected in the NOCHC sample with carboxymethyl substitution degree of 0.3 compared with

that of 0.5 in the initial stage because the latter has a denser network structure. The subsequent near-zero order release occurring in all the NOCHC samples was probably correlated with the IBU molecules that were tightly cross-linked with polymer chains via intermolecular forces included hydrophobic interaction, electrostatic attraction and hydrogen bonding. This was favorable for the stabilization of polymer-drug network and led to a lower drug mobility. Therefore, the IBU released in the second stage was mainly dependent on the swelling of polymer-drug network whose rate was relatively low compared with that in the first stage. In addition, diffusion rate in the second stage is much higher than that in the first stage because the highly swollen polymer network became loose and full of water. Hence, the IBU release in the second stage was considered as a swelling control mechanism.

7.4. Conclusion

Amphipathic hydrogel derived from chemically-modified chitosan was successfully synthesized through bearing both carboxymethyl and hexanoyl substitutions. The pH-sensitivity was dependent on the degree and nature of such substitution. Moreover, hexanoyl substitution enhanced significantly the swelling ratio and pH-sensitivity by changing intermolecular interaction and the state of water. Improved encapsulation efficiency and less busting release behaviors for ibuprofen were achieved for the sample with high hexanoyl and carboxymethyl substitution. It is feasible to employ NOCHC hydrogel as a novel and potential amphipathic carrier to effectively encapsulate and deliver numerous amphipathic drugs, such as vancomycin and naproxen, for cell encapsulation or wound dressing material with excellent water-retention ability and pre-designed drug release function for enhanced therapeutic efficacy.

Table 7-1: Sample name and corresponding estimation of substitution degree by ^{1}H-NMR.

	Degree of substitution	
	Carboxymethyl group	Hexanoyl group
Chitosan	0	0
NOCC-2	0.32	0
NOCHC-2A	0.32	0.26
NOCHC-2B	0.32	0.46
NOCC-3	0.50	0
NOCHC-3A	0.50	0.26
NOCHC-3B	0.50	0.48
	Carboxymethyl group	Palmityl group
NOCPC	0.50	0.40

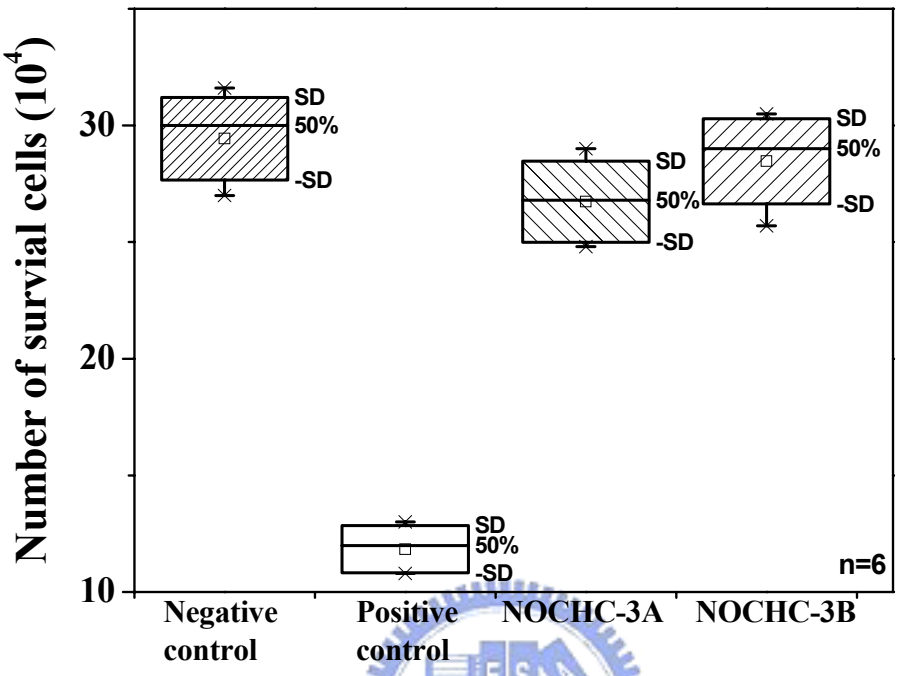

Figure 7-1. Cytotoxicity of NOCHC samples with carboxymethyl substitution degree of 0.5.

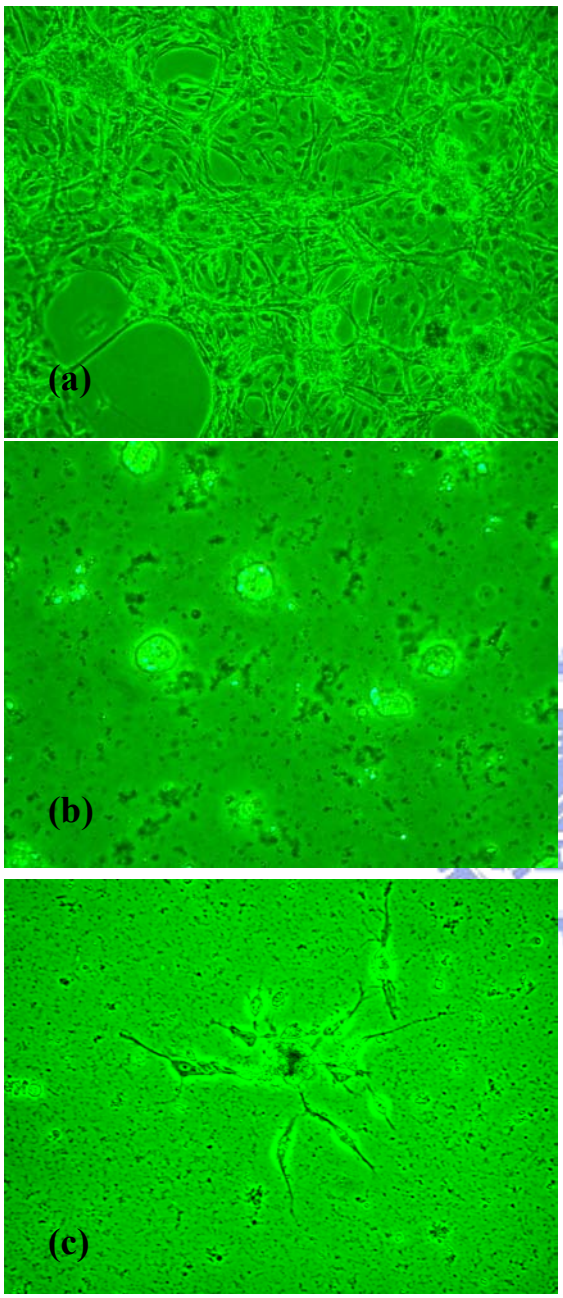

Figure 7-2. Cell morphology on the 6-well plates (a), NOCHC-2A immobilized plates and (b) NOCHC-2B immobilized plates after cell seeding for 24 h.

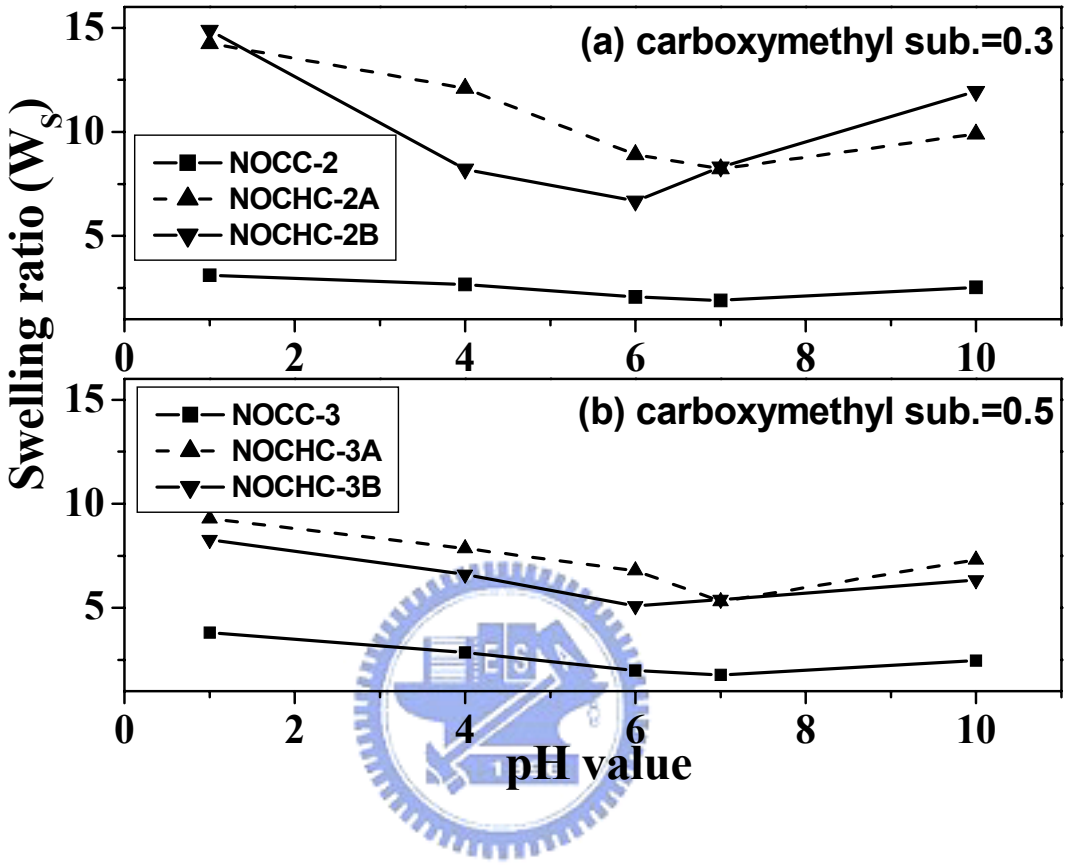

Figure 7-3. Dependence of carboxymethyl and hexanoyl groups on pH values.

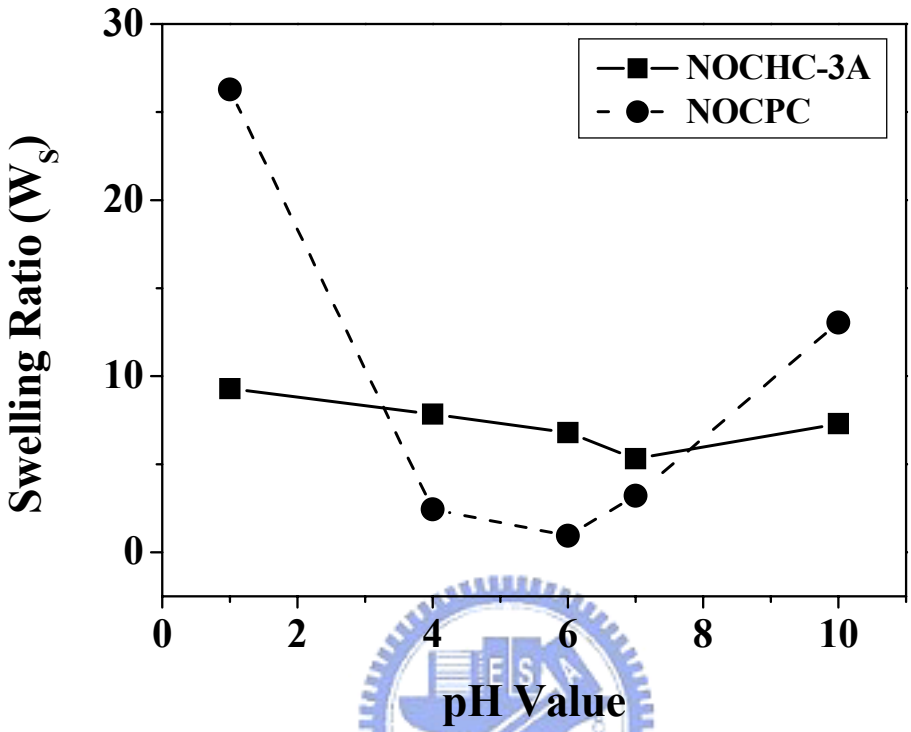

Figure 7-4. Dependence of the swellng ratio of NOCHC-3A and NOCPC samples on pH values.

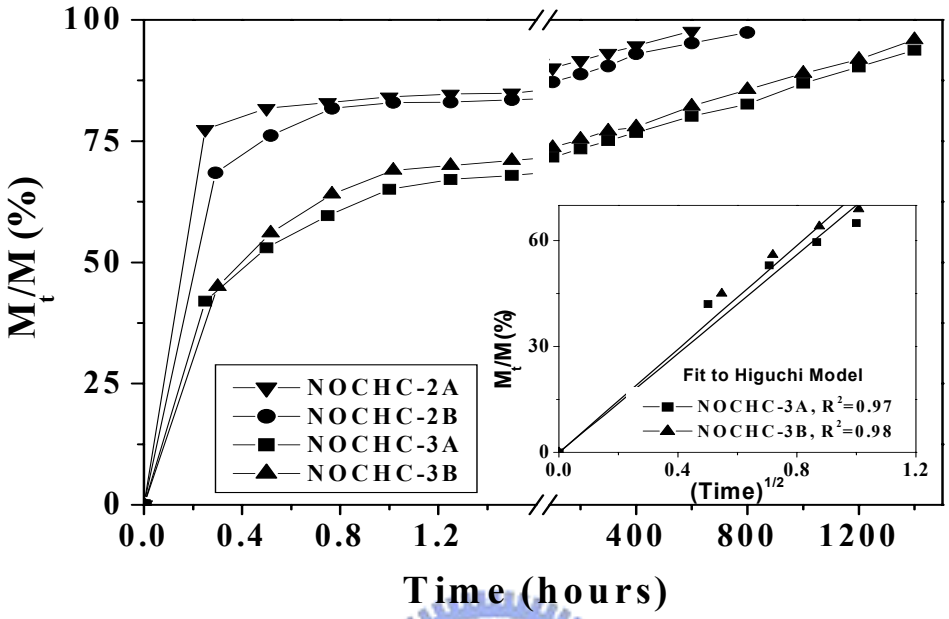

Figure 7-5. Ibuprofen release profiles of NOCHC samples.

CHAPTER 8

Effect of Hydroxyapatite Nanoparticles on Ibuprofen Release from Carboxymethyl-hexanoyl chitosan / *O*-hexanoyl chitosan Hydrogel

8.1. Introduction

Hydrogel-based scaffold has been used for delivering cells with bioactive agents [140]. In recent years, much attention has been focused on chitosan (CS) hydrogels for cartilage tissue engineering and bone substitute with controlled release function because CS is structurally similar to natural glycosaminoglycan (GAG) [139, 164, 165].

Chitosan is a cationic polysaccharide with an isoelectric point (IEP) of 6.2. It is soluble in diluted acids and the resulting gelled-solution aggregates under neutral physiological conditions [166], which is unfavorable for encapsulating the bioactive agents which denature in acidic environments. On the other hand, many amphiphilic bioactive agents, such as vancomycin and ibuprofen, prefer to be dissolved in water-miscible organic solvents. On this base, novel carboxymethyl-hexanoyl chitosan (NOCHC) with amphiphilic and water-soluble nature was synthesized for the first time via selecting *N,O*-carboxymethyl chitosan (NOCC) as a starting precursor. The highly swollen NOCHC under neutral physiological conditions can be considered to be a candidate hydrogel-based material for delivering cells, growth factors and the therapeutic agent with partial hydrophobicity.

However, therapeutic agents rapidly release from highly swollen hydrogel due to its loose structure [167]. In order to extend the drug release period of NOCHC hydrogel, biodegradable microspheres made of hydrophobic *O*-hexanoyl chitosan (OHC) were embedded within the NOCHC matrix, which is expected to achieve sustained release behaviors. On the other hand, the drug release kinetics (permeability and diffusion exponent) of chitosan can be further regulated by the incorporation of Ca-deficient hydroxyapatite

(CDHA, Ca/P = 1.5) nanoparticles since it has long been employed to improve the mechanical strength and osteoconductivity of chitosan [58, 116, 168]. However, the influence of the nanofiller on the resulting physical characteristics of the polymeric phase has been not consistently reported due to differing polymer characteristics and various extent of polymer-nanofiller interaction [126, 127], implying that the role of the CDHA nanoparticle in the NOCHC and OHC may be critical and is worth further exploring.

Therefore, the major research objective of this study is to explore the role of CDHA nanoparticle in the release behavior of ibuprofen (IBU, an anti-inflammatory drug with amphiphilic nature) released from NOCHC and OHC. In addition, sustained and sequential release of IBU from the NOCHC/OHC microsphere-embedded hydrogel was also investigated. This study is expected to provide a fundamental understanding of the amphiphilic NOCHC hydrogel used for medical applications and in particular, drug delivery.

8.2. Experiment materials and methods

8.2.1 Materials

Chitosan (M_w = 215,000 g $\cdot$ mol^{-1}) with 80% degree of deacetylation was supplied from Aldrich-Sigma. Ibuprofen was purchased from Aldrich-Sigma (I4883).

8.2.2 Methods

8.2.2.1 Synthesis NOCHC and OHC

NOCHC was synthesized using NOCC as a starting precursor. The synthesis of NOCC with a controlled degree of substitution has been reported [169]. In brief, 5 g of chitosan were dissolved in isopropanol (50 ml) at room temperature while being stirred for 30 minutes. The resulting suspension was gently mixed with 12.5 ml of NaOH solution (13.3 N), followed by mixing with 7 g of chloroacetic to prepare the NOCC sample with carboxymethyl substitutions of 0.5. This suspension was stirred for 30 minutes and heated to 60 ^{o}C for 4

hours, followed by filtration and washing by methanol solution. After drying, the obtained NOCC sample (2 g) was dissolved in distilled water (50 ml) while being stirred for 24 hour. The resulting solution was mixed with methanol (50 ml) at room temperature, followed by the addition of hexanoyl anhydride (0.7 ml) with hexanoyl substitution of 0.26. Following the reaction time of 12 hours, the resulting solution was collected by dialysis membrane (Aldrich-Sigma, D6191).

Synthesis of OHC has been reported [170]. In brief, chitosan (3 g) was suspended in 40 ml of methanesulfonic acid. This mixture was then mixed with hexanoyl anhydride (28.64 ml) and stirred at 60 ^{o}C for 6 hours followed by fast cooling to room temperature. The pH value was adjusted to 7 by neutralization with NaOH. The resulting precipitate was filtered, washed and dialyzed to remove the unreacted acid and ions followed by overnight drying at 60 °C.

8.2.2.2 Material characterization

Proton nuclear magnetic resonance spectroscopy (^{1}H-NMR) spectra were used to confirm the sites and degrees of substitution. The samples were dissolved in D_2O and the spectra were recorded by NMR spectrometer (Varian unityinova 500) at 270 MHz. Dynamic mechanical analysis (DMA) was performed on cut strips (2 cm long and 0.5 cm wide) using a TA Instruments 2980 dynamic mechanical analyzer from -130 to 50 ^{o}C with a frequency of 1 Hz and a heating rate of 3 ^{o}C/min. The samples were dried in a vacuum chamber with P_2O_5 for 72 hours prior to the DMA test. The morphology of CDHA incorporated in composite membranes was observed through the use of transmission electron microscopy (TEM, JEOL-2000FX). The microsphere-embedded hydrogel implant was observed via using scanning electron microscopy (SEM, JOEL- JSM-6500F).

8.2.2.3 Drug-loaded NOCHC-based and OAC-based monolithic membranes

Hydroxyapatite nanoparticle suspension containing calcium-deficient hydroxyapatite

(CDHA) nanoparticles with a Ca/P molar ratio of 1.5 were fabricated by the co-precipitation method with $Ca(CH_3COO)_2$ and H_3PO_4 as Ca and P precursors, respectively [171]. The resulting hydroxyapatite suspensions with various CDHA concentrations were mixed with NOCHC/3 % ethanol solution (7.5 mg/ml, 100 ml) and ibuprofen/3 % ethanol solution (6 mg/ml, 50 ml). The mixtures were cross-linked with genipin solution (1% (w/v)) at 50 ^{o}C for 48 hours. The cross-linked NOCHC-CDHA hybrid composites with various CDHA amounts (0%, 1%, 5%, 10%) loaded with ibuprofen (weight ratio of ibuprofen/NOCHC = 40 %) were obtained after air drying at room temperature for 5 days. On the other hand, for the preparation of IBU-loaded OHC-CDHA hybrid composites, the above-mentioned hydroxyapatite suspensions were filtered and dried at room temperature for 2 hours. The obtained precipitates were then re-suspended in butanol. These suspensions with various CDHA concentrations were mixed with the OHC/dichloromethane polymeric solution (15 mg/ml, 50 ml) and the ibuprofen/ethanol solution (70 mg/ml, 10 ml). OHC-CDHA hybrid composites with various CDHA amounts (0%, 1%, 5%, 10%) were obtained following solvent evaporation and post vacuum drying at 80 ^{o}C for 48 hours.

8.2.2.4 Preparation of NOCHC/OHC microsphere-embedded hydrogel

The NOCHC/OHC microsphere-embedded sponge was fabricated via using the oil-in-water emulsion method. In brief, 1 ml of the above-mentioned IBU-loaded OHC/dichloromethane solution was added into 3 ml of IBU-loaded NOCHC/3 % ethanol solution with ultrasonic vibration followed by liquid N_2 quenching and vacuum drying at -80 ^{o}C for 48 hours (lyophilization).

8.2.2.5 Drug release test

The IBU-loaded composite membrane (~50 mg) was rinsed with distilled water, followed by carrying out the release test in the quartz cuvette containing release medium (50

ml) with constant rotary-shaking at 37 ^{o}C. The release medium (phosphate-buffered solution, pH 7.4) was withdrawn for each juncture and replaced with an equivalent volume of fresh buffer. UV-visible spectroscopy (Agelent 8453) was used for the characterization of absorption peak at 264.4 nm to determine the released amount of ibuprofen through the use of pre-determined standard concentration-intensity calibration curve. The drug release profile was presented by plotting (M_t/M)-t curve, where M_t is the amount of drug released at time t, M is the amount of drug released at equilibrium state.

8.3. Results and discussion

Carboxymethyl-hexanoyl chitosan was synthesized via using NOCC as a starting precursor. Upon substitution reaction, hydrogen atoms in some of amino groups (*N*-position) can be replaced by the hexanoyl groups. Figure 8-1 shows the molecular structures and the ^{1}H-NMR spectra of NOCHC and NOCC. As shown in Figure 8-1(a), the chemical shifts at 0.75 ppm (-CH_3), 1.06 ppm (-$C_\gamma H_2$-$C_\delta H_2$-), 1.28 ppm (-$C_\delta H_2$-), 1.48 ppm (-$C_\beta H_2$-) and 2.18 ppm (-CO-$C_\alpha H_2$-) were assigned to the protons in the hexanoyl group. Moreover, the chemical shift at 3.22 ppm was assigned to the proton at the amide bonding. On the other hand, the chemical shifts at 4.2 and 4.4 ppm were designated to the protons of –CH_2–COO^- at C2 (*N*-position) and at C6 (*O*-position) of the NOCHC, respectively. This demonstrates hexanoyl substitution occurring on some of the amino sites of the *N,O*-carboxymethyl chitosan.

In this study, synthesized CDHA nano-powder was dispersed into the NOCHC solution, where the NOCHC was derived from the NOCC sample with the carboxymethyl group. The resulting solution showed a low viscosity at pH 7 and was favorable for the dispersion of CDHA nanoparticles, as evidenced by TEM photographs shown in Figure 8-2(a). The TEM image indicates that the needle-like CDHA nanoparticles (SAD pattern of CDHA is shown in Figure 8-2(b)), with dimensions of 10-20 nm in diameter and 70-100 nm in length, dispersed in the NOCHC matrix. Also shown in Figure 8-2(c), CDHA nanoparticles were also

well-dispersed in the OHC matrix. It can be explained as follows: Following the aqueous synthesis process, the CDHA nanoparticles collected from the filter paper can be re-suspended in butanol without aggregation because the high surface tension of residual water around CDHA particles can be significantly lowered by butanol. In addition, electrostatic attraction between NH_3^+ (OHC chains) and PO_4^{3-} (negative-charged sites of CDHA crystals) could provide the stable force for colloid, which favors the dispersion of CDHA.

The influence of CDHA nanoparticles on the release profile of IBU from the OHC-CDHA monolithic membranes is shown in Figure 8-3. It was found that a single-stage release with a diffusion-controlled mechanism was observed for the pure OHC membrane and also the OHC-CDHA hybrid membrane containing 1% of CDHA. This was due to the hydrophobic nature of OHC that limits water accessibility. However, as CDHA content increased to 5%, a two-stage behavior was observed. For the diffusion-controlled stage (first stage) of all OHC-CDHA hybrids, the path length of diffusion was increased as the amount of the well-dispersed CDHA nanoparticles was increased, resulting in a lower diffusion coefficient. On the other hand, for the OHC-CDHA hybrid membranes containing CDHA of 5% and 10%, it was found that the first release stage was followed by a fast release stage which was due to the degradation of OHC [172]. The degradation of hydrophobic OHC was enhanced by the well-dispersed CDHA nanoparticles (without strong filler-polymer interaction) which can significantly reduce the hydrophobic interaction (physical cross-link). This could be further evidenced by dynamic mechanical analysis (DMA) as shown in Figure 8-4(a). The height of α-peak was increased and the T_g of OHC was decreased as the CDHA content increased, suggesting the degree of cross-linking decreased with increasing CDHA content [120]. Accordingly, the OHC degradation rate was enhanced causing a high second-stage release rate. Furthermore, once degradation occurs, the long-range molecular motion (i.e., relaxation rate) of OHC in the second release stage will be further enhanced. Consequently, the release rate of the second stage was significantly raised through increasing

CDHA content.

The differing influences of CDHA nanoparticles on the release profiles of the NOCHC-CDHA monolithic membranes are shown in Figure 8-5(a). As it can be seen, a bursting release behavior was observed for the pure NOCHC sample due to its high swelling ratio (loose intermolecular structure). However, the release profile was altered as the NOCHC samples were incorporated with CDHA. The diffusion exponents (n) of the NOCHC samples incorporated with CDHA of 1% to 10% can be determined by plotting Log(M_t/M)-Log(t) and using Eqn. 8-(1):

$$(M_t/M) = kt^n \qquad 8\text{-}(1)$$

where k is a constant and n is diffusion exponent related to the diffusion mechanism. As shown in Figure 8-5(b), a non-Fickian ($0.5 < n < 1$, diffusion rate ~ swelling rate) diffusion was observed for the NOCHC membranes incorporated with CDHA of 1% and 5%. As the amount of CDHA was further increased to 10%, a Fickian diffusion ($n = 0.5$, diffusion rate << swelling rate) was observed, indicating that the drug release followed a diffusion-controlled mechanism. This can be further explained in terms of the influence of CDHA on swelling rate and diffusion rate as follows. Based on our previous study, well-dispersed CDHA nanoparticles are acting as a physical cross-linker in hydrophilic chitosan derivate [173], which was contrary to the case of OHC. This was attributed to the fact that the filler-polymer interaction of NOCHC-CDHA was stronger than that of OHC-CDHA [124, 125], which was evidenced by the DMA curve shown in Figure 8-4(b). It was found that the α-peak broadened as CDHA content increased, suggesting that the extent of cross-link increased with increasing CDHA content [173]. Hence, the swelling rate decreased with increasing CDHA content. However, a swelling-controlled mechanism was not observed for the sample with a CDHA content of 10%. On the contrary, the n value was observed to decrease with increasing CDHA content (i.e., towards to diffusion-controlled mechanism), suggesting that CDHA plays a more significant role in the diffusion rate than the swelling rate. This is due to the fact that

well-dispersed CDHA nanoparticles act as a diffusion barrier, causing a significant decrease in the diffusion coefficient as mentioned previously. Moreover, strong filler-drug interaction (electrostatic attraction: CDHA-$Ca^{2+}\cdots^{-}$OO=C-IBU) and high cross-link extent (tight intermolecular structure) also probably lowered the mobility of IBU diffusing through NOCHC matrix. Therefore, the diffusion-controlled mechanism became dominant in this condition.

Recently, sequential release of dual growth factors has been reported because of its potential to enhance wound healing and osteogenesis [96]. In addition, the concept of using combination antibiotic therapy to decrease antibiotic-resistance has been reported [97, 136]. Moreover, many hydrophobic bioactive agents, such as paclitaxel and naproxen, should preferably be dissolved in organic solvents. Therefore, it is feasible to design a microsphere-embedded hydrogel to efficiently encapsulate a variety of bioactive agents with a wide range of hydrophilic/hydrophobic nature for either simultaneous release or sequential release via regulating the amount of CDHA nano-phase. Based on those reasons, the hydrophobic OHC microspheres were incorporated into the amphiphilic NOCHC matrix to form a porous sponge as shown in Figure 8-6. As can be seen, microspheres with a diameter of 0.7-1.5 um were uniformly embedded in the NOCHC matrix. This was due to the similar structure (i.e., both containing hexanoyl and amino groups) and counter-charged character (COO^- in NOCHC, NH_3^+ in OHC) which are favorable for the dispersion and stability of hydrophobic microspheres in the hydrophilic matrix without the use of surfactant. The sequential release behavior of the NOCHC/OHC microsphere-embedded hydrogel is shown in Figure 8-7. As can be seen, the fast release profile of the highly swollen hydrogel such as NOCHC could be altered by incorporating the microspheres or nanospheres made of hydrophobic OHC, where a sequential release behavior was observed. It can then be concluded that the release profile of the NOCHC hydrogel could be manipulated by the incorporation of CDHA nanoparticles and OHC microspheres.

8.4. Conclusion

Novel biocompatible hybrid composites consisting of NOCHC amphiphilic hydrogel and hydrophobic OHC microspheres with sequential release behaviors were successfully synthesized for drug delivery purpose. It was found that drug release kinetics of the hydrophilic phase (NOCHC) and the hydrophobic phase (OHC) were both affected by the incorporation of CDHA nanoparticles. Hence, CDHA nanocrystal could concurrently play roles as a bioactive filler and drug release regulator. This study may provide valuable information for a better design of chitosan hydrogel-based drug-loaded implant with improved bioactivity and controlled drug release function.

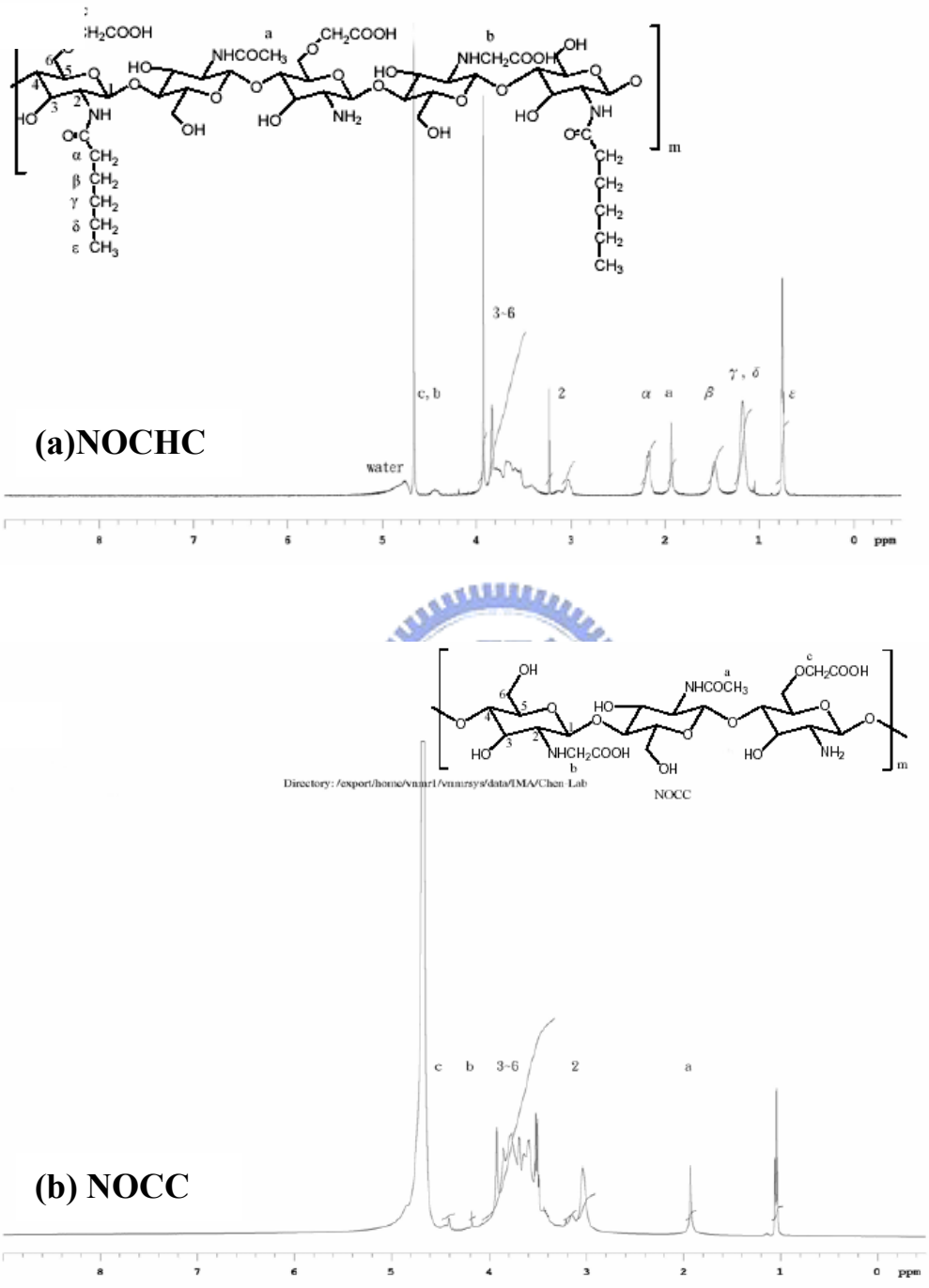

Figure 8-1. Proton NMR spectra and molecular structures of (a) NOCHC and (b) NOCC.

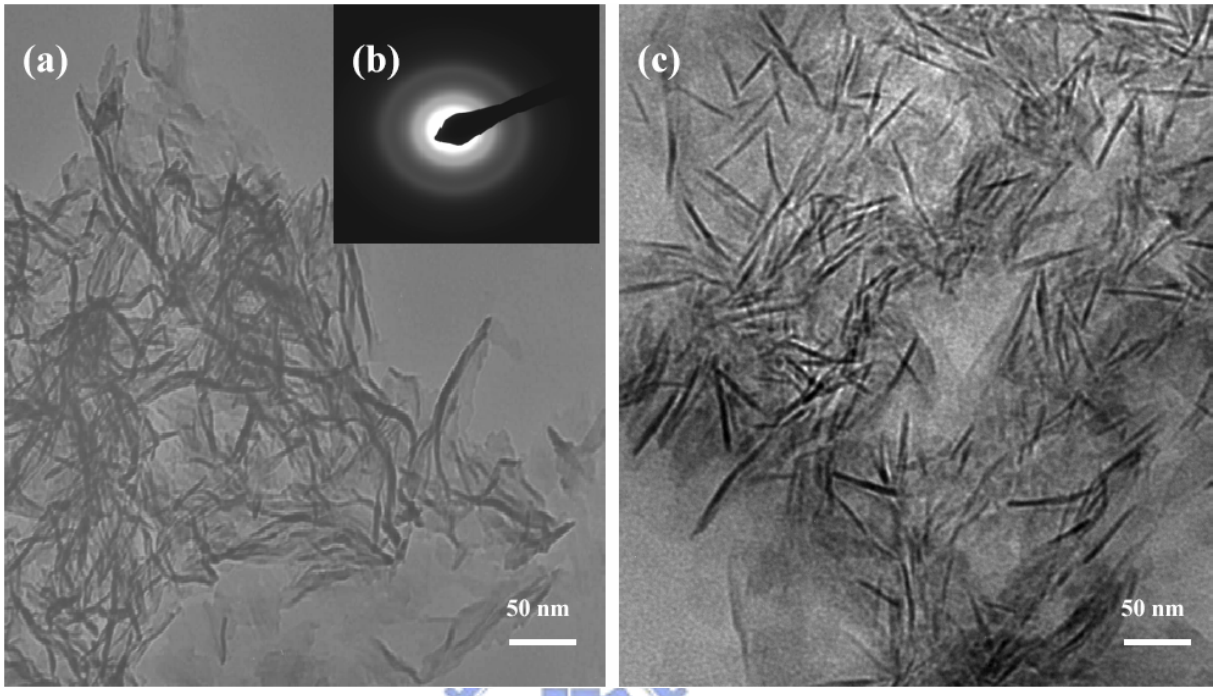

Figure 8-2. TEM images of (a) NOCHC-CDHA nano-composite membrane, (b) selected-area electron diffraction (SAD) pattern of CDHA, and (c) OHC-CDHA nano-composite membrane.

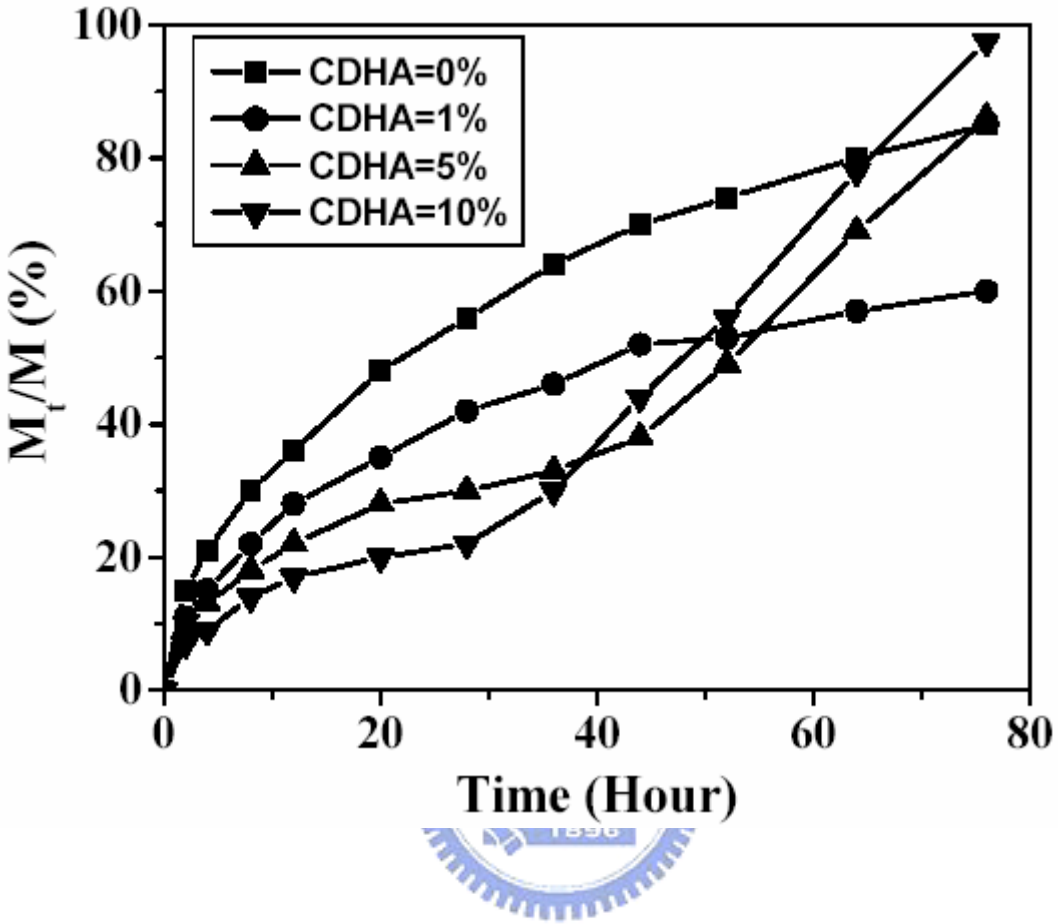

Figure 8-3. Influence of CDHA amount on the release profiles of OHC-CDHA monolithic membranes.

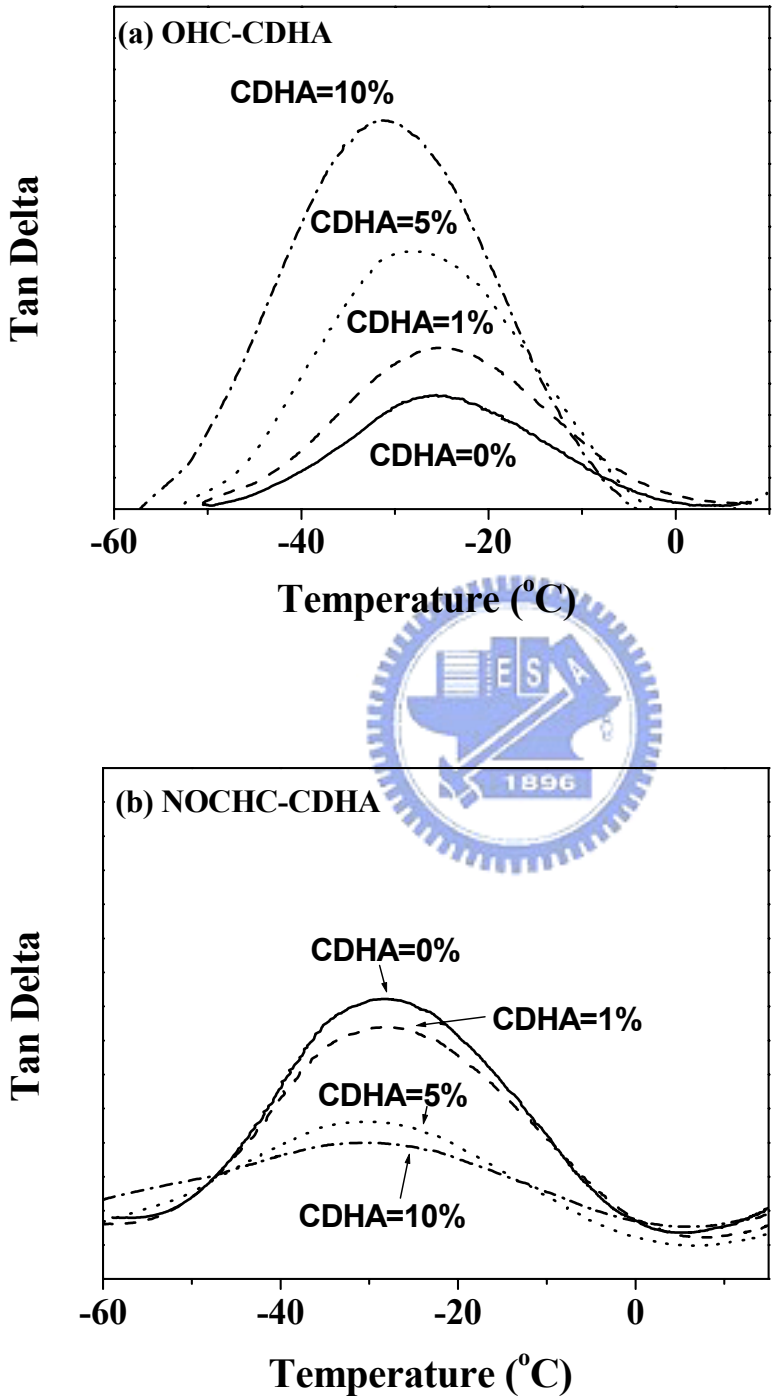

Figure 8-4. DMA curves of (a) OHC-CDHA and (b) NOCHC-CDHA monolithic membranes.

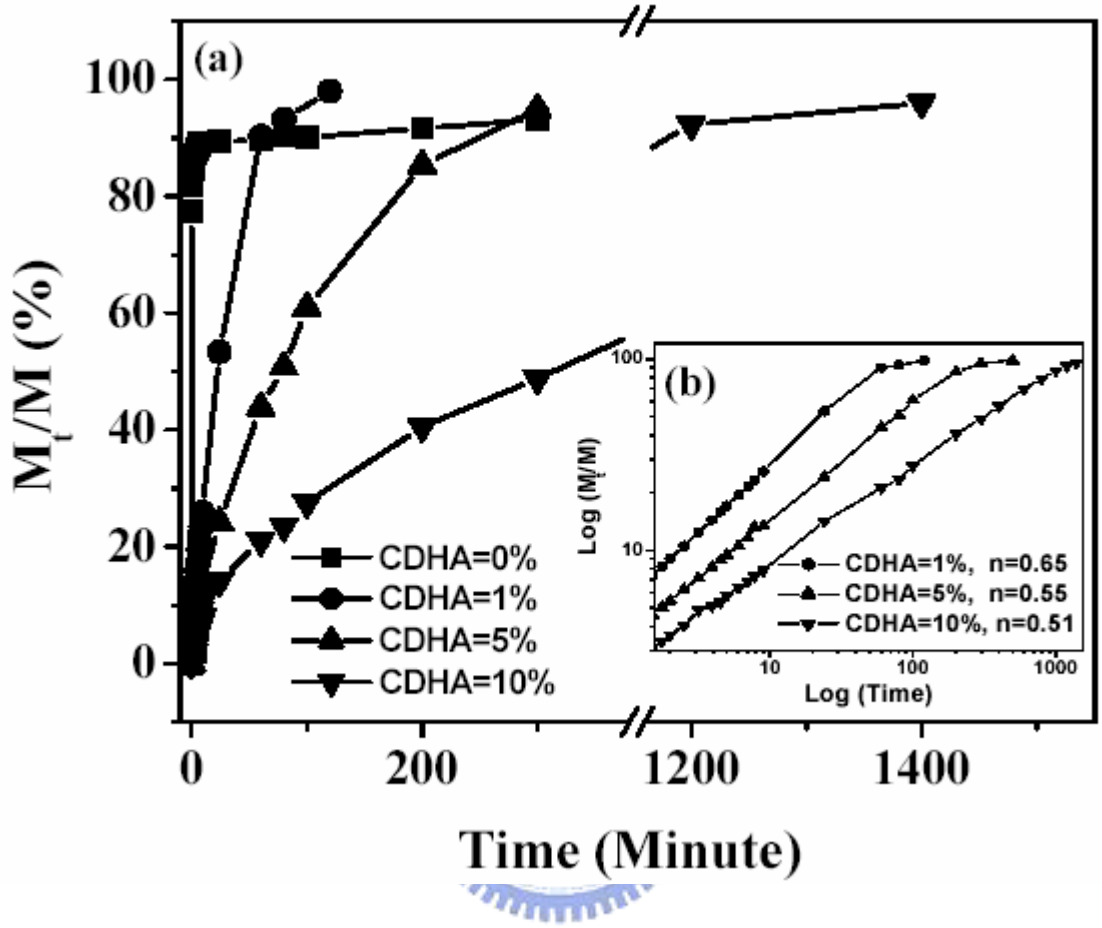

Figure 8-5. Influence of CDHA amount on the release profiles of NOCHC-CDHA monolithic membranes: (a) Linear scale; (b) logarithmic scale.

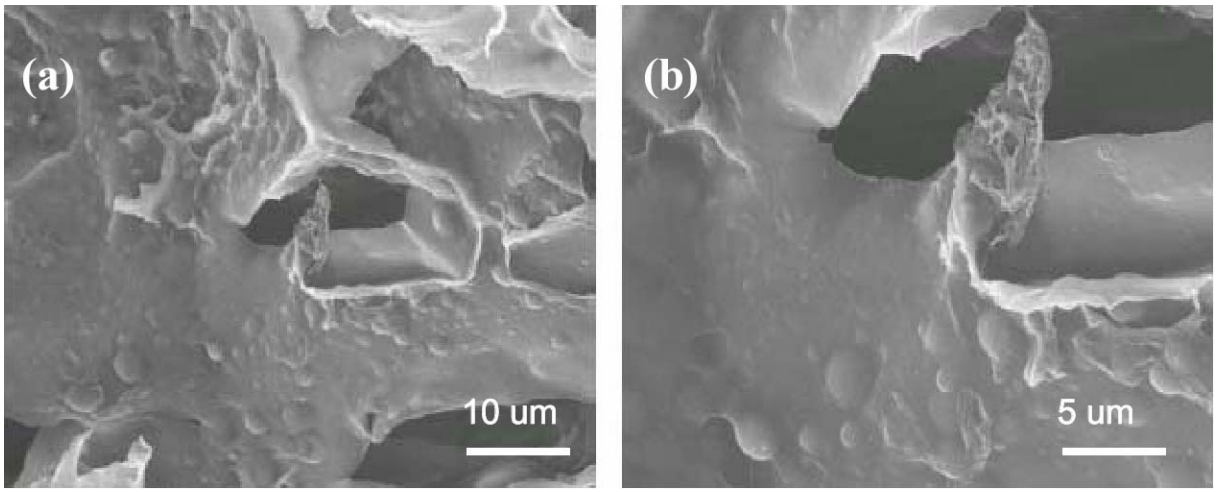

Figure 8-6. SEM images of NOCHC/OHC microsphere-embedded porous sponge: (a) 2500X; (b) 5000X.

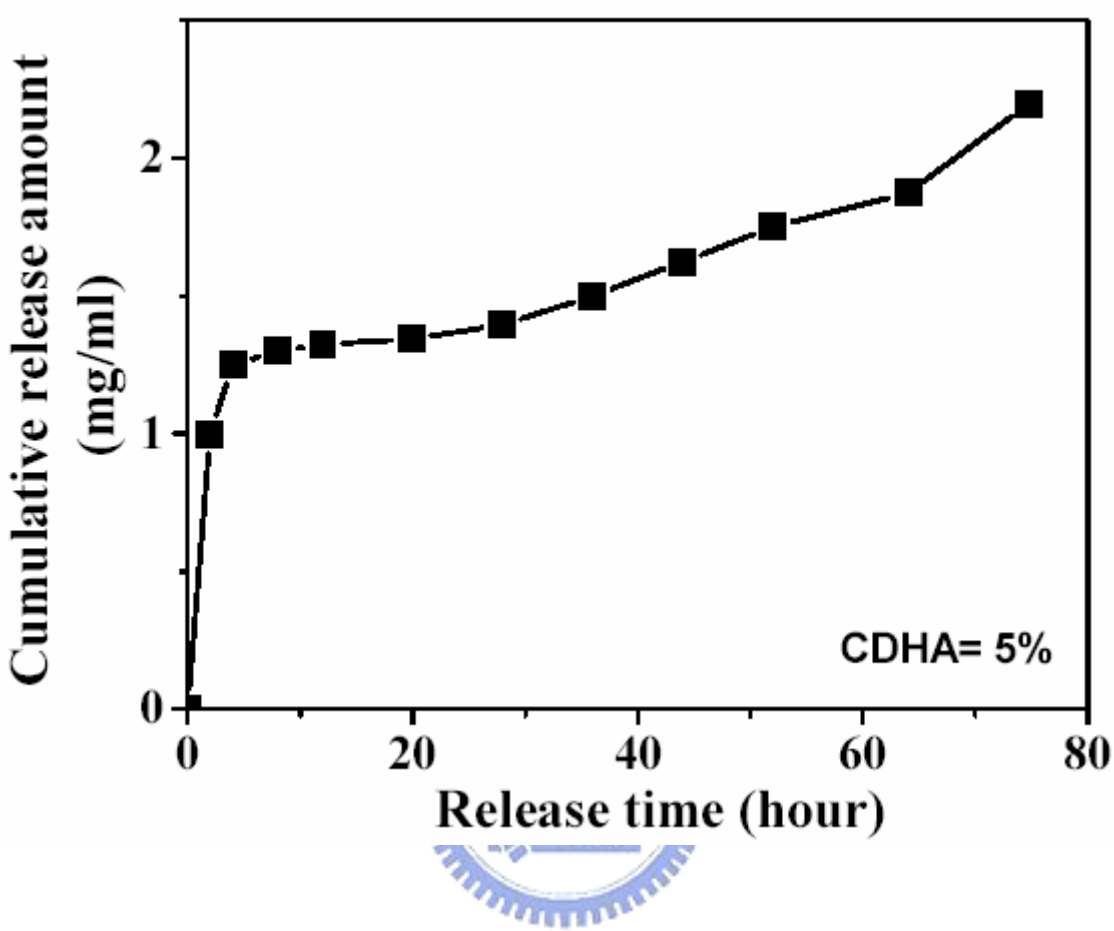

Figure 8-7. Sequential release profile of NOCHC/OHC microsphere-embedded sponge.

CHAPTER 9

Conclusions

9.1. Influence of the aspect ratio of bioactive nano-fillers on rheological behavior of PMMA-based orthopedic materials

The influence of particle aspect-ratio on packing efficiency is significant and a critical value of the aspect ratio was determined to be 8.8. With increasing the aspect ratio, especially above the critical value, the nano-needles result in an extensive contact between the particles upon which a poorer packing efficiency, higher yield strength and poorer flowability of the mixture suspension can be observed. The maximum solid loadings of nano-CDHA particles with aspect ratio 7, 10, and 17 were determined to be 28%, 31% and 57% respectively.

9.2. BSA-loaded calcium-deficient hydroxyapatite nano-carriers for controlled drug delivery

The amount of BSA uptake was dependent on the solution pH and processing variation. Moreover, both synthetic process and pH value upon synthesis significantly altered the drug release behaviors of BSA-loaded CDHA nano-crriers. It is feasible to employ the CDHA nano-carrier to load protein, such as acid growth factor and acid protein-drug conjugation, as component of bone substitutes or as a reinforced filler together with a pre-designed drug release function for particular therapeutic effect.

9.3. Drug release behaviour of CDHA/Chitosan nanocomposites-Effect of CDHA nanoparticles

Both the amount of CDHA incorporated and the synthetic process altered significantly the extent of filler-polymer interaction, which influences strongly the diffusion exponent and permeability of CDHA/chitosan nanocomposites. Hence, CDHA nanocrystal could concurrently play the roles as bioactive nanofiller and drug-release regulator. This study may provide valuable information for a better design of chitosan-based orthopedic devices with improved bioactivity and controlled drug release function.

9.4. Synthesis and characterization of amphiphatic carboxymethyl-hexanoyl chitosan hydrogel

Amphiphatic hydrogel derived from chemically-modified chitosan was successfully synthesized through bearing both carboxymethyl and hexanoyl substitutions. Water-absorption ability decreased with increasing substitution of the carboxymethyl group but was significantly increased with the introduction of the hexanoyl group because it altered the number of water-binding sites and the state of water under low humidity and the fully-swollen condition, respectively. Moreover, compared with NOCC, NOCHC also demonstrated enhanced water-retention ability. Besides, the pH-sensitivity was dependent on the degree and nature of such substitution. The hexanoyl substitution enhanced significantly the swelling ratio and pH-sensitivity by changing intermolecular interaction and the state of water. On the other hand, improved encapsulation efficiency and less busting release behaviors for ibuprofen were achieved for the sample with high hexanoyl and carboxymethyl substitution. Moreover, release behaviors of NOCHC can be regulated via incorporating the hydrophobic OHC microspheres and CDHA nanoparticles into NOCHC matrices. It was found that drug release kinetics of the hydrophilic phase (NOCHC) and the hydrophobic phase (OHC) were both affected by the incorporation of CDHA nanoparticles. Hence, CDHA nanocrystal could concurrently play roles as a bioactive filler and drug release regulator. It is

feasible to employ NOCHC hydrogel as a potential amphipathic carrier to effectively encapsulate amphipathic drugs an cell for wound dressing material with excellent water-retention ability and pre-designed drug release function.

REFERENCE

[1] Wilson M, Nanotechnology, Chapman & Hall/CRC, 2002.

[2] Bonnell DA, "Materials in nanotechnology: New structures, new properties, new complexity", J. Vac. Sci. Technol., A 21, pp. 194-206, 2003.

[3] Rosei F, "Nanostructured surfaces: challenges and frontiers in nanotechnology", J. Phys.: Condens. Matter., 16, pp. S1373-S1436, 2004.

[4] Kenneth, J. Klabunde, Nanoscale Materials in Chemistry, John Wiley & Sons, Inc, 2001.

[5] Ratner BD, Biomaterials Science : An Introduction to Materials in Medicine, San Diego Elsevier, 1996.

[6] Teoh SH, Engineering Materials for Biomedical Applications, Hackensack, NJ, Singapore World Scientific Publishing Co., 2004.

[7] Osborn JF, Implantatwerkstoff hydroxylapatitikeramik grundlagen, Kliniske Anwendung Quintessenz, Springer-Verlag A.G., Berlin, 1985.

[8] De Groot K, "Bioceramic consisting of calcium phosphate salts", Biomaterials, 1, pp. 47-50, 1980.

[9] Bauer G, Hohenberger G, Ursachen des unterschiedliches Verhaltens von bioactiven Calciumphosphatkeramiken im Organismus (Causes of behavioral variation of bioactive calcium phosphate ceramics in living organisms), Ber. Dtsch. Keram. Ges. 1989.

[10] Jarcho M, "The future of hydroxyapatite ceramics", Bioceramics 1, Vol. 1, Shiyaku-EuroAmerica Inc., Tokyo-Sant Louis, 1989.

[11] Koutsopoulos S, "Synthesis and characterization of hydroxyapatite crystals: a review study on the analytical methods", J. Biomed. Mater. Res., 62, pp. 600-609, 2002.

[12] Currey JD, Handbook of composites Vol. 4, Elsevier Science Publishers B. V. 1983.

[13] Kay MI, Young RA, Posner RA, "Crystal structure of hydroxyapatite", Nature, 204, pp. 1050-1052, 1964.

[14] Posner AS, Perloff A, Diorio AF, “Refinement of the hydroxyapatite structure”, Acta Cryst., 11, pp. 308, 1958.

[15] Elliott JC, Young RA, “Conversion of single crystals of Chlorapatite into single crystals of hydroxyapatite”, Nature, 214, pp. 904-906, 1967.

[16] Rangavittal N, Landa-Canovas AR, Gonzales-Calbet, JM, Vallet-Regi M, “Structural study and stability of hydroxyapatite and β-tricalcium phosphate: Two important bioceramics”, J Biomed. Mater. Res., 51, pp. 660-668, 2000.

[17] Raynaud S, Champion E, Bernache-Assollant D, “Calcium phosphate apatites with variable Ca/P atomic ratio II. Calcination and sintering”, Biomaterials, 23, pp. 1073-1080, 2002.

[18] Hench LL, “Mechanisms of hydroxyapatite formation on porous gel-silica substrates”, J. Sol-Gel Sci. Technol., 7, pp. 59-68, 1995.

[19] Weber FA, Charnley J, J. Bone Joint Surg., 57 B, pp. 297, 1975.

[20] Ciapetti G, Granchi D, Cenni E, Savarino L, Cavedagna D, Pizzoferrato A, “Cytotoxic effect of bone cements in HL-60 cells: distinction between apoptosis and necrosis”, J. Biomed. Mater. Res., 52, pp. 338-345, 2000.

[21] Kusy RP,“Characterization of self-curing acrylic bone cements”, J. Biomed. Mater. Res., 12, pp. 271-305, 1978.

[22] Dalby MJ, Di Silvio L, Harper EJ, Bonfield W, “In vitro evaluation of a new polymethylmethacrylate cement reinforced with hydroxyapatite”, J. Mater. Sci.-Mater. Med., 10, pp. 793-796, 1999.

[23] Aizawa M, Ito M, Itatani K, Suemasu H, Nozue A, Okada I, Matsumoto M, Ishikawa M, Matsumoto H, Toyama Y, “In vivo and in vitro evaluation of the biocompatibility of the hydroxyapatite-PMMA hybrid materials having mechanical property similar to that of cortical bone”, Key Eng. Mater., 218, pp. 465-468, 2002.

[24] Lee RR, Ogiso M, Watanabe A, Ishihara K, “Examination of hydroxyapatite filled 4-META/MMA-TBB adhesive bone cement in in-vitro and in-vivo environment”, J. Biomed. Mater. Res., 38, pp. 11-16, 1997.

[25] Moursi AM, Winnard AV, Winnard PL, Lannutti JJ, Seghi RR, “Enhanced osteoblast response to a polymethylmethacrylate-hydroxyapatite composite”, Biomaterials, 23, pp. 133-144, 2002.

[26] Liu Q, de Wijn JR, van Blitterswijk, “Covalent bonding of PMMA, PBMA, and poly(HEMA) to hydroxyapatite particles”, J. Biomed. Mater. Res., 40, pp. 257-263, 1998.

[27] Majeti N.V. Ravi Kumar, “A review of chitin and chitosan applications”, React. Funct. Polym., 46, pp.1-27, 2000.

[28] Eugene K, Lee YL, “Implantable applications of chitin and chitosan”, Biomaterials, 24, pp. 2339-2349, 2003.

[29] Keisuke K, “Controlled functionalization of the polysaccharide chitin”, Prog. Polym. Sci., 26, pp. 1921-1971, 2001.

[30] Sashiwa H, Shigemasa Y, Roy R, “Chemical modification of chitosan part 2 - Novel N-alkylation of chitosan via Michael type reaction”, Chem. Lett., 8, pp. 862-863, 2000.

[31] Yalpani M, Hall LD, “Some chemical and analytical aspects of polysaccharide modifications. III. Formation of branched-chain, soluble chitosan derivatives”, Macromolecules, 17, pp. 272-281, 1984.

[32] Hirano S, Ohe Y, Ono H, “Selective N-acylation of chitosan”, Carbohydr. Res., 47, pp. 315, 1976.

[33] Hirano S, “The blood compatibility of chitosan and N-acyl chitosans”, J. Biomed. Mater. Res., 19, pp. 413-417, 1985.

[34] Sashiwa H, Shigemasa Y, Roy R, "Chemical modifications of chitosan. Part 5 - Homogeneous *N,O*-acylation of chitosan in dimethyl sulfoxide with cyclic acid anhydrides", Chem. Lett., 10, pp. 1186-1187, 2000.

[35] Kurita K, "Controlled functionalization of the polysaccharide chitin", Prog. Polym. Sci., 26, pp. 1921-1971, 2001.

[36] Fujii S, Kumagai H, Noda M, "Preparation of poly(acyl)chitosans", Carbohydr. Res., 83, pp. 389-393, 1980.

[37] Hirano S, Miura O, Yamaguchi R, "N-acylchitosan gel preparation of partially and heterogeneously N-acylated chitosans", Agri. Biol. Chem., 9, pp. 1755-1759, 1977.

[38] Nishimura SI, Kohgo O, Kurita K, Kuzuhara H, "Chemospecific manipulations of a rigid polysaccharide: syntheses of novel chitosan derivatives with excellent solubility in common organic solvents by regioselective chemical modifications", Macromolecules, 24, pp. 4745-4748, 1991.

[39] Kennedy R, "Prevention of experimental postoperative peritoneal adhesions by *N,O*-carboxymethyl chitosan", Surgery, 120 , pp. 866-870, 1996.

[40] Muzzarelli RAA, Tanfani F, Emanuelli M, Mariotti S, "*N*-(carboxymethylidene)chitosans and *N*-(carboxymethyl)chitosans: Novel chelating polyampholytes obtained from chitosan glyoxylate", Carbohydr. Res., 107, pp. 199-214, 1982.

[41] Lillo LE, Matsuhiro B, "Chemical modifications of carboxylated chitosan", Carbohydr. Polym., 34, pp. 397-401, 1997.

[42] Holme KR, Perlin AS, "Chitosan *N*-sulfate. A water-soluble polyelectrolyte", Carbohydr. Res., 302, pp. 7-12, 1997.

[43] Focher B, Massoli A, Torri G, Gervasini A, Morazzoni F, "High molecular weight chitosan 6-*O*-sulfate. Synthesis, ESR and NMR characterization", Macromol. Chem. Phys., 187, pp. 2609-2620, 1986.

[44] Zhu AP, Shan B, Yuan YL, Shen J, "Preparation and blood compatibility of phosphorylcholine-bonded O-butyrylchitosan", Polym. Int., 52, pp. 81-85, 2003.

[45] Heras A, Rodriguez NM, Ramos VM, Aguiio E, "*N*-methylene phosphonic chitosan: a novel soluble derivative", Carbohydr. Polym., 44, pp. 1-8, 2001.

[46] Wenming X, Peixin X, Qin L, "Preparation and antibacterial activity of a water-soluble chitosan derivative", Carbohydr. Polym., 50, pp. 35-40, 2002.

[47] Zhishen J, Dongfen S, Weiliang X, "Synthesis and antibacterial activities of quaternary ammonium salt of chitosan", Carbohydr. Res., 333, pp. 1-6, 2001.

[48] Kato Y, Onishi H, Machida Y, "Biological characteristics of lactosaminated *N*-succinyl-chitosan as a liver-specific drug carrier in mice", J. Control. Release, 70, pp. 295-307, 2001.

[49] Skorik Y, Gomes CAR, Vasconcelos TSD, Yatluk YG, "*N*-(2-Carboxyethyl)chitosans: regioselective synthesis, characterisation and protolytic equilibria", Carbohydr. Res., 338, pp. 271-276, 2003.

[50] Rabea EI, Badawy ME-T, Rogge TM, Stevens CV, Smagghe G, Hofte M, Steurbaut W, In Proceedings of the 9th International Chitin-Chitosan Conference; Montereal, Que´bec, Canada, pp. 103, 2003.

[51] Zhang C, Qineng P, Hongjuan Z, Jian S, "Synthesis and characterization of water-soluble *O*-succinyl-chitosan", Eur. Polym. J., 39, pp. 1629-1634, 2003.

[52] Martin L, Wilson CG, Koosh F, Uchegbu IF, "Sustained buccal delivery of the hydrophobic drug denbufylline using physically cross-linked palmitoyl glycol chitosan hydrogels", Eur. J. Pharm. Biopharm., 55, pp. 35-45, 2003.

[53] Ramos VM, Rodrý´guezb NM, Rodrý´gueza MS, Herasc A, Agullo E, "Modified

chitosan carrying phosphonic and alkyl groups", Carbohydr. Polym., 51, pp. 425-429, 2003.

[54] Zhanga C, Ping Q, Zhang H, Shen J, "Preparation of *N*-alkyl-*O*-sulfate chitosan derivatives and micellar solubilization of taxol", Carbohydr. Polym., 54, pp. 137-141, 2003.

[55] Tong Y, Wang S, Xu J, Chua B, He C, "Synthesis of *O,O*-dipalmitoyl chitosan and its amphiphilic properties and capability of cholesterol absorption", Carbohydr. Polym., 60, pp. 229-233, 2005.

[56] Li BQ, Hu QL, Qian XZ, Fang ZP, Shen JC, "Bioabsorbable chitosan/hydroxyapatite composite rod prepared by in-situ precipitation for internal fixation of bone fracture", ACTA Polym. Sin., 6, pp. 828-833, 2002.

[57] Chen F, Wang ZC, Lin CJ, "Preparation and characterization of nano-sized hydroxyapatite particles and hydroxyapatite/chitosan nano-composite for use in biomedical materials", Mater. Lett., 57, pp. 858-861, 2002.

[58] Zhao F, Yin YJ, Lu WW, Leong JC, Zhang WJ, Zhang JY, Zhang MF, Yao KD, "Preparation and histological evaluation of biomimetic three-dimensional hydroxyapatite/chitosan-gelatin network composite scaffolds", Biomaterials, 23, pp. 3227-3234, 2002.

[59] Sivakumar M, Manjubala I, Rao KP, "Preparation, characterization and in-vitro release of gentamicin from coralline hydroxyapatite-chitosan composite microspheres", Carbohydr. Polym., 49, pp. 281-288, 2002.

[60] Yamaguchi I, Tokuchi K, Fukuzaki H, Koyama Y, Takakuda K, Monma H, Tanaka J, "Preparation and mechanical properties of chitosan/hydroxyapatite nanocomposites", Key Eng. Mater., 192-1, pp. 673-676, 2000.

[61] Langer R, "Polymeric delivery systems for controlled drug release", Chem. Eng. Commun., 6, pp.1-48, 1980.

[62] Wang TT, Kwei TK, Frisch HL, “Diffusion in glassy polymers III”, J. Polym. Sci., 7, pp. 2019-2028, 1968.

[63] Siepmann J, Peppas NA, “Modeling of drug release from delivery systems based on hydroxypropyl methylcellulose (HPMC)”, Adv. Drug Deliv. Rev., 48, pp. 39-157, 2001.

[64] Higuchi T, “Rate of release of medicaments from ointment bases containing drugs in suspensions”, J. Pharm. Sci., 50, pp. 874-875, 1961.

[65] Ritger PL, Peppas NA, “A simple equation for description of solute release. I. Fickian and non-Fickian release from non-swellable devices in the form of slabs, spheres, cylinders or discs”, J. Control. Release, 5, pp. 23-36, 1987.

[66] Ritger PL, Peppas NA, “A simple equation for description of solute release II. Fickian and anomalous release from swellable devices”, J. Control. Release, 5, pp. 37-42, 1987.

[67] Hopfenberg HB, “Controlled release from erodible slabs, cylinders, and spheres”, Controlled Release Polymeric Formulations, ACS Symp. Ser. No. 33. American Chemical Society, Washington, 1976.

[68] Heller J, Baker RW, “Theory and practice of controlled drug delivery from bioerodible polymers”, Controlled Release of Bioactive Materials, Academic Press, New York, 1980.

[69] Amstutz HC, Gruen T, “Clinical application of polymethylmethacrylate for total joint replacement”, Current practice of orthopaedic surgery, St. Louis, CV Mosby Company, 1973.

[70] Vasquez B, Elvira C, Levenfeld B, “Application of tertiary amines with reduced toxicity to the curing process of acrylic bone cements”, J. Biomed. Mater. Res., 34, pp. 129-136, 1997.

[71] Oonishi H, “Mechanical and chemical bonding of artificial joints”, Clin. Mater., 5, pp. 217-233, 1990.

[72] Downes S, "Methods of improving drug release from poly(methyl methacrylate) bone cement", Clin. Mater., 7, pp. 227-231, 1991.

[73] Vallo CI, Montemartini MA, Fanorich MA, Porto Lopez JM, Candrado TR, "Polymethylmethacrylate based bone cement modified with hydroxyapatite", J. Biomed. Mater. Res., 48, pp. 174-178, 1999.

[74] Sogal A, Hulbert SF, "Mechanical properties of a composite bone cement; polymethylmethacrylate and hydroxyapatite", Bioceramics, 5, pp. 213-224, 1992.

[75] Dalby MJ, DiSivio L, Harper EJ, Bonefield W, "Increasing hydroxyapatite incorporation into poly(methyl methacrylate) cement increases osteoblast adhesion and responses", Biomaterials, 23, pp. 569-576, 2002.

[76] Hench LL, Wilson J, "Surface-active biomaterials", Science, 226, pp. 630-636, 1984.

[77] Heisa U, Osborn JF, Dune F, "Hydroxyapatite ceramic as a bone substitute", Int. Orthop., 14, pp. 329-338, 1990.

[78] Nanes CR, Simske SJ, Sachdeva R, Wolford LM, "Long-term growth and apposition of porous hydroxyapatite implants", J. Biomed. Mater. Res., 36, pp. 560-563, 1997.

[79] Bigi A, Boanini E, Panzavolta S, Roveri N, "Biomimetic Growth of Hydroxyapatite on Gelatin Films Doped with Sodium Polyacrylate", Biomacromolecules, 1, pp. 752-756, 2000.

[80] Bigi A, Boanini E, Panzavolta S, Roveri N, Rubini K, "Bonelike apatite growth on hydroxyapatite-gelatin sponges from simulated body fluid", J. Biomed. Mater. Res., 59, pp. 709-714, 2002.

[81] Chang MC, Ko CC, Douglas WH, "Preparation of hydroxyapatite-gelatin nanocomposite", Biomaterials, 24, pp. 2853-2862, 2003.

[82] Wang X, Li Y, Wei J, de Groot K, "Development of biomimetic

nano-hydroxyapatite/poly(hexamethtlene adipamide) composites", Biomaterials, 23, pp. 4787-4791, 2002.

[83] Joseph R, McGregor WJ, Martyn MT, Tammer KE, Coates PD, "Effect of hydroxyapatite morphology/surface area on the rheology and processability of hydroxyapatite filled polyethylene composites", Biomaterials, 23, pp. 4295-4302, 2002.

[84] Bercea M, Navard P, "Shear dynamics of aqueous suspensions of cellulose whiskers" Macromolecules, 33, pp. 6011-6016, 2000.

[85] Yuan J, Murry HH, "The importance of crystal morphology on the viscosity of concentrated suspensions of kaolins", Appl. Clay. Sci., 12, pp. 209-219, 1997.

[86] Bouyer E, Gitzhofer F, Boulos MI, "Morphological study of hydroxyapatite nanocrystal suspension", J. Mater. Sci. Mater. Med., 8, pp. 523-531, 2000.

[87] Bagley EB, "End correlations in capillary flow of polyethylene", J. App. Phys., 28, pp. 624-627, 1958.

[88] Casson N, "A flow Equation for pigment oil suspensions of the printing types", Rheology of disperse systems, Pergamon Press, London, 1959.

[89] Liu DM, "Control of yield stress in low-temperature ceramic injection moldings", Ceram. Int., 25, pp. 587-592, 1999.

[90] Liu DM, "Particle packing and rheological property of highly-concentrated ceramic suspensions: phi(m) determination and viscosity prediction", J. Mater. Sci., 35, pp. 5503-5507, 2000.

[91] Gorbunoff MJ, "The interaction of proteins with hydroxyapatite", Anal. Biochem., 136, pp. 425-432, 1984.

[92] Barroug A, Glimcher MJ, "Hydroxyapatite crystals as a local delivery system for cisplatin: adsorption and release of cisplatin in vitro", J. Orthopaed. Res., 20, pp.

274-280, 2002.

[93] Goller G, Oktar FN, “Sintering effects on mechanical properties of biologically derived dentine hydroxyapatite”, Mater. Lett., 56, pp. 142-147, 2002.

[94] Koempel JA, Patt BS, O’Grady K, Wozney J, Toriumi1 DM, “The effect of recombinant human bone morphogenetic protein-2 on the integration of porous hydroxyapatite implants with bone the amount of bone growth into the implant”, J. Biomed. Mater. Res., 41, pp. 359-363, 1998.

[95] Yaylaoglu MB, Korkusuz P, Örs Ü, Korkusuz F, Hasirci V, “Development of a calcium phosphate-gelatin composite as a bone substitute and its use in drug release”, Biomaterials, 20, pp. 711-719, 1999.

[96] Raiche AT, Puleo DA, “In vitro effects of combined and sequential delivery of two bone growth factors”, Biomaterials, 25, pp. 677-685, 2004.

[97] Tatman OM, Gurcan S, Ozer B, Shokrylanbaran N, “Annual trends in antibiotic resistance of nosocomial Acinetobacter baumannii strains and the effect of synergistic antibiotic combinations”, Microbiologica, 27, pp. 21-28, 2004.

[98] Barlow GD, Nathwani D, “Sequential antibiotic therapy”, Curr. Opin. Infect. Dis., 13, pp. 599-607, 2000.

[99] Ijntema KI, Heuvelsland WJM, Dirix CAMC, Sam AP, “HA microcarriers for biocontrolled release of protein drugs”, Int. J. Pharm., 112, pp. 215-224, 1994.

[100] Ueno Y, Futagawa H, Takagi Y, Ueno A, Mizushim Y, “Drug-incorporating calcium carbonate nanoparticles for a new delivery system”, J. Control. Release, 103, pp. 93-98, 2005.

[101] Matsumoto T, Okazaki M, Inoue M, Yamaguchi S, Kusunose T, Toyonaga T, Hamada Y, Takahashi J, “Hydroxyapatite particles as a controlled release carrier of protein”, Biomaterials, 25, pp. 3807-3812, 2004.

[102] Rhee SH, Lee JD, “Nucleation of hydroxyapatite crystal through chemical interaction

with collagen", J. Am. Ceram. Soc., 83, pp. 2890-2892, 2002.

[103] Ellingsen JE, "A study on the mechanism of protein adsorption to TiO_2", Biomaterials, 12, pp. 593-596, 1991.

[104] Kandori K, Saito M, Saito H, Yasukawa A, Ishikawa T, "Adsorption of protein on non-stoichiometric calcium-strontium hydroxyapatite", Colloid. Surf. A-Physicochem. Eng. Asp., 94, pp. 225-230, 1995.

[105] Liou SC, Chen SY, Liu DM, "Synthesis and characterization of needlelike apatitic nanocomposite with controlled aspect ratios", Biomaterials, 24, pp. 3981-3988, 2003.

[106] Matsumoto T, Okazaki M, Inoue M, Hamada Y, Taira M, Takahashi J, "Crystallinity and solubility characteristics of hydroxyapatite adsorbed amino acid", Biomaterials, 23, pp. 2241-2247, 2002.

[107] Nicolopoulos S, Gonza'lez-Calbet JM, Alonso MP, Gutierrez-Rios MT, de Frutos MI, Vallet-Regi M, "Characterization by TEM of local crystalline changes during irradiation damage of hydroxyapatite compounds", J. Solid State Chem., 116, pp. 265-274, 1995.

[108] Hlady V, Furedi-Milhofer H, "Absorption of HAS on precipitated hydroxyapatite", J. Colloid Interface Sci., 69, pp. 460-467, 1979.

[109] Dee KC, Puleo DA, Bizios R, An Introduction to Tissue-Biomaterial Interactions, Wiley & Sons, Inc., New Jersey, 2002, pp. 39-45.

[110] Garnett J, Dieppe P, "The effects of serum and human albumin on calcium hydroxyapatite crystal growth", Biochem. J., 266, pp. 863-868, 1990.

[111] Kandori K, Sawai S, Yamamoto Y, Saito H, Ishikawa T, "Adsorption of albumin on calcium hydroxyapatite", Colloid Surf. A-Physicochem. Eng. Asp., 68, pp. 283-289, 1992.

[112] Wassell DTH, Hall RC, Embery G, "Adsorption of BSA onto hydroxyapatite", Biomaterials, 16, pp. 697-702, 1995.

[113] Manson ST, The Calculation of Photoionization Cross Sections: An Atomic View, In

Topics in Applied Physics, Vol. 26, Springer-Verlag, New York.

[114] Sailaja GS, Velayudhan S, Sunny MC, Sreenivasan K, Varma HK, Ramesh P, "Hydroxyapatite filled chitosan-polyacrylic acid polyelectrolyte complexes", J. Mater. Sci., 38, pp. 3653-3662, 2003.

[115] Ahn JS, Choi HK, Chun MK, Ryu JM, Jung JH, Kim YU, Cho CS, "Release of triamcinolone acetonide from mucoadhesive polymer composed of chitosan and poly(acrylic acid) in vitro", Biomaterials, 23, pp. 1411-1416, 2002.

[116] Ito M, Hidaka Y, Nakajima M, Yagasaki H, Kafrawy AH, "Effect of hydroxyapatite content on physical properties and connective tissue reactions to a chitosan–hydroxyapatite composite membrane", J. Biomed. Mater. Res., 45, pp. 204-208, 1999.

[117] Yin YJ, Ye F, Cui JF, Zhang FJ, Li XL, Yao KD, "Preparation and characterization of macroporous chitosan-gelatin beta-tricalcium phosphate composite scaffolds for bone tissue engineering", J. Biomed. Mater. Res., A 67, pp. 844-855, 2003.

[118] Geiger M, Li RH, Friess W, "Collagen sponges for bone regeneration with rhBMP-2", Adv. Drug. Deliver. Rev., 55, pp. 1613-1629, 2003.

[119] Yamaguchi I, Iizuka S, Osaka A, Monmad H, Tanaka J, "The effect of citric acid addition on chitosan/hydroxyapatite composites", Colloid Surf. A-Physicochem. Eng. Asp., 214, pp. 111-118, 2003.

[120] Sperling LH, Introduction to physical polymer science, Second edition, John Wiley & Sons, New York, 1992.

[121] Kesenci K, Fambri L, Migliaresi C, Piskin E, "Preparation and properties of poly(L-lactide)/hydroxyapatite composites", J. Biomat. Sci-Polym. E., 11, pp. 617-632, 2000.

[122] Arrighi V, McEwen IJ, Qian H, Serrano Prieto MB, "The glass transition and interfacial layer in styrene-butadiene rubber containing silica nanofiller", Polymer, 44, pp.

6259-6266, 2003.

[123] Goh HW, Goh SH, Xu GQ, Pramoda KP, Zhang WD, "Dynamic mechanical behavior of in situ functionalized multi-walled carbon nanotube/phenoxy resin composite", Chem. Phys. Lett., 373, pp. 277-283, 2003.

[124] Lu H, Nutt S, "Restricted relaxation in polymer nanocomposites near the glass transition", Macromolecules, 36, pp. 4010-4016, 2003.

[125] Huang YQ, Zhang YQ, Hua YQ, "Studies on dynamic mechanical and rheological properties of LLDPE/nano-SiO2 composites", J. Mater. Sci. Lett., 22, pp. 997-998, 2003.

[126] Strawhecker KE, Manias E, "Crystallization behavior of poly(ethylene oxide) in the presence of Na^+ montmorillonite fillers", Chem. Mater., 15, pp. 844-849, 2003.

[127] Ash BJ, Schadler LS, Siegel RW, "Glass transition behavior of alumina/polymethylmethacrylate nanocomposites", Mater. Lett., 55, pp. 83-87, 2002.

[128] Hu Q, Li B, Wang M, Shen J, "Preparation and characterization of biodegradable chitosan/hydroxyapatite nanocomposite rods via in situ hybridization: a potential material as internal fixation of bone fracture", Biomaterials, 25, pp. 779-785, 2004.

[129] Peppas NA, Franson NM, "The swelling interface number as a criterion for prediction of diffusional solute release mechanism in swellable polymers", J. Appl. Polym. Sci., 21, pp. 983-997, 1983.

[130] Miyajima M, Koshika A, Okada J, Ikeda M, "Mechanism of drug release from poly(L-lactic acid) matrix containing acidic or neutral drugs", J. Control. Release, 60, pp. 199-209, 1999.

[131] Tien CL, Lacroix M, Ispas-Szabo P, Mateescu MA, "N-acylated chitosan: hydrophobic matrices for controlled drug release", J. Control. Release, 93, pp. 1-13, 2003.

[132] Peppas NA, "Analysis of Fickian and non-Fickian drug release from polymers", Pharm. Acta. Helv., 60, pp. 110-111, 1985.

[133] Peppas NA, Korsmeyer RW, “Dynamically swelling hydrogels in controlled release applications”, Hydrogels in Medicine and Pharmacy, Vol. 3, CRC Press, Boca Raton, 1986.

[134] Seo J, Han H, “Water diffusion studies in polyimide thin films”, J. Appl. Polym. Sci., 82, pp. 731-737, 2001.

[135] Wronski TJ, Ratkus AM, Thomsen JS, Vulcan Q, Mosekilde L, “Sequential treatment with basic fibroblast growth factor and parathyroid hormone restores lost cancellous bone mass and strength in the proximal tibia of aged ovariectomized rats”, J. Bone Miner. Res., 16, pp. 1399-1407, 2001.

[136] Miller YW, Eady EA, Lacey RW, Cove JH, Joanes DN, Cunliffe WJ, “Sequential antibiotic therapy for acne promotes the carriage of resistant staphylococci on the skin of contacts”, J. Antimicrob. Chemother., 38, pp. 829-837, 1996.

[137] Borden M, El-Amin SF, Attawia M, Laurencin CT, “Structural and human cellular assessment of a novel microsphere-based tissue engineered scaffold for bone repair”, Biomaterials, 24, pp. 597-609, 2003.

[138] Ishihara M, Obara K, Ishizuka T, Fujita M, Sato M, Masuoka K, Saito Y, Yura H, Matsui T, Hattori H, Kikuchi M, Kurita A, “Controlled release of fibroblast growth factors and heparin from photocrosslinked chitosan hydrogels and subsequent effect on *in vivo* vascularization”, J. Biomed. Mater. Res., 64A, pp. 551-559, 2003.

[139] Kim SE, Park JH, Cho YW, Chung H, Jeong SY, Lee EB, Kwon IC, “Porous chitosan scaffold containing microspheres loaded with transforming growth factor-β1: Implications for cartilage tissue engineering”, J. Control. Release, 91, pp. 365-374, 2003.

[140] Drury JL, Mooney DJ, “Hydrogels for tissue engineering: scaffold design variables and applications”, Biomaterials, 24, pp. 4337-4351, 2003.

[141] Kurita K, Ikeda H, Yoshida Y, Shimojoh M, Harata M, “Chemoselective protection of

the amino groups of chitosan by controlled phthaloylation: Facile preparation of a precursor useful for chemical modifications", Biomacromolecules, 3, pp. 1-4, 2002.

[142] Sashiwa H, Kawasaki N, Nakayama A, Muraki E, Yamamoto N, Aiba S-I, "Chemical Modification of Chitosan. 14: Synthesis of Water-Soluble Chitosan Derivatives by Simple Acetylation", Biomacromolecules, 3, pp. 1126-1128, 2002.

[143] de Queiroz AAA, Ferraz HG, Abraham GA, Fernandez MD, Bravo AL, Roman JS, "Development of new hydroactive dressings based on chitosan membranes: Characterization and in vivo behavior", J. Biomed. Mater. Res., 64A, pp.147-154, 2003.

[144] Koyano T, Minoura N, Nagura M, Kobayashi K, "Attachment and growth of cultured fibroblast cell on PVA/chitosan blended hydrogels", J. Biomed. Mater. Res., 39, pp. 486-490, 1998.

[145] Temenoff JS, Park H, Jabbari E, Sheffield TL, LeBaron RG, Ambrose CG, Mikos AG, **"***In vitro* osteogenic differentiation of marrow stromal cells encapsulated in biodegradable hydrogels", J. Biomed. Mater. Res., 70A, pp. 235-244, 2004.

[146] Chen LY, Du YM, Zeng XQ, "Relationships between the molecular structure and moisture-absorption and moisture-retention abilities of carboxymethyl chitosan: II. Effect of degree of deacetylation and carboxymethylation", Carbohydr. Res., 338, pp. 333-340, 2003.

[147] Missirlis D, Tirelli N, Hubbell JA, "Amphiphilic hydrogel nanoparticles. Preparation, characterization, and preliminary assessment as new colloidal drug carriers", Langmuir, 21, pp. 2605-2613, 2005.

[148] Cleary J, Bromberg LE, Magner E, "Diffusion and release of solutes in Pluronic-*g*-poly(acrylic acid) hydrogels", Langmuir, 19, pp. 9162-9172, 2003.

[149] Can Z, Ping QN, Zhang HJ, Jian S, "Preparation of *N*-alkyl-*O*-sulfate chitosan derivatives and micellar solubilization of taxol", Carbohydr. Polym., 54, pp. 137-141, 2003.

[150] Guan YL, Shao L, Yao KD, "A study on correlation between water state and swelling kinetics of chitosan-based hydrogels", J. Appl. Polym. Sci., 61, pp. 2325-2335, 1996.

[151] Vashuk EV, Vorobieva EV, Basalyga II, Krutko NP, "Water-absorbing properties of hydrogels based on polymeric complexes", Mater. Res. Innov., 4, pp. 350-352, 2001.

[152] Vazquez B, Roman JS, Peniche C, Cohen ME, "Polymeric hydrophilic hydrogels with flexible hydrophobic chains. Control of the hydration and interactions with water molecules", Macromolecules, 30, pp. 8440-8446, 1997.

[153] Morillon V, Debeaufort F, Capelle M, Blond G, Voilley A, "Influence of the physical state of water on the barrier properties of hydrophilic and hydrophobic films", J. Agric. Food. Chem., 48, pp. 11-16, 2000.

[154] Barrow RE, Ramirez RJ, Zhang XJ, "Ibuprofen modulates tissue perfusion in partial-thickness burns", Burns, 26, pp. 341-346, 2000.

[155] Sugimoto M, Morimoto M, Sashiwa H, Saimoto H, Shigemasa Y, "Preparation and characterization of water-soluble chitin and chitosan derivatives", Carbohyd. Polym., 36, pp. 49-59, 1998.

[156] Agrawal AM, Manek RV, Kolling WM, Neau SH, "Water distribution studies within microcrystalline cellulose and chitosan using differential scanning calorimetry and dynamic vapor sorption analysis", J. Pharm. Sci., 93, pp. 1766-1779, 2004.

[157] Sen M, Guven O, "Dynamic deswelling studies of poly(N-vinyl-2-pyrrolidone/itaconic acid) hydrogels swollen in water and terbinafine hydrochloride solutions", Eur. Polym. J., 38, pp. 751-757, 2002.

[158] Smith BC, Infrared spectral interpretation: a systematic approach, Boca Raton: CRC Press, 1999.

[159] Bajpai SK, "Swelling-deswelling behavior of poly(acrylamide-co-maleic acid) hydrogels", J. Appl. Polym. Sci., 80, pp. 2782-2789, 2001.

[160] Tamai Y, Tanaka H, Nakanishi K, "Molecular dynamics study of polymer-water

interaction in hydrogels 1. Hydrogen-bond structure", Macromolecules, 29, pp. 6750-6760, 1996.

[161] Rodriguez R, Alvarez-Lorenzo C, Concheiro A, "Interactions of ibuprofen with cationic polysaccharides in aqueous dispersions and hydrogels rheological and diffusional implications", Eur. J. Pharm. Sci., 20, pp. 429-438, 2003.

[162] Azad AK, Sermsintham N, Chandrkrachang S, Stevens WF, **"**Chitosan membrane as a wound-healing dressing: Characterization and clinical application", J. Biomed. Mater. Res., 69B, pp. 216-222, 2004.

[163] Lee DH, Kim JW, Suh KD, "Amphiphilic urethane acrylate hydrogels: pH sensitivity and drug-releasing behaviors", J. Appl. Polym. Sci., 72, pp. 1305-1311, 1999.

[164] Suh JKF, Matthew HWT, "Application of chitosan-based polysaccharide biomaterials in cartilage tissue engineering: a review", Biomaterials, 21, pp. 2589-2598, 2000.

[165] Lee JY, Nam SH, Im SY, Park YJ, Lee YM, Seol YJ, Chung CP, Lee SJ, "Enhanced bone formation by controlled growth factor delivery from chitosan-based biomaterials", J. Control. Release, 78, pp. 187-197, 2002.

[166] Lee KY, Mooney DJ, "Hydrogels for tissue engineering", Chem. Rev., 101, pp. 1869-1879, 2001.

[167] Royce SM, Askari M, Marra KG, "Incorporation of polymer microspheres within fibrin scaffolds for the controlled delivery of FGF-1", J. Biomater. Sci.-Polym. Ed., 15, pp. 1327-1336, 2004.

[168] Sivakumar M, Rao KP, "Preparation, characterization, and *in vitro* release of gentamicin from coralline hydroxyapatite-alginate composite microspheres", J. Biomed. Mater. Res. Part A, 65, pp. 222-228, 2003.

[169] Chen SC, Wu YC, Mi FL, Lin YH, Yu LC, Sung HW, "A novel pH-sensitive hydrogel composed of *N*,*O*-carboxymethyl chitosan and alginate cross-linked by genipin for

protein drug delivery", J. Control. Release, 96, pp. 285-300, 2004.

[170] Badawy MEI, Rabea EI, Rogge TM, Stevens CV, Smagghe G, Steurbaut W, Hofte M, "Synthesis and fungicidal activity of new *N*,*O*-Acyl chitosan derivatives", Biomacromolecules, 5, pp. 589-595, 2004.

[171] Liu TY, Chen SY, Liu DM, "Influence of the aspect ratio of bioactive nanofillers on rheological behavior of PMMA-based orthopedic materials", J. Biomed. Mater. Res. Part B: Appl. Biomater., 71B, pp. 116-122, 2004.

[172] Siepmann J, Gopferich A, "Mathematical modeling of bioerodible, polymeric drug delivery systems", Adv. Drug Deliv. Rev., 48, pp. 229-247, 2001.

[173] Liu TY, Chen SY, Li JH, Liu DM, "Study on drug release behavior of CDHA/Chitosan nanocomposites-Effect of CDHA nanoparticles", J. Control. Release, 112, pp. 88-95, 2006.

PERSONAL INFORMATION

劉澤英

58 年 9 月 10 日出生於基隆

學歷:

1. 學士: 逢甲大學材料科學與工程系　　82畢

2. 碩士: 台灣大學材料科學與工程研究所　84畢

3. 博士: 交通大學材料科學與工程研究所　91入學

經歷:

1. 華通電腦股份有限公司 製程研發工程師　84-86

2. 華通電腦股份有限公司 製程研發課課長　86-88

3. 華通電腦股份有限公司 技術開發部 副理　88-91

PUBLICATION

1. SCI 論文(2002-2006)

1-1. **Tse-Ying Liu**, San-Yuan Chen, Dean-Mo Liu. Influence of the aspect ratio of bioactive nanofillers on rheological behavior of PMMA-based orthopedic materials. **Journal of biomedical material research 71B (2004) 116–122.**

1-2. **Tse-Ying Liu,** San-Yuan Chen, Dean-Mo Liu, Sz-Chian Liou. On the study of BSA-loaded calcium-deficient hydroxyapatite nano-carriers for controlled drug delivery. **Journal of controlled release 107 (2005) 112–121.**

1-3. **Tse-Ying Liu**, San-Yuan Chen, Jo-Hao Li and Dean-Mo Liu. Study on drug release behaviour of CDHA/Chitosan nanocomposites-Effect of CDHA nanoparticles. **Journal of controlled release 112 (2006) 88-95.**

1-4. **Tse-Ying Liu**, Ting-Yu Liu, San-Yuan Chen, Shian-Chuan Chen and Dean-Mo Liu. Study on sequential release behaviors of carboxymethyl-hexanoyl chitosan/*O*-hexanoyl chitosan hydrogel: Role of hydroxyapatite Nanoparticles. **Journal of nanoscience and nanotechnology 6 (2006) 1-7.**

1-5. Ting-Yu Liu, Shang- Hsiu Hu, **Tse-Ying Liu**, Dean-Mo Liu and San-Yuan Chen. Magnetic-sensitive behavior of intelligent ferrogels for controlled release of drug. **Langmuir. Accepted.**

1-6. **Tse-Ying Liu**, San-Yuan Chen, Yi-Ling Lin and Dean-Mo Liu. Synthesis and characterization of amphiphilic carboxymethyl-hexanoyl chitosan hydrogel. **Submitted to Langmuir.**

1-7. Yen-Yu Liu, **Tse-Ying Liu**, San-Yuan Chen and Dean-Mo Liu. Characterization and controlled drug release of SiO_2/pHEMA hybrid. **Submitted to Journal of membrane science.**

1-8. **Tse-Ying Liu**, San-Yuan Chen, Yi-Ling Lin and Dean-Mo Liu. Synthesis and characterization of amphiphilic carboxymethyl-hexanoyl chitosan hydrogel: pH sensitivity and drug release behaviors. **Submitted to Biomacromolecules.**

1-9. **Tse-Ying Liu**, San-Yuan Chen, Jo-Hao Li, Manipulation of Drug Release Behaviors of Chitosan-based Orthopedic Nano-composites by PAA-coated CDHA Nanoparticles.

2. 研討會論文 (2002-2006)

2-1. **T.Y. Liu**, J.H. Li, S.C. Chen, S.Y. Chen, 2004/11/17, Effects of Ca-deficient hydroxyapatite nanoparticles on the drug release behaviors of Chitosan based composites for the use of orthopedics, 中華民國材料年會2004, 新竹. (Oral Presentation)

2-2. **T.Y. Liu**, J.H. Li, S.C. Chen, S.Y. Chen, 2004/12/18, CDHA 奈米顆粒之 PAA 披覆對 Chitosan 骨科複合材料藥物釋放性質研究, 中華民國生醫年會 2004, 台南. (Oral Presentation)

2-3. **T.Y. Liu**, J.H. Li, S.C. Chen, S.Y. Chen, 2005/4/24, Study on the drug release behaviours of chitosan/CDHA nanocomposite - Effect of CDHA nanoparticles on diffusion exponent, 6th Asian-Pacific Conference on Medical and Biological Engineering (APCMBE 2005), Japan.

2-4. **T. Y. Liu**, J. Li, S. Chen, S. Chen, 2005/4/29, Manipulation of Drug Release Behaviors of Chitosan-based Orthopedic Nano-composites by PAA-coated CDHA Nanoparticles, 30th Annual Meeting and Exposition of the Society for Biomaterials (SFB 2005). Tennessee, U.S. (Post Presentation)

2-5. **T.Y. Liu**, Y. L. Lin, S.C. Chen, S.Y. Chen, D.M. Liu, 2005/06/17, Study on Sequential Release Behaviors of Carboxymethyl-hexanoyl Chitosan/Acylation Chitosan Scaffold, 32nd Annual Meeting & Exposition of the Controlled Release Society (CRS 2005), Miami, U.S.

2-6. **T.Y. Liu**, Y. L. Lin, S.C. Chen, 2005/11/26, Characterization of Novel Amphiphilic Carboxymethyl-hexanoyl Chitosan Hydrogel: Water-retention Ability and Drug Release Behaviors, 中華民國藥物制放及生醫材料學會2005年會, 新竹. (Oral Presentation)

2-7. **T.Y. Liu**, Y.L. Lin, S.Y. Chen and D.M. Liu, 2005/12/9, Synthesis and Characterization of Amphiphilic Ccarboxymethyl-hexanoyl Chitosan Hydrogel , The 12th International Conference on Biomedical Engineering (ICMBE 2005), Singapore.

2-8. **T.Y Liu**, T.Y. Liu, S.Y. Chen, S.C. Chen and D.M. Liu. 2006/2/17, Study on Sequential Release Behaviors of Carboxymethyl-hexanoyl Chitosan/*O*-hexanoyl Chitosan Hydrogel: Role of Hydroxyapatite Nanoparticles, National Institute of Pharmaceutical Education and Research (NIPER-NANO-2006): Nanotechnology in Advanced Drug Delivery, India.

2-9. J.H. Li, T.Y. Liu, **T.Y. Liu** and S.Y. Chen, 2003/11, The preparation and release properties investigation of Organic/ inorganic in-situ process of chitosan/CDHA hydrogel beads, 中華民國生醫年會 2003, 台北.

2-10. **T.Y. Liu,** Y. L. Lin, S.Y. Chen and D.M. Liu, Characterization of Novel Amphiphilic Carboxymethyl-hexanoyl Chitosan Hydrogel: pH-sensitivity and Drug Release Behaviors, 33th Annual Meeting & Exposition of the Controlled Release Society (CRS 2006), Amsterdam, Netherlands. Oral presentation Accepted .

3. 專利:

1. 中華民國專利：印刷電路板壓合承載盤止滑裝置 (證書號：115291)

2. 美國專利："Synthesis and Develoment of Novel Hemocompatible Comopsites". (94 年送件專利審查中))

3. 中華民國及美國專利：一種由微囊胞聚集體所構成的支架及其製造方法 (95 年送件申請中)

4. 一種具有親疏水雙性及酸鹼敏感性的中性水膠材料(專利說明書撰寫中)